

Distribution Agreement

In presenting this thesis as a partial fulfillment of the requirements for a degree from Emory University, I hereby grant to Emory University and its agents the non-exclusive license to archive, make accessible, and display my thesis in whole or in part in all forms of media, now or hereafter now, including display on the World Wide Web. I understand that I may select some access restrictions as part of the online submission of this thesis. I retain all ownership rights to the copyright of the thesis. I also retain the right to use in future works (such as articles or books) all or part of this thesis.

Taylor L. Dover

April 13, 2021

Unusual Paradigms in Selective Synthesis:

Part 1: Toward the Synthesis of Racemic and Enantioenriched HIOC;

Part 2: Fluorinated Alcohols: Powerful Promoters for the Ring-Opening Reactions of Epoxides
with Carbon Nucleophiles

by

Taylor L. Dover

Frank E. McDonald
Adviser

Chemistry

Frank E. McDonald
Adviser

Jose Soria
Committee Member

Eladio Abreu
Committee Member

2021

Unusual Paradigms in Selective Synthesis:

Part 1: Toward the Synthesis of Racemic and Enantioenriched HIOC;

Part 2: Fluorinated Alcohols: Powerful Promoters for the Ring-Opening Reactions of Epoxides
with Carbon Nucleophiles

By

Taylor L. Dover

Frank E. McDonald

Adviser

An abstract of
a thesis submitted to the Faculty of Emory College of Arts and Sciences
of Emory University in partial fulfillment
of the requirements of the degree of
Bachelor of Science with Honors

Chemistry

2021

Abstract

Unusual Paradigms in Selective Synthesis:

Part 1: Toward the Synthesis of Racemic and Enantioenriched HIOC;

Part 2: Fluorinated Alcohols: Powerful Promoters for the Ring-Opening Reactions of Epoxides
with Carbon Nucleophiles

By Taylor L. Dover

N-[2-(5-hydroxy-1*H*-indol-3-yl)ethyl]-2-oxopiperidine-3-carboxamide (HIOC) exhibits protective activity against light-induced retinal damage in animal models, and thus has considerable therapeutic potential. Due to its stereogenic center, asymmetric synthesis methods are of great interest. This thesis will describe improvements in the synthesis of racemic HIOC, as well as the development of asymmetric synthesis methods for two analogs of the carboxylic acid precursor. Our selective synthesis strategy employs porcine liver esterase (PLE) in two different capacities: selective hydrolysis of the ester precursor and a multi-step process that includes an enzymatic desymmetrization and a cyclization step. We also discuss preliminary computational studies of PLE, and the challenges associated with these efforts.

The coupling of terminal alkynes and epoxides using mild catalytic methods is a long-standing challenge in synthetic chemistry. As part of initial efforts toward a strategy employing dual activation of the alkyne nucleophile and the epoxide electrophile, we developed an extensive review of fluorinated alcohol solvents in epoxide ring-opening reactions with carbon nucleophiles. The unique physical properties of these solvents enable interesting reactivity paradigms, which are rarely observed in typical organic solvents.

Unusual Paradigms in Selective Synthesis:

Part 1: Toward the Synthesis of Racemic and Enantioenriched HIOC;

Part 2: Fluorinated Alcohols: Powerful Promoters for the Ring-Opening Reactions of Epoxides
with Carbon Nucleophiles

By

Taylor L. Dover

Frank E. McDonald

Adviser

A thesis submitted to the Faculty of Emory College of Arts and Sciences
of Emory University in partial fulfillment
of the requirements of the degree of
Bachelor of Science with Honors

Chemistry

2021

Acknowledgements

I would like to thank my committee members: Prof. Frank McDonald, Dr. Jose Soria, and Dr. Eladio Abreu. Without you all, I would not have this wonderful opportunity.

Prof. McDonald, without your mentorship—both in chemistry and in life—I would not have grown to be the researcher and person I am today. Whether processing grief, or processing an NMR spectrum, you've always been there for me, and I am forever grateful for that. I especially appreciate the attention and care you dedicate to each member of the McDonald laboratory. Your expertise as a PI and dedication as a mentor are characteristics I have sought after in each of my graduate school discussions.

Dr. Soria, since our time in CHEM 150, you've remained one of my biggest supporters. I attribute my decision to study chemistry to my wonderful experiences in your courses, and I'm incredibly grateful to continue working with you as a teaching assistant. Working with you in this capacity has been one of the most valuable experiences of my undergraduate career, and these experiences have solidified a passion for education that continues to guide my career goals.

Dr. Abreu, though we've only known each other for a short time, you've consistently supported my research and personal endeavors. It has been a pleasure working with you as part of the Scientific Research and Mentoring Theme Hall. Your continued interest in my development as a scientist and mentor shines through in each of our conversations, and I'm incredibly grateful to have you as part of my honors thesis committee.

I am also grateful to my fellow scientists in the McDonald laboratory. Our camaraderie has made my time in the McDonald laboratory outstanding. I especially thank my mentor, Dr. Christopher Walker. You have been a valuable resource as I have strengthened my skills in the lab, and I would consider myself very fortunate to find a laboratory mentor like you in graduate school.

Though my committee was limited in size, I would like to additionally acknowledge a few individuals that have left a lasting mark on my experience at Emory: Dr. Antonio Braithwaite, Mr. Michael McCormick, Prof. Susanna Widicus Weaver, Prof. Tracy McGill, Dr. Megan Friddle, Dr. Jennifer Hayward, and a host of other amazing instructors and mentors.

I would especially like to thank countless friends and family members for their continued support, guidance, and inspiration throughout Emory and throughout life. I also thank God for blessing me with the ability to attend Emory and thrive during my time here, both as a student and as a researcher.

Last, but not least, I would also like to thank the United States Department of Defense (W81XWH-18-1-0700), Emory College of Arts & Sciences Program to Enhance Research & Scholarship, and the Scientific Research & Mentoring Theme Hall, for funding my research and the dissemination thereof.

Table of Contents

Chapter 1: Developments Toward an Optimized Synthesis of Racemic HIOC

1.1 Background & Physiology of the BDNF/TrkB Interaction	1
1.2 Overview of Relevant Small-Molecule, Serotonin-Derived Therapeutics	5
1.3 Overview of the Published HIOC Synthesis	6
1.4 Mechanistic Concerns in the CDI Coupling	7
1.5 Initial Attempts at HIOC Synthesis	8
1.6 Revisions to the Synthesis of 2-Oxopiperidine-3-carboxylic Acid	9
1.7 A Variant Route to 2-Oxopiperidine-3-carboxylic Acid	11
1.8 Revisions to the Final Step of the HIOC Synthesis	12
1.9 Conclusions	13

Chapter 2: Developments Toward an Enantioselective Synthesis of HIOC

2.1 The Importance of Stereochemistry in Therapeutics	14
2.2 Chemoenzymatic Assays for Enantioselective Hydrolysis	15
2.3 Time Trials and Attempts at Configurational Assignment	17
2.4 Progress toward preparing the C ^a -methyl derivative of HIOC	18
2.5 Relevant Background for the Analysis of PLE Enantioselectivity	23
2.6 Initial Challenges in the Analysis of PLE Enantioselectivity	25
2.7 Computational Molecular Docking Studies	26
2.8 Further Challenges in the Analysis of PLE Enantioselectivity	27
2.9 Concluding Thoughts	29

Chapter 3: Fluorinated Alcohols: Powerful Promoters for Ring-Opening Reactions of Epoxides with Carbon Nucleophiles

3.1 Overview	31
3.2.1 Introduction	34

3.2.2 Properties of Fluorinated Alcohol Solvents	36
3.2.3 Safety of Fluorinated Alcohol Solvents and Implications in Green Chemistry	37
3.3.1 Intermolecular Carbon-Carbon Bond-Forming Reactions	38
3.3.2 Intramolecular carbon-carbon bond-forming reactions	44
3.4.1 Ring-opening reactions with organopalladium intermediates arising from directed C-H functionalization	51
3.4.2 Scope of reactions and conditions	53
3.4.3 Mechanistic Proposals	56
3.5 Ring-opening reactions with terminal alkyne nucleophiles	59
3.6 Ring-opening reactions of aziridines with carbon nucleophiles	64
3.7 Conclusions	65
Chapter 4: Experimental Details	
4.1 Notes	67
4.2 Protocols	67
4.3 Computational Details	72
References	73

Figures, Schemes, Tables, and Equations

Figures

- Figure 1.1.1: **(A)** Illustration of the “Neurotrophic Factor Hypothesis”: neurons that obtain the necessary target-derived neurotrophic factors ultimately survive and differentiate, while those that do not eventually die off. **(B)** Illustration of alternative routes of obtaining neurotrophic factors, including autocrine and paracrine routes. 2
- Figure 1.1.2: Simplified illustration of the TrkB receptor domain and the tyrosine residues implicated in some of the downstream signaling pathways. 3
- Figure 1.2.1: Structures of *N*-acetylserotonin (NAS) and *N*-[2-(5-hydroxy-1*H*-indol-3-yl)ethyl]-2-oxopiperidine-3-carboxamide (HIOC), two serotonin derivatives with activity as TrkB agonists. 6
- Figure 1.4.1: **(A)** Summary of the literature-proposed mechanisms for the CDI (**5**) coupling of carboxylic acids **7** with amines **12** to produce amides **13**. **(B)** The exact mechanism of the reaction remains undetermined, with the second phase (**8**→**11**) remaining contested in the chemical literature. 8
- Figure 2.1.1: Structures of (*R*)- and (*S*)-thalidomide. While the (*R*) enantiomer is therapeutic, the (*S*) enantiomer exhibits teratogenic properties. 14
- Figure 2.3.2: Structure of the C^α-methyl derivative of HIOC (**18**). 18
- Figure 2.4.1: Structures of nipecotic acid (**19**), 2-oxopiperidine-3-carboxylic acid (**4**), and the C^α-methyl derivative of 2-oxopiperidine-3-carboxylic acid (**21**). 18
- Figure 2.5.1: Schematic illustration of the revised Jones model for the selectivity of PLE. The H_L (hydrophobic, large) sector has undergone significant revision since the original specification of ≈33 cubic Å given in ref. 62. 23
- Figure 2.5.2: Application of the Jones Model to **24**, which illustrates the cause of the preferential production of (*R*)-**25**. 24
- Figure 2.7.1: Methyl 2-phenylacetate (**28**) and ethyl 2-phenylacetate (**29**)—two substrates used as our model system. The computed binding affinities and the literature-reported Michaelis constants are also shown. 26
- Figure 2.7.2: Structure of phenylacetic acid, the hydrolysis product of both **28** and **29**. 26
- Figure 2.8.1: Structure of PLE, with the particularly troublesome external cavity highlighted. To induce binding within the binding pocket, the Gridbox in AutoDock Vina was set to exclude this region. 28

Figure 2.9.1: Illustration of the Entrance Channel, flanked by the two entrance helices, highlighted in blue and red.	30
Figure 3.1.1: Proposed structures for bastimolide A and bastimolide B, two antimalarial natural products with moderate activity against drug-resistant <i>P. falciparum</i> strains.	31
Figure 3.1.2: Excerpt from the synthesis of RK-397, an anti-cancer natural product.	33
Figure 3.2.1.2: Structures of fluorinated alcohol solvents.	35
Figure 3.2.2.2: Aggregation of HFIP, depicting hydrogen bond donation with 1,4-dioxane.	37
Figure 3.3.1.2: The electrophilic aromatic alkylation mechanism promoted by hydrogen bonding and the ionizing power of TFE.	40
Figure 3.3.2.6: Possible mechanisms for cycloisomerization.	48
Figure 3.4.1.1: Directing groups for palladium acetate-catalyzed C-H functionalization / epoxide alkylation.	52
Figure 3.4.1.2: Representative epoxides for palladium-catalyzed C-H functionalization / epoxide alkylation.	53
Figure 3.4.3.2: Partial catalytic cycles involving 2-phenylpyridine alkylation, with a Pd(IV) intermediate (path a) vs. redox-neutral pathway (path b). Determined at the B2PLYP/DGDZVP level of theory, in acetic acid ($\epsilon = 6.25$).	58
Figure 3.5.2: Scope of product dihydropyrans (124-127) arising from epoxide substrates 37 (a) and 101 (b).	62
Figure 3.5.3: Individual steps via alkynyl alcohols 128 and 129 .	63
Figure 4.3.1: Sample Workflow for AutoDock Vina Docking Calculations.	72
Schemes	
Scheme 1.3.1: Synthetic route to HIOC from a commercially available ester precursor, ethyl 2-oxopiperidine-3-carboxylate (3).	7
Scheme 1.6.1: Conversion of ethyl 2-oxopiperidine-3-carboxylate (3) into 2-oxopiperidine-3-carboxylic acid (4) as reported by Setterholm <i>et al.</i>	9
Scheme 1.6.2: Condensed scheme leading to the isopropyl ester byproduct 14 in the work-up protocol for 4 .	10

Scheme 1.7.1: Synthesis of 4 from <i>tert</i> -butyl 2-oxopiperidine-3-carboxylate (15) using an acidic hydrolysis.	12
Scheme 1.8.1: Step two of the synthetic protocol yielding HIOC.	12
Scheme 2.3.1: Steglich esterification procedure with (<i>1R,2S</i>)- <i>trans</i> -2-phenyl-1-cyclohexanol (16) to provide derivatized product 17 .	17
Scheme 2.4.2: Synthetic route to provide diethyl 2-(3-(1,3-dioxoisoindolin-2-yl)propyl)-2-methylmalonate (24) from the substitution reaction between diethyl 2-methylmalonate (22) and <i>N</i> -(3-bromopropyl)phthalimide (23).	19
Scheme 2.4.3: Synthetic route to provide (<i>R</i>)-5-(1,3-dioxoisoindolin-2-yl)-2-(ethoxycarbonyl)-2-methylpentanoic acid ((<i>R</i>)- 25) from the PLE-catalyzed desymmetrization of 2-(3-(1,3-dioxoisoindolin-2-yl)propyl)-2-methylmalonate (24).	20
Scheme 2.4.4: Synthetic route to provide 1-(<i>tert</i> -butyl) 3-ethyl (<i>S</i>)-2-(3-(1,3-dioxoisoindolin-2-yl)propyl)-2-methylmalonate ((<i>S</i>)- 26) from (<i>R</i>)-5-(1,3-dioxoisoindolin-2-yl)-2-(ethoxycarbonyl)-2-methylpentanoic acid ((<i>R</i>)- 25).	21
Scheme 2.4.5: Synthetic route to <i>tert</i> -butyl (<i>S</i>)-3-methyl-2-oxopiperidine-3-carboxylate ((<i>S</i>)- 20) from 1-(<i>tert</i> -butyl) 3-ethyl (<i>S</i>)-2-(3-(1,3-dioxoisoindolin-2-yl)propyl)-2-methylmalonate ((<i>S</i>)- 26) via phthalimide cleavage and regioselective cyclization.	21
Scheme 2.4.6: Synthetic route to (<i>S</i>)-3-methyl-2-oxopiperidine-3-carboxylic acid ((<i>S</i>)- 21) from <i>tert</i> -butyl (<i>S</i>)-3-methyl-2-oxopiperidine-3-carboxylate ((<i>S</i>)- 20) via acid hydrolysis.	22
Scheme 2.4.7: Synthetic route to the (<i>S</i>) enantiomer of the C ^a -methyl derivative of HIOC ((<i>S</i>)- 18) via a CDI coupling of serotonin-HCl (6) with (<i>S</i>)-3-methyl-2-oxopiperidine-3-carboxylic acid ((<i>S</i>)- 21).	22
Scheme 2.6.1: Illustration of the enantioselective hydrolysis of 2-oxopiperidine-3-carboxylate esters 27 (where the dark blue circle represents one of a variety of linear and branched alkyl chains) to provide (<i>R</i>)- and (<i>S</i>)-2-oxopiperidine-3-carboxylic acid (4).	25
Scheme 3.2.1.1: Representative examples of epoxide electrophiles reacting with carbon nucleophiles, <i>without</i> fluorinated alcohol solvents.	35
Scheme 3.3.1.3: Representative scope of epoxide substrates in TFE-promoted alkylations of indoles.	41
Scheme 3.3.1.5: Alkylations of other electron-rich aromatic compounds with (<i>R</i>)-styrene oxide.	43

Scheme 3.3.1.6: 3 atom + 2 atom annulations of aryl-substituted epoxides with aryl alkenes.	44
Scheme 3.3.2.2: HFIP-promoted cyclization of the sensitive epoxyether 65 .	45
Scheme 3.3.2.8: HFIP / Ph ₄ PBF ₄ -promoted cyclization of squalene oxide (80).	51
Scheme 3.4.2.1: Pd-catalyzed C-H functionalization with 2-pyridyl and <i>N</i> -methoxyamide directing groups, with regioselective epoxide alkylation.	54
Scheme 3.4.2.2: Pd-catalyzed C-H functionalization with carboxylic acid directing group, with regioselective epoxide alkylation.	55
Scheme 3.4.2.3: Pd-catalyzed C-H functionalization with an <i>O</i> -methyl ketoxime directing group, promoting regioselective epoxide alkylation.	55
Scheme 3.4.2.4: Pd-catalyzed C-H functionalization with <i>N</i> -acyl directing groups, with regioselective epoxide alkylation.	56
Scheme 3.4.3.1: Kinetic isotope rate study and a stoichiometric experiment with palladacycle 109 from 2-phenylpyridine (84).	57
Scheme 3.4.3.3: A stoichiometric experiment with palladacycle 115 from <i>meta</i> -toluic acid, and a mechanistic proposal based on the stereochemistry of 102 .	59
Scheme 3.6.1: Palladium-catalyzed C-H functionalization of an arylcarboxylic acid with addition to an <i>N</i> -tosylaziridine, promoted by HFIP.	64
Scheme 3.6.2: Three-component coupling of an isonitrile, an <i>N</i> -tosylaziridine, and malononitrile (119) to form tetrahydropyridone imines, promoted by tetrabutylphosphonium acetate in HFIP.	65

Tables

Table 2.1.1: Chemoenzymatic Condition Assays. Investigation of the enzymatic enantioselective hydrolysis of ethyl 2-oxopiperidine-3-carboxylate (3).	16
Table 3.2.2.1: Selected properties of HFIP and TFE, compared with ethanol and water.	36
Table 3.2.3.1: Toxicity of HFIP and TFE.	37
Table 3.3.1.1: TFE-promoted alkylations of indoles 36 with (<i>R</i>)-styrene oxide (37).	39
Table 3.3.1.4: Comparing the effects of TFE vs. HFIP and water on alkylation with spiroepoxyoxindole (48).	42
Table 3.3.2.1: Solvent screening for cycloisomerization of epoxide 63 .	45

Table 3.3.2.3: Acid-catalyzed, HFIP-promoted cycloisomerization of neopentyl epoxide 67.	46
Table 3.3.2.4: Alkyl vs. ether tethers, and regioselectivity of monomethoxy aromatic substrates.	47
Table 3.3.2.5: Cycloisomerizations of methylcycloalkyl epoxide substrates 71 .	47
Table 3.3.2.7: HFIP / additive-promoted tricyclizations of epoxydiene 76 .	50
Table 3.5.1: Three-component reactions of phenylacetylene with propylene oxide and active methylene compounds.	61

Equations

Equation 4.1.1: ^1H NMR conversion estimate for the PLE-catalyzed hydrolysis of ethyl 2-oxopiperidine-3-carboxylate.	67
---	----

CHAPTER 1: Developments Toward an Optimized Synthesis of Racemic HIOC

1.1 Background & Physiology of the BDNF/TrkB Interaction

Neurotrophins—such as Neurotrophin-4 (NT-4) and Brain-Derived Neurotrophic Factor (BDNF)—are polypeptides which serve to regulate neuronal survival, growth, and differentiation.^{1, 2} These macromolecules represent only a subset of the broader family of neurotrophic factors, which are implicated in neuronal development.¹ This crucial role is embodied in the “Neurotrophic Factor Hypothesis,” which presents a simple premise: given a supply of a neurotrophic factor, developing neurons compete in an effort to obtain part of this limited resource from a given target (Figure 1.1.1 A).¹ Neurons that successfully obtain these factors ultimately survive and differentiate, while those that do not eventually die off.³ While this basic premise holds, some evidence suggests that other routes, such as paracrine and autocrine modes, may play an essential role, especially with regard to certain neurotrophins, such as BDNF (Figure 1.1.1 B).^{1, 4-6} Nonetheless, this conception provides a useful avenue for the development of therapeutics for related dysfunctions.^{1, 7}

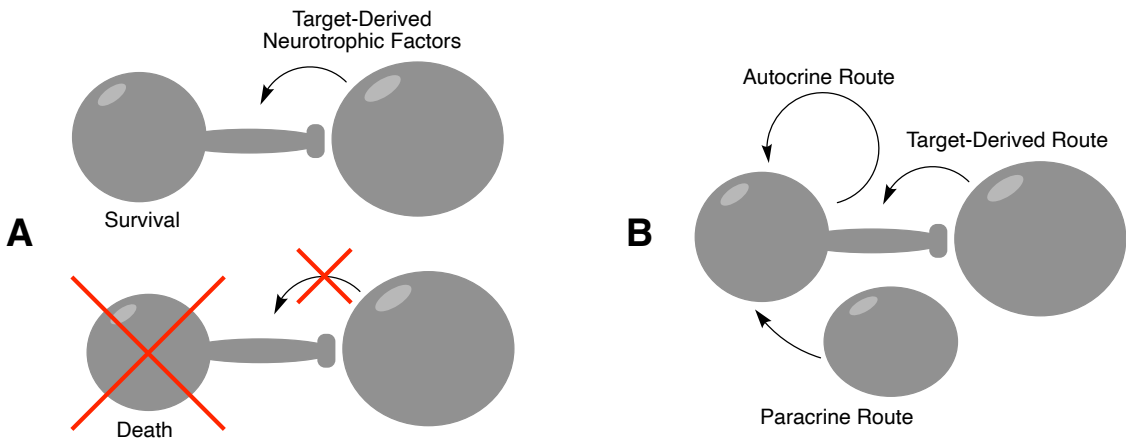


Figure 1.1.1: (A) Illustration of the “Neurotrophic Factor Hypothesis”: neurons that obtain the necessary target-derived neurotrophic factors ultimately survive and differentiate, while those that do not eventually die off. (B) Illustration of alternative routes of obtaining neurotrophic factors, including autocrine and paracrine routes. Figure adapted from ref. 1.

Neurotrophins appear to regulate the aforementioned neuronal survival, growth, and differentiation via the careful interplay of the Trk family of receptors (comprised of TrkA, TrkB, and TrkC) and the p75 neurotrophin receptor (p75^{NTR} or p75^{NTTR}).^{1,2,8} The Trk family of receptors promote neuronal survival, growth, and differentiation, while the p75NTR generally exhibits the opposite effect, promoting apoptosis instead, an effect that is greatly amplified in the case of pro-Nerve Growth Factor (pro-NGF) binding.^{8,9} This balance is further complicated by some reports which suggest that p75NTR binding may augment the effects of the Trk receptor via, for example, downstream activation of the NF-κB transcription factor.^{2,10} Additionally, while the Trk receptors exhibit selective binding, the p75NTR shows a similar, low-level affinity for several neurotrophins.^{8,11} This low-level affinity can be greatly amplified by pro-neurotrophins, which provide the mature neurotrophin upon cleavage.^{8,9}

Before we address therapeutics for neurotrophic factor-related dysfunction, let us narrow our focus to the interaction of BDNF with the TrkB receptor. BDNF is one of two neurotrophic factors with strong binding affinities toward the TrkB receptor and one of four fully characterized neurotrophins found in mammals.¹¹ The interaction between BDNF and TrkB occurs most prominently via one of two immunoglobulin (Ig) domains; however, the receptor domain of TrkB is composed of additional cysteine clusters and leucine repeats (Figure 1.1.2).^{11, 12}

As a receptor tyrosine kinase, TrkB's downstream effects—including neuronal survival and differentiation—result from autophosphorylation outside of the activation loop.^{2, 11, 13, 14} Some of these downstream signaling pathways include (Figure 1.1.2):^{2, 11, 13, 15, 16}

- (i) Ras/PI3K/Akt (Protein Kinase B),
- (ii) Ras/MEK/MAPK, and
- (iii) Phospholipase C- γ 1 (PLC- γ 1).

Pathways (i) and (ii) are associated with phosphorylation of tyrosine 515, while pathway (iii) is associated with phosphorylation of tyrosine 816.^{14, 17}

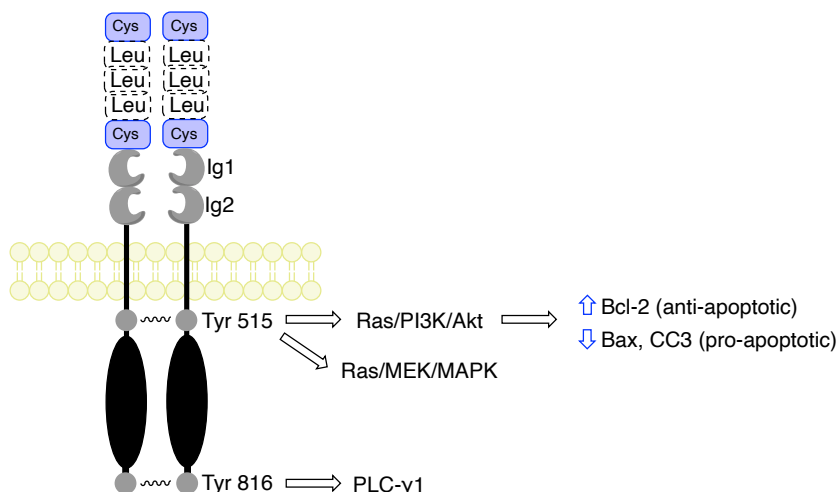


Figure 1.1.2: Simplified illustration of the TrkB receptor domain and the tyrosine residues implicated in some of the downstream signaling pathways. Adapted from ref. 12 and 17.

Notably, the Ras/PI3K/Akt pathway features a few downstream targets implicated in the regulation of apoptosis—Bcl-2 (anti-apoptotic, up-regulated), Bax (pro-apoptotic, down-regulated), and cleaved caspase 3 (CC3, pro-apoptotic, down-regulated).¹⁸ These effects are valuable for apoptosis-induced disease states, such as traumatic brain injury (TBI) and light-induced retinal degeneration (LIRD), as well as neurodegenerative disorders such as Alzheimer's Disease and Parkinson's Disease.¹⁸⁻²⁰

In the past, several studies have demonstrated that the mRNAs coding for the expression of TrkB and BDNF (as well as the related NT-4 neurotrophin) appear to be upregulated after mild to moderate traumatic brain injuries (TBIs).²¹⁻²⁴ Given these considerations, some researchers have noted the possible therapeutic potential of administering supplementary neurotrophic factors.²⁵⁻²⁸ As supported by their limited use, these neurotrophic factors represent poor therapeutic agents for several reasons, including:²⁵⁻²⁸

- (i) poor oral bioavailability, as a result of
 - (a) poor solubility and permeability, as well as
 - (b) an inability to cross through the blood-brain and blood-cerebrospinal fluid barriers;
- (ii) short *in vivo* half-lives, due to proteolytic degradation; and
- (iii) a high potential for pleiotropic effects, such as apoptosis arising from p75NTR binding.

Others have opted for a different approach, instead using small-molecule therapeutics to circumvent some of these issues. To date, several promising candidates for TrkB agonists appear in the literature.^{25, 27-29} However, this approach begs a fundamental question: can a single (or small number of) interaction site(s) between TrkB and a small molecule replicate the plethora of protein-protein interactions necessary to replicate all of the physiological effects of BDNF binding?²⁷ As Longo and Massa note, this is quite unlikely for any sort of small-molecule/neurotrophin receptor

interaction. However, these researchers propose that complete replication is not necessary, and the presence of promising TrkB agonists supports this assertion.²⁷ Consequently, they propose the term “neurotrophin receptor-modulating ligands,” rather than “neurotrophin mimetics.” Recognizing this important distinction, these scientists acknowledge a few important considerations, including:

- (i) the inability to induce endogenous production, thereby requiring continuous administration;
- (ii) a potential for unintended effects, as was also expected with the administration of native neurotrophins; and
- (iii) a decreased ability to restrict these off-target effects to a specific region of the body, since some small molecules may more easily cross the blood-brain barrier.

1.2 Overview of Relevant Small-Molecule, Serotonin-Derived Therapeutics

The Iuvone and McDonald laboratories are particularly interested in two serotonin-derived small-molecule neurotrophin receptor-modulating ligands, namely, *N*-acetylserotonin (NAS, **1**) and *N*-[2-(5-hydroxy-1*H*-indol-3-yl)ethyl]-2-oxopiperidine-3-carboxamide (HIOC, **2**), as shown in Figure 1.2.1. NAS, a biosynthetic precursor to melatonin, activates TrkB in a manner that does not depend on endogenous BDNF; this activation provided neuroprotective and antidepressant effects in animal studies.¹⁶ Additionally, recent studies have established that NAS can act against TBI-related blood-brain barrier disruption, cell death, and apoptosis activation.¹⁸ Consistent with these observations, these researchers found increased levels of anti-apoptotic Bcl2, and decreased levels of pro-apoptotic Bax and CC3.¹⁸ Despite its potential therapeutic benefits, NAS has a relatively short half-life, which has raised concerns about its viability for exogenous administration in long-term neurodegenerative disease.^{16, 19} Noting this, Jang and coworkers proposed developing

a more stable derivative, which was later identified in the form of HIOC.^{16, 19} In contrast to NAS, HIOC exhibited effective protection against light-induced retinal degeneration (LIRD) (*Ghai & Iuvone, unpublished results*) and exhibited a greater half-life, at 45 min - 1 h in retinas.^{19**, 30} This compound could cross both the blood-brain and the blood-retinal barriers.³⁰

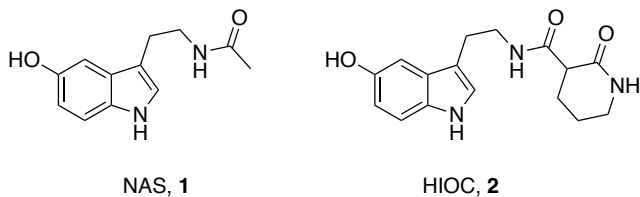
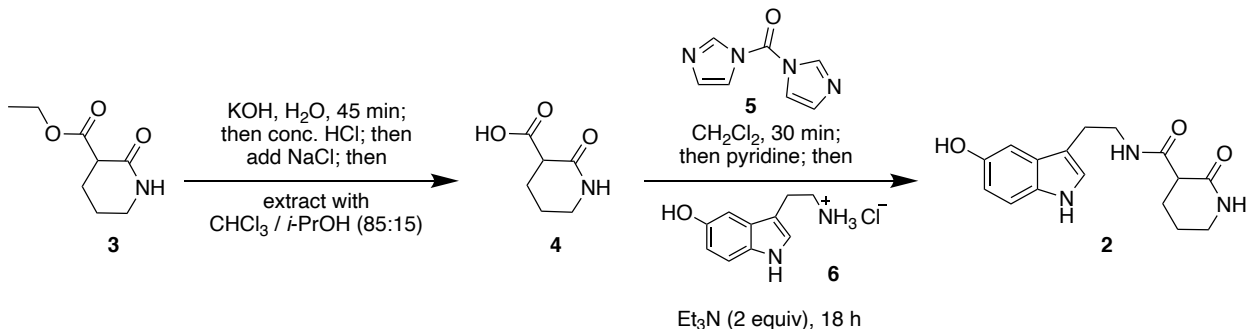


Figure 1.2.1: Structures of *N*-acetylserotonin (NAS) and *N*-[2-(5-hydroxy-1*H*-indol-3-yl)ethyl]-2-oxopiperidine-3-carboxamide (HIOC), two serotonin derivatives with activity as TrkB agonists.

1.3 Overview of the Published HIOC Synthesis

In 2015, the McDonald laboratory completed the first published synthesis of HIOC (Scheme 1.3.1).³¹ While its synthesis appeared trivial at first, the development of this route was riddled with challenges. For example, the literature does not report a method for the isolation of compound **4**. Consequently, our laboratory previously found that a salting-out assisted extraction with a chloroform/isopropanol mixture was suitable.³¹ Additionally, the coupling between **4** and serotonin-HCl (**6**) proved challenging, requiring the use of *N,N'*-Carbonyldiimidazole (CDI, **5**), a peptide-coupling reagent.^{31, 32}



Scheme 1.3.1: Synthetic route to HIOC from a commercially available ester precursor, ethyl 2-oxopiperidine-3-carboxylate (**3**).

1.4 Mechanistic Concerns in the CDI Coupling

Adding to the complexity of this coupling, there is a great deal of uncertainty regarding the mechanism by which CDI couples a terminal amine salt with a carboxylic acid. These complexities are summarized in Figure 1.4.1.^{32, 33-35} Additionally, there is some uncertainty (not illustrated) regarding whether intermediate **8** or intermediate **11** is the species that undergoes *N*-acylation with amine **12**. While the exact mechanism of this reaction is not the subject of our inquiry, this represents a promising area for future investigation.

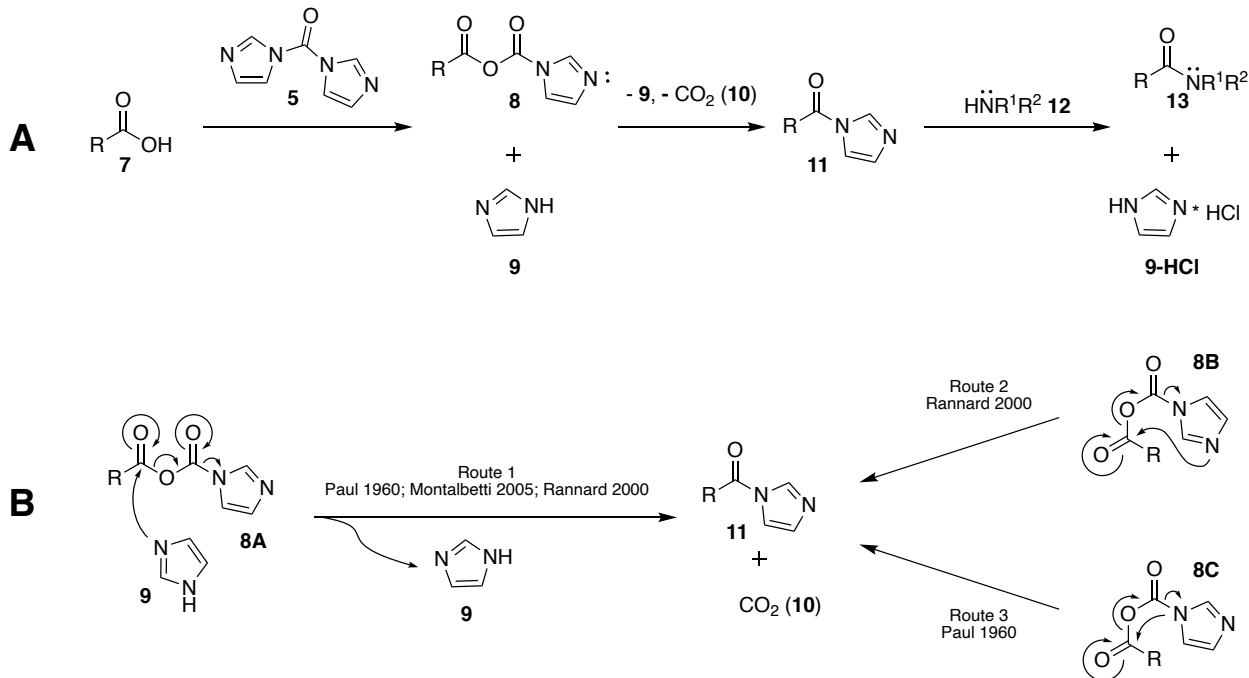


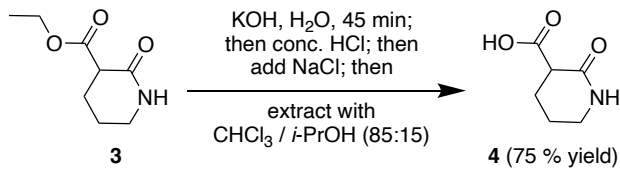
Figure 1.4.1: (A) Summary of the literature-proposed mechanisms for the CDI (**5**) coupling of carboxylic acids **7** with amines **12** to produce amides **13**. **(B)** The exact mechanism of the reaction remains undetermined, with the second phase (**8**→**11**) remaining contested in the chemical literature.

1.5 Initial Attempts at HIOC Synthesis

Recognizing the technically challenging nature of the synthesis of HIOC, my first task upon joining the McDonald laboratory was to replicate the published route (Scheme 1.3.1 above), working closely with Dr. Christopher Walker, a postdoctoral scholar in our laboratory. After a few attempts, I produced HIOC in 40 % yield and good purity (only trace impurities via ¹H NMR). During this process, however, we noted a few shortcomings in the published procedure. Herein we document our revisions, including some which may prove beneficial to less-experienced experimentalists.³¹

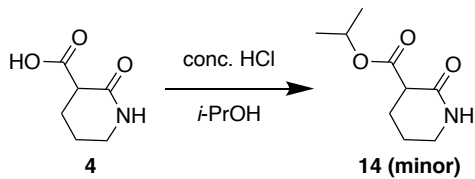
1.6 Revisions to the Synthesis of 2-Oxopiperidine-3-carboxylic Acid

Regarding the first step of the transformation (Scheme 1.6.1), a few revisions are noteworthy. First, argon (or other inert gas) is not necessary for the success of this reaction, and the transformation may be completed in a loosely capped flask. Additionally, we have observed generally better yields when using anhydrous magnesium sulfate ($MgSO_4$) as the drying agent, rather than the reported anhydrous sodium sulfate (Na_2SO_4). In cases where sodium sulfate was employed, we have noted a few instances of the disappearance of the carboxyl O-H in 1H -NMR and IR spectra. Further studies are warranted to determine if these observations are correlated.



Scheme 1.6.1: Conversion of ethyl 2-oxopiperidine-3-carboxylate (**3**) into 2-oxopiperidine-3-carboxylic acid (**4**) as reported by Setterholm *et al.*³¹

A final point which sparked a few later inquiries concerns the acidification step. While the published protocol provides a quantitative estimate of the amount of concentrated hydrochloric acid (HCl) added, we have noted that the pH should be carefully monitored throughout the addition, so as to not drop below $\sim 3\text{-}4$. In instances where this occurred, we often observed Fischer esterification in the subsequent extraction, and lower yields were generally observed. The possibility of a Fischer esterification (Scheme 1.6.2) is a pervasive threat in this synthetic approach, and the formation of the isopropyl ester (**14**) was noted by Setterholm and coworkers.³¹ Unfortunately, what proved to be the best conditions for extraction (namely, 85:15 $CHCl_3/i\text{-PrOH}$ after acidification), also proved to be favorable for this side reaction.



Scheme 1.6.2: Condensed scheme leading to the isopropyl ester byproduct **14** in the work-up protocol for **4**.

As part of our continued optimization of this protocol, we attempted to identify alternative, less-sensitive conditions. In one of our early tests, we opted to avoid an extraction altogether, instead quenching the excess potassium hydroxide (KOH), returning to a basic pH, and boiling off the water to provide the carboxylate salt. Acidification with concentrated trifluoroacetic acid (TFAA, chosen to avoid introducing significant amounts of water into the system) and further solvation in acetonitrile (MeCN) provided a white paste after solvent evaporation. While this experiment seemed promising, ultimately $^1\text{H-NMR}$ analysis suggested we had not isolated our desired product.

Satisfied with the solubility of our product in acetonitrile, we sought to employ the solvent in a formal extraction step. Unfortunately, acetonitrile is miscible with water. This led to an informative literature search, wherein we identified a report that employed magnesium sulfate as a salting-out reagent in liquid-liquid extraction with acetonitrile.³⁶ Noting the benefits of sodium chloride in our own extraction, this find was encouraging. However, this method suffered one major flaw: the combination of acetonitrile and a strong aqueous base (such as the KOH used here) has been contraindicated on a process scale, due to the potential for a runaway reaction.³⁷

These pitfalls forced us to reevaluate the synthetic protocol and instead opt for only one equivalent of KOH, as opposed to our typical use of ~4.2 equivalents. As expected, this dramatic decrease led to a significantly longer reaction time. Gratifyingly, however, we did observe

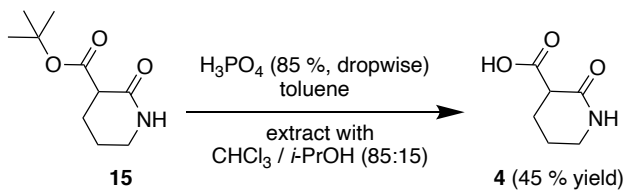
significant conversion after ~72 hours. Extraction with ethyl acetate (to remove residual starting material), followed by our revised extraction with MeCN/MgSO₄ provided a mixture of products. Recognizing that a carboxylate might more easily be isolated, we repeated this protocol with an additional basification step (using aqueous sodium bicarbonate) after acidification. This was to ensure that: (a) any unreacted KOH was quenched, (b) the carboxylate was present, and (c) no strongly nucleophilic bases were present in the final solution. Though the resultant product was still largely impure, careful chromatography might provide the pure product.

To conclude our discussion of product **4**, we acknowledge a useful “experiment” induced by the COVID-19 pandemic. As part of the studies described in Chapter 2 of this thesis, a sample of **4** was prepared for comparative analysis. Unfortunately, the sudden closure of the McDonald laboratory at the onset of the COVID-19 pandemic led to this sample being unintentionally stored under ambient condition for several months (in total, more than 1 year, 4 months). Recent NMR analysis revealed no noticeable difference between this sample and a freshly prepared one, indicating the sample did not undergo decarboxylation upon standing for 16 months. This represents a marked increase in our understanding of the long-term stability of this product. Additionally, the literature suggests that similar species (namely, malonic acid and its carboxylate derivatives) exhibit a pH-dependent decarboxylation rate, with the protonated form exhibiting a greater rate constant than the mono- and di-carboxylate variants.³⁸

1.7 A Variant Route to 2-Oxopiperidine-3-carboxylic Acid

In addition to synthesizing **4** from an ethyl ester precursor, we have also attempted to prepare **4** from the *tert*-butyl ester precursor **15** (Scheme 1.7.1). Although **15** is not commercially available, this reagent was isolated by Dr. Christopher Walker as a byproduct from an attempted

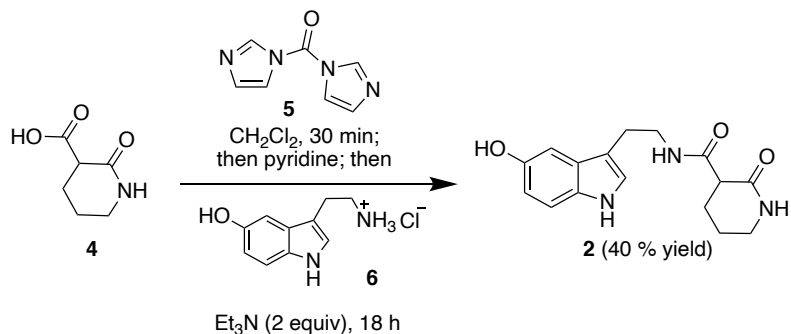
extraction of **4** with *tert*-butanol under acidic conditions. While the true value of this will become especially apparent in Chapter 2, this accomplishment serves to highlight that the quest for an alternative route to **4** need not directly involve the ethyl ester and may not require basic hydrolysis conditions.



Scheme 1.7.1: Synthesis of **4** from *tert*-butyl 2-oxopiperidine-3-carboxylate (**15**) using an acidic hydrolysis. See Ch. 4: Experimental, Note 1.

1.8 Revisions to the Final Step of the HIOC Synthesis

Fortunately, few modifications to the final step of the HIOC synthetic protocol are warranted (Scheme 1.8.1). Most notably, we found that a set of on-frit washings with acetone were beneficial after washing with warm diethyl ether (Et_2O). Additionally, azeotroping with toluene, while likely useful, was not absolutely necessary.



Scheme 1.8.1: Step two of the synthetic protocol yielding HIOC.

1.9 Conclusions

The synthesis of HIOC, though challenging, was eventually accessible as I became further acquainted with synthetic chemistry. While some issues are noted herein, the optimization process remains fluid, and may become the challenge of process chemists in the future.

CHAPTER 2: Developments Toward an Enantioselective Synthesis of HIOC

2.1 The Importance of Stereochemistry in Therapeutics

Stereochemistry is an exceedingly important concept in drug development. Under achiral conditions, differing enantiomers behave effectively the same; however, when placed in a chiral environment, such as those in the body, each enantiomer can behave differently.³⁹ While in some cases differing enantiomers vary only in efficacy, in other cases—such as the infamous thalidomide (Figure 2.1.1)—one enantiomer can have devastating effects.^{39, 40, 41} Moreover, in this unfortunate instance, simply isolating one enantiomer was insufficient, drawing attention to the need to consider *in vivo* racemization, in addition to the varying effects of single stereoisomers.⁴⁰

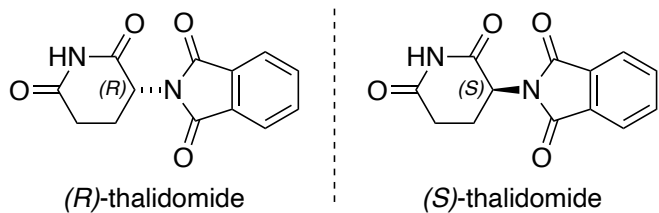


Figure 2.1.1: Structures of (*R*)- and (*S*)-thalidomide. While the (*R*) enantiomer is therapeutic, the (*S*) enantiomer exhibits teratogenic properties.⁴⁰

Broadly, Nguyen and coworkers describe three main categories of chiral drugs:⁴²

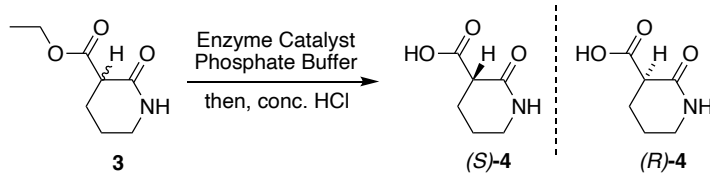
- (i) Racemates with only one active (or effective) stereoisomer, which is termed the *eutomer*;
 - (ii) Racemates with both stereoisomers showing therapeutic activity; and
 - (iii) Enantiomers that can undergo chiral inversion such that: (a) a mixture of enantiomers converts to a single enantiomer *in vivo*, or (b) a single enantiomer racemizes *in vivo*.

Altogether, these considerations illustrate the multitude of complexities that must be considered in developing therapeutic agents with stereogenic centers.

2.2 Chemoenzymatic Assays for Enantioselective Hydrolysis

Motivated by the successful enzymatic synthesis of a related compound, we sought to develop enzymatic conditions to prepare 2-oxopiperidine-3-carboxylic acid in an enantioenriched form.⁴³ In 2007, Hu and coworkers attempted to develop an enzymatic route to enantioenriched 2-butyl-3-hydroxypropionic acid using conditions suitable for a process scale.⁴⁴ These researchers found that, while both porcine (pig) liver esterase (PLE) and α -chymotrypsin were capable of facilitating the reaction, PLE was preferable for a process-scale production. Correspondingly, we applied similar conditions to ethyl 2-oxopiperidine-3-carboxylate (**3**) and found that PLE effectively catalyzed the reaction. However, via analysis of the ¹H-NMR spectrum (cf. δ (DMSO-d₆) = 1.12 vs. 1.00), we found only trace amounts of the ethyl ester precursor, precluding the likelihood of an enantioenriched sample. As such, we began investigating other esterases and lipases. The results of these investigations are summarized in Table 2.2.1.

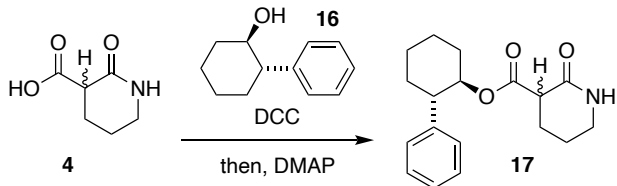
Table 2.2.1: Chemoenzymatic Condition Assays. Investigation of the enzymatic enantioselective hydrolysis of ethyl 2-oxopiperidine-3-carboxylate (**3**).



Enzyme	Conditions	Results & Notes
Porcine Liver Esterase	pH 7; r.t. (normal workup) ^{31, 44}	Nearly quantitative conversion
Porcine Liver Esterase	pH 7; r.t. (lit. workup) ⁴⁴	Nearly quantitative conversion; lit. workup was not successful
Porcine Pancreas Esterase	pH 7; r.t. ⁴⁴	No apparent conversion
Porcine Pancreas Esterase	pH 7.6; T \approx 37 °C ⁴⁵	No apparent conversion
Amano Lipase PS SD from <i>Burkholderia cepacia</i>	pH 7.5; T \approx 30 °C ⁴⁵	No apparent conversion
Amano Lipase PS SD from <i>Burkholderia cepacia</i>	pH 7.0; T \approx 50 °C ⁴⁶	No apparent conversion
Amano Lipase from <i>Pseudomonas fluorescens</i>	pH 8.0; T \approx 55 °C ^{47, 48}	Limited conversion (ca. 11 % after >48 hours)
Amano Lipase from <i>Pseudomonas fluorescens</i>	pH 8.0; T \approx 55 °C ^{47, 48} (newer bottle)	Limited Conversion (<1 % after 26 hours)
Amano Lipase from <i>Pseudomonas fluorescens</i>	pH 8.0; T \approx 55 °C ^{47, 48} (newer bottle, reduced conc.) ⁴⁹	Limited Conversion (< 1% after 29 hours)
Amano Lipase from <i>Pseudomonas fluorescens</i>	pH 8.0; r.t. ^{44, 47, 48}	Limited Conversion
Amano Lipase from <i>Pseudomonas fluorescens</i>	pH 7; T \approx 55 °C ^{44, 47, 48}	Limited Conversion (ca. 5 % after 26 hours)
Amano Lipase from <i>Pseudomonas fluorescens</i>	pH 7.5; T \approx 25 °C ⁴⁹ (newer bottle, reduced conc.) ⁴⁹	Limited Conversion (ca. 7 % after 28 hours)
Amano A 12 Lipase from <i>Aspergillus niger</i>	pH 7.4; T \approx 40 °C ⁵⁰	Limited Conversion (<1 % after 24 hours)
Amano A 12 Lipase from <i>Aspergillus niger</i>	pH 8; T \approx 40 °C ⁵⁰	Limited Conversion (<1 % after 24 hours)

2.3 Time Trials and Attempts at Configurational Assignment

On the basis of these results, we decided it would be best to further investigate PLE via time trials. Consequently, we analyzed a series of aliquots taken at 1 hour, 2 hours, and 3 hours. Gratifyingly, after 1 hour, we observed ca. 22 % conversion; however, the time points after 2 hours showed greater than 50 % conversion. In our attempts to analyze the enantiomeric composition of the 1-hour sample, we conducted a control analysis via Steglich esterification of the racemic acid with (*1R,2S*)-*trans*-2-phenyl-1-cyclohexanol (**16**), an established chiral auxiliary reagent (Scheme: 2.3.1).⁵¹⁻⁵³



Scheme 2.3.1: Steglich esterification procedure with (*1R,2S*)-*trans*-2-phenyl-1-cyclohexanol (**16**) to provide derivatized product **17**.

Though we intended to follow this experiment with a similar protocol using (*1S,2R*)-*trans*-2-phenyl-1-cyclohexanol, much to my chagrin, the $^1\text{H-NMR}$ spectrum of **17** appeared to be too dilute and/or impure for useful analysis. Rather than analyze this product further, we began working toward the C^α -methyl derivative of HIOC (**18**, Figure 2.3.2)—for which a *partial* literature preparation exists.^{54, 55} Later studies on the configurational stability of 2-oxopiperidine-3-carboxylic acid (**4**) revealed that this choice was a fortunate one. Dr. Christopher Walker, a postdoctoral fellow in the McDonald laboratory, recently found that HIOC—which is derived from 2-oxopiperidine-3-carboxylic acid—racemizes in phosphate buffer quite rapidly (Walker *et al.*, *in preparation*). Consequently, an enantioselective preparation of this nature would likely be

therapeutically futile, as the buffer was intended to simulate physiological conditions. Additionally, as we used a similar phosphate buffer in our enzymatic enantioselective hydrolysis, Dr. Walker's findings may further complicate this methodology.

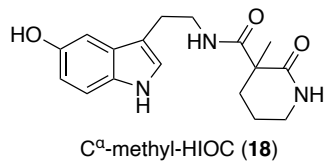


Figure 2.3.2: Structure of the C^α-methyl derivative of HIOC (18).

2.4 Progress toward preparing the C^α-methyl derivative of HIOC

In 2013, Banerjee and coworkers reported a unified route to orthogonally protected $\alpha^{2,2}$ - and $\beta^{2,2}$ -methyllysine derivatives.⁵⁴ This route served as the basis for a later report detailing a stereoselective route to δ -lactam derivatives, and specifically those similar to nipecotic acid (**19**, Figure 2.4.1).⁵⁵ Gratifyingly, this later article provided a method to prepare the C^α-methyl derivative of *tert*-butyl 2-oxopiperidine-3-carboxylate (**20**). In chapter one, we demonstrated that acid hydrolysis of *tert*-butyl 2-oxopiperidine-3-carboxylate (**15**) could potentially provide the carboxylic acid. In tandem with Dr. Christopher Walker's synthetic route to C^α-methyl HIOC, this framework presents a plausible route to enantioenriched C^α-methyl HIOC, which, in principle, should be less subject to racemization *in vivo*.

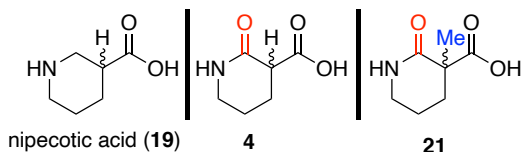
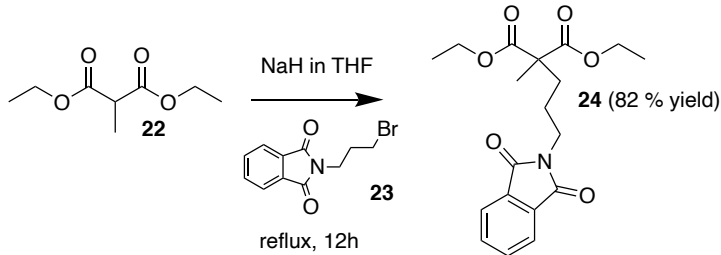


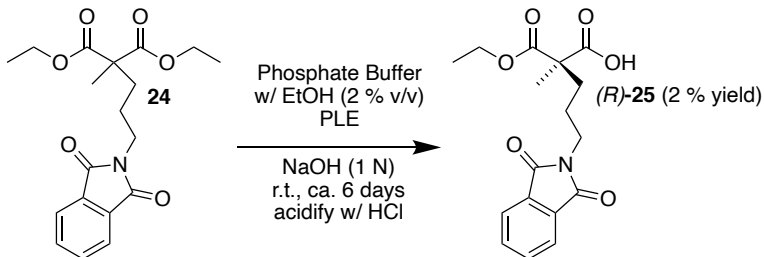
Figure 2.4.1: Structures of nipecotic acid (**19**), 2-oxopiperidine-3-carboxylic acid (**4**), and the C^α-methyl derivative of 2-oxopiperidine-3-carboxylic acid (**21**).

The preparation of *tert*-butyl (*S*)-3-methyl-2-oxopiperidine-3-carboxylate begins with a conceptually simple substitution reaction between diethyl 2-methylmalonate (**22**) and *N*-(3-bromopropyl)phthalimide (**23**, Scheme 2.4.2).



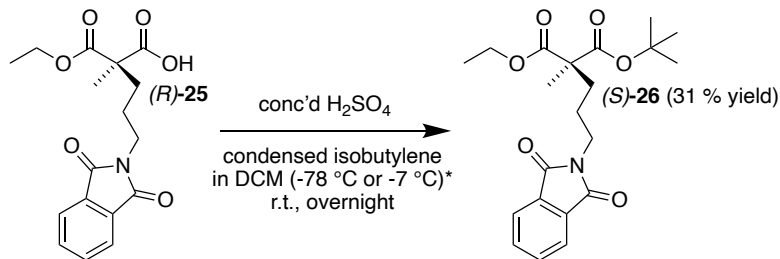
Scheme 2.4.2: Synthetic route to provide diethyl 2-(3-(1,3-dioxoisoindolin-2-yl)propyl)-2-methylmalonate (**24**) from the substitution reaction between diethyl 2-methylmalonate (**22**) and *N*-(3-bromopropyl)phthalimide (**23**).

The substitution step is followed by a PLE-catalyzed enantioselective desymmetrization to provide the half-ester product (**25**, Scheme 2.4.3). Though the propyl chain was desirable for creating a δ -lactam, the authors also reported that this chain length gave the highest enantioselectivity out of a series of alkyl chains.⁵⁴ This result, per the authors, is consistent with the Jones model for PLE enantioselectivity (see section 2.5).^{54, 56} One important consideration in this step is the inclusion of 2 % (v/v) ethanol as a co-solvent with the phosphate buffer. In an earlier paper by Smith and coworkers, addition of 2 % (v/v) ethanol as a co-solvent afforded a notable increase in enantioselectivity in the desymmetrization of a related substrate.⁵⁷



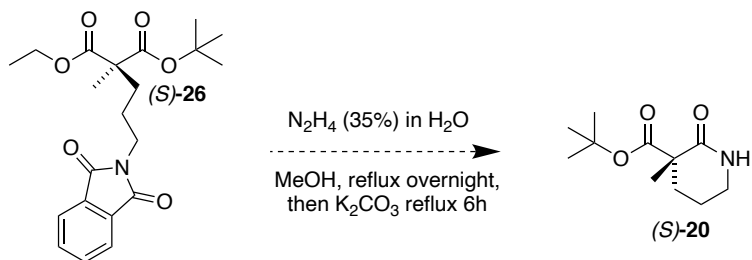
Scheme 2.4.3: Synthetic route to provide (*R*)-5-(1,3-dioxoisindolin-2-yl)-2-(ethoxycarbonyl)-2-methylpentanoic acid ((*R*)-**25**) from the PLE-catalyzed desymmetrization of 2-(3-(1,3-dioxoisindolin-2-yl)propyl)-2-methylmalonate (**24**).

The next step in this process is considerably more technically challenging, requiring the low-temperature condensation of gaseous isobutylene, followed by immediate transfer to a sealable reaction tube. Though specific instructions on how this should be done were not provided in either of the specifying articles, an *Org. Synth.* preparation suggested condensation into a test-tube resting in a dry ice-acetone bath, followed by immediately pouring into the reaction tube.⁵⁸ In tandem with concentrated sulfuric acid, this step serves to replace the carboxylic acid moiety with a *tert*-butyl ester (Scheme 2.4.4). The literature procedure recommends cooling the reaction vessel to -7 °C, the boiling point of isobutylene.^{54, 55, 59} While we originally suspected this may have been a mistake and this value should have been -78 °C (a typical temperature given for a dry ice-acetone bath), we are now inclined to explore the published temperature (which can be obtained via an ice bath with salt) in greater depth.



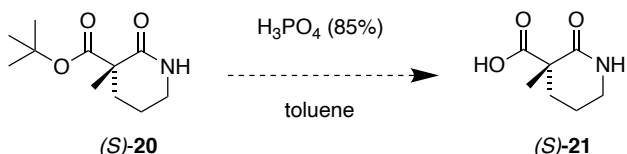
Scheme 2.4.4: Synthetic route to provide 1-(*tert*-butyl) 3-ethyl (*S*)-2-(3-(1,3-dioxoisoindolin-2-yl)propyl)-2-methylmalonate ((*S*)-26) from (R)-5-(1,3-dioxoisoindolin-2-yl)-2-(ethoxycarbonyl)-2-methylpentanoic acid ((R)-25).

To date, we have only been able to replicate this process in any quantifiable yield up to the formation of the *tert*-butyl ester. However, for completeness, we provide the remaining steps, which we expect to lead to an enantioenriched form of the C^a-methyl derivative of HIOC. After creating the *tert*-butyl ester, the next reported step entails employing a hydrazine solution and potassium carbonate to cleave the phthalimide and induce cyclization via a preferential nucleophilic acyl substitution of the more-accessible ethyl ester (Scheme 2.4.5).



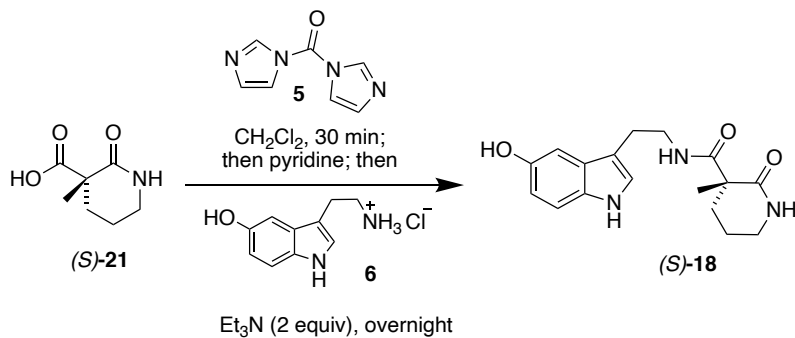
Scheme 2.4.5: Synthetic route to *tert*-butyl (*S*)-3-methyl-2-oxopiperidine-3-carboxylate ((*S*)-20) from 1-(*tert*-butyl) 3-ethyl (*S*)-2-(3-(1,3-dioxoisoindolin-2-yl)propyl)-2-methylmalonate ((*S*)-26) via phthalimide cleavage and regioselective cyclization.

At this point, the remaining steps have been developed with the racemic compound by Dr. Christopher Walker, but these have not yet been tested on a single enantiomer form. Experiments to come will reveal the efficacy of these steps. As discussed in chapter one, *tert*-butyl 2-oxopiperidine-3-carboxylate (**15**) might be cleaved via acid hydrolysis; we expect the reaction to proceed similarly with the C^a-methyl derivative (Scheme 2.4.6).



Scheme 2.4.6: Synthetic route to (S)-3-methyl-2-oxopiperidine-3-carboxylic acid ((S)-**21**) from *tert*-butyl (S)-3-methyl-2-oxopiperidine-3-carboxylate ((S)-**20**) via acid hydrolysis.

Following the creation of the carboxylic acid, the racemic acid can be converted to the C^a-methyl derivative of HIOC via a CDI coupling with serotonin, in a similar manner to the CDI coupling in chapter one (Scheme 2.4.7).³¹



Scheme 2.4.7: Synthetic route to the (S) enantiomer of the C^a-methyl derivative of HIOC ((S)-**18**) via a CDI coupling of serotonin-HCl (**6**) with (S)-3-methyl-2-oxopiperidine-3-carboxylic acid ((S)-**21**). In previous experiments, Dr. Christopher Walker noted that 3-methyl-2-oxopiperidine-3-carboxylic acid (\pm -**21**) required a longer reaction time than 2-oxopiperidine-3-carboxylic acid (**4**).

As a concluding note for this section, we acknowledge that a route is also provided to prepare the (*R*) enantiomer.^{54, 55} Should we complete the synthesis of the (*S*) enantiomer in the coming weeks, this may become an additional area of focus.

2.5 Relevant Background for the Analysis of PLE Enantioselectivity

As a serine hydrolase, PLE serves as a stereoselective catalyst with a high tolerance for a variety of esters.⁶⁰ This tolerance is a consequence of a particularly complex binding pocket, which is currently best understood with the Jones model (Figure 2.5.1).^{56, 61} This model proposes a four-sector binding pocket consisting of two polar sectors (P_F and P_B , denoting **Front** and **Back**, respectively) and two hydrophobic sectors (H_L and H_S , denoting **Large** and **Small**, respectively) arranged around a so-called “serine sphere,” where the catalytic activity occurs.^{56, 61}

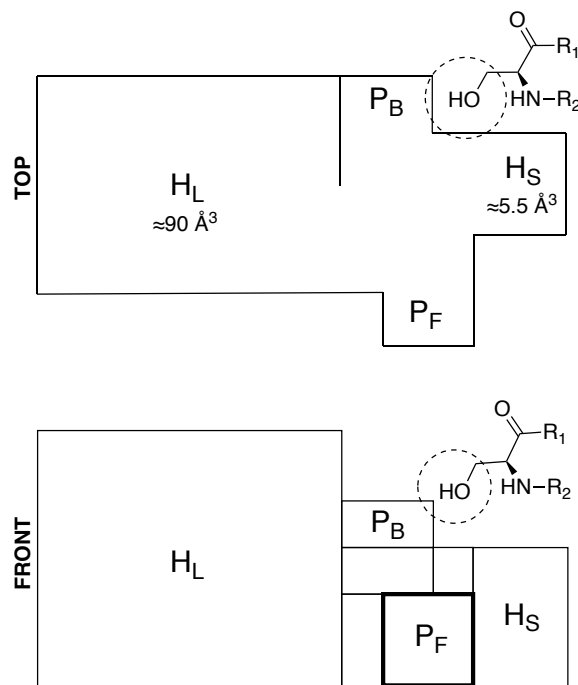


Figure 2.5.1: Schematic illustration of the revised Jones model for the selectivity of PLE. The H_L (hydrophobic, large) sector has undergone significant revision since the original specification of ≈ 33 cubic \AA given in ref. 61. Figure adapted from ref. 56.

Though the model has been further refined over time—specifically, the reported size of the H_L sector has increased significantly—it is particularly helpful in explaining the apparent reversal of stereoselectivity that can result when the confines of the H_S sector of the binding pocket are exceeded.^{56, 61} This reversal is often explained by the so-called “Circe Effect,” which asserts, **by extension**, that the restricted motion and prearrangement of substrates upon binding to an enzyme serves to reduce the entropic cost of a reaction.⁶¹⁻⁶³ While this effect has seen some opposition in the enzymology community in recent years, it nonetheless provides a useful starting point.⁶³ In essence, a substrate will attempt to conform into the H_S sector until it no longer fits, after which the H_L sector will begin to be occupied and a subsequent change in stereoselectivity results.⁶¹ We have illustrated the observed selectivity for the formation of (*R*)-**25** using the Jones Model in Figure 2.5.2.

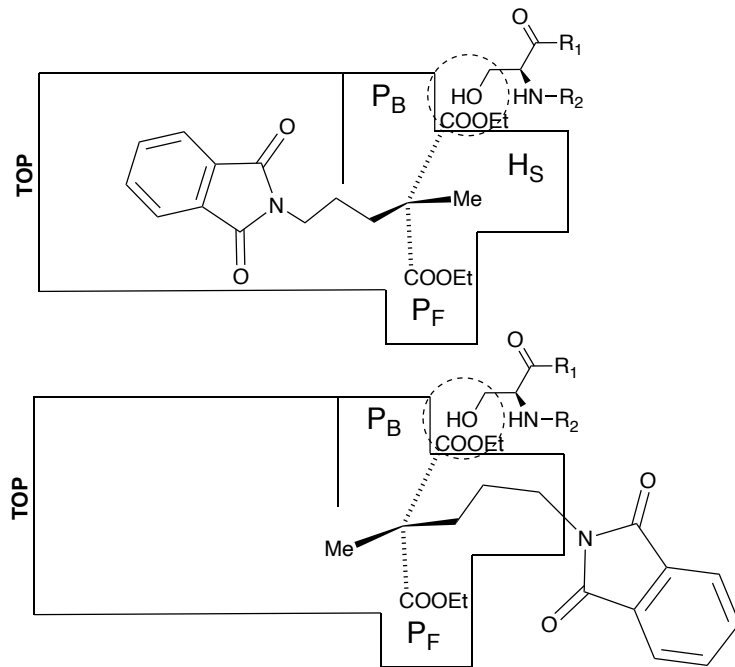
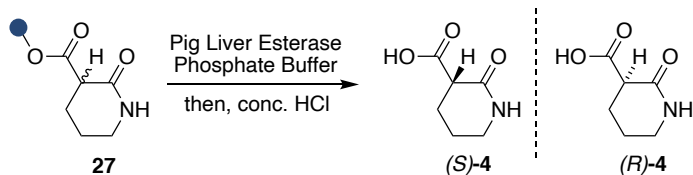


Figure 2.5.2: Application of the Jones Model to **24**, which illustrates the cause of the preferential production of (*R*)-**25**.

2.6 Initial Challenges in the Analysis of PLE Enantioselectivity

Commercial PLE is a mixture of several isozymes, with at least 6 isozymes currently known.^{57, 60} In spite of this, an X-ray crystallographic structure is only available for one isozyme (PLE5), which is reported to exhibit differing active site interactions relative to other isozymes, per an earlier homology model based on human carboxyl esterase (hCE).^{60, 64} Though in bulk, PLE is usually treated as one entity, individual isozymes provide variable enantioselectivities.^{60, 65, 66} Together, these factors complicate detailed theoretical analyses of the selectivity of PLE for various esters **27** (Scheme 2.6.1), an issue not faced by experimental structure-selectivity relationship (SSR) studies.^{67, 68}

Previous theoretical work has established that molecular docking studies are capable of predicting the enantioselectivity of various esterases for several substrates, though some esterases are seemingly more amenable to this analysis.⁶⁹ To date, however, no studies report molecular docking studies of this nature for PLE. After we determined that I would not return to the laboratory for the Fall 2020 semester, we wondered if we could fill this gap in the literature with computational modeling. Dr. Christopher Walker, a postdoctoral fellow in the McDonald laboratory, has significant experience in using AutoDock Vina, an open-source molecular docking program, which provided a route toward starting this analysis.⁷⁰



Scheme 2.6.1: Illustration of the enantioselective hydrolysis of 2-oxopiperidine-3-carboxylate esters **27** (where the dark blue circle represents one of a variety of linear and branched alkyl chains) to provide *(R)*- and *(S)*-2-oxopiperidine-3-carboxylic acid (**4**).

2.7 Computational Molecular Docking Studies

As part of building familiarity with AutoDock Vina and PyMOL, while also verifying the likelihood of this method matching experimental observations, we sought to find a pair of similar substrates (**28** & **29**, Figure 2.7.1) with known kinetic data (namely Michaelis constants, K_m).⁷⁰⁻⁷² We hypothesized that this information could be used to qualitatively verify the viability of the molecular docking-determined affinities. Gratifyingly, our results, though fairly close, were consistent with the Michaelis constants (i.e., the larger Michaelis constant corresponded to the structure with the weaker binding affinity).

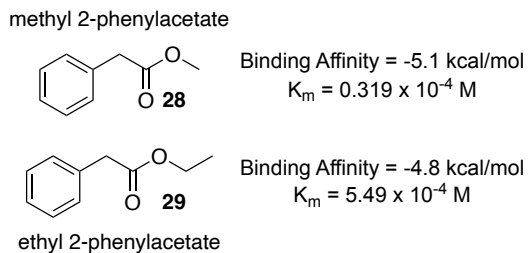


Figure 2.7.1: Methyl 2-phenylacetate (**28**) and ethyl 2-phenylacetate (**29**)—two substrates used as our model system. The computed binding affinities and the literature-reported Michaelis constants are also shown.⁷²

Though both **28** and **29** provide the same product, phenylacetic acid (**30**, Figure 2.7.2), we were curious to see how well this product could bind to the active site. Interestingly, this product exhibited the strongest binding affinity, compared to **28** and **29**. However, the significance of this result, if any, is not immediately clear.

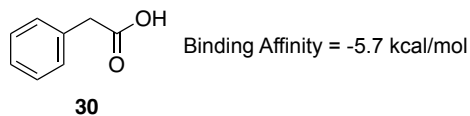


Figure 2.7.2: Structure of phenylacetic acid, the hydrolysis product of both **28** and **29**.

2.8 Further Challenges in the Analysis of PLE Enantioselectivity

While the literature proposes the residues comprising the active site for several isoenzymes of Porcine Liver Esterase, our initial studies with PLE isoenzyme variant 5 (PDB ID: 5FV4) revealed that our model substrates did not bind the ligands near the reported site, preferring instead an external cavity (see Figure 2.8.1).^{60, 64} After inspection of this binding site, we opted to further decrease the size of the Gridbox, fearing that the large size of our initial Gridbox may have led to a false positive (see Ch. 4: Experimental, Note 2). Upon using a smaller Gridbox, which excluded this external region, we received comparable binding affinities, likely due to the heightened ability to optimize the conformation near the reported active site within the exhaustiveness parameters.

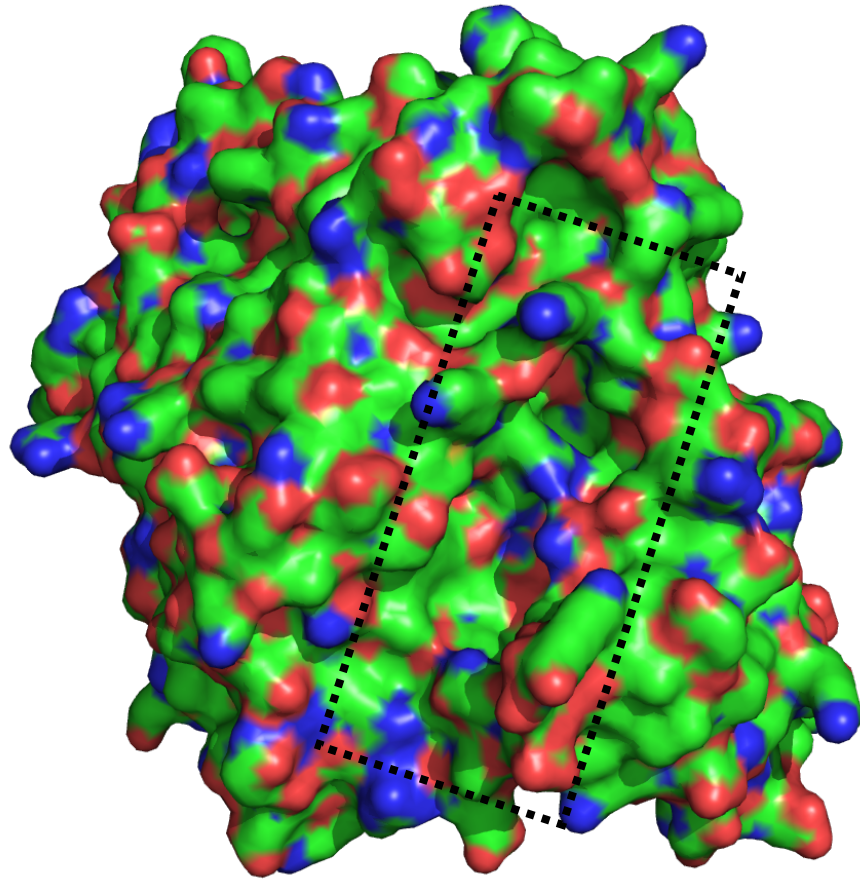


Figure 2.8.1: Structure of PLE, with the particularly troublesome external cavity highlighted. To induce binding within the binding pocket, the Gridbox in AutoDock Vina was set to exclude this region. Image via PyMOL.⁷¹

Additionally, as noted earlier, molecular docking does not present a facile way to model transition states due to the rigid nature imposed on the receptor. For completeness, we acknowledge that two leading routes exist for AutoDock Vina: the two-point attractor method, and the flexible side-chain method.⁷³ More details on these techniques, which we did not employ, can be found in ref. 73.

2.9 Concluding Thoughts

Ultimately, though theoretical analysis could be promising for future studies, the framework needed to perform this work rigorously is simply not yet established. While workarounds may allow for the simulation of some flexibility, molecular docking favors a static enzyme. Additionally, some researchers propose the active site may not play the main role in stereoselectivity, suggesting that the entrance channel (Figure 2.9.1) may be partially responsible for these effects.^{60, 74} Recognizing these challenges, and my ability to return to lab in January 2021, we determined that completing the enantioselective synthesis of the C^a-methyl derivative is a more valuable pursuit, which complements the expertise of our laboratory.

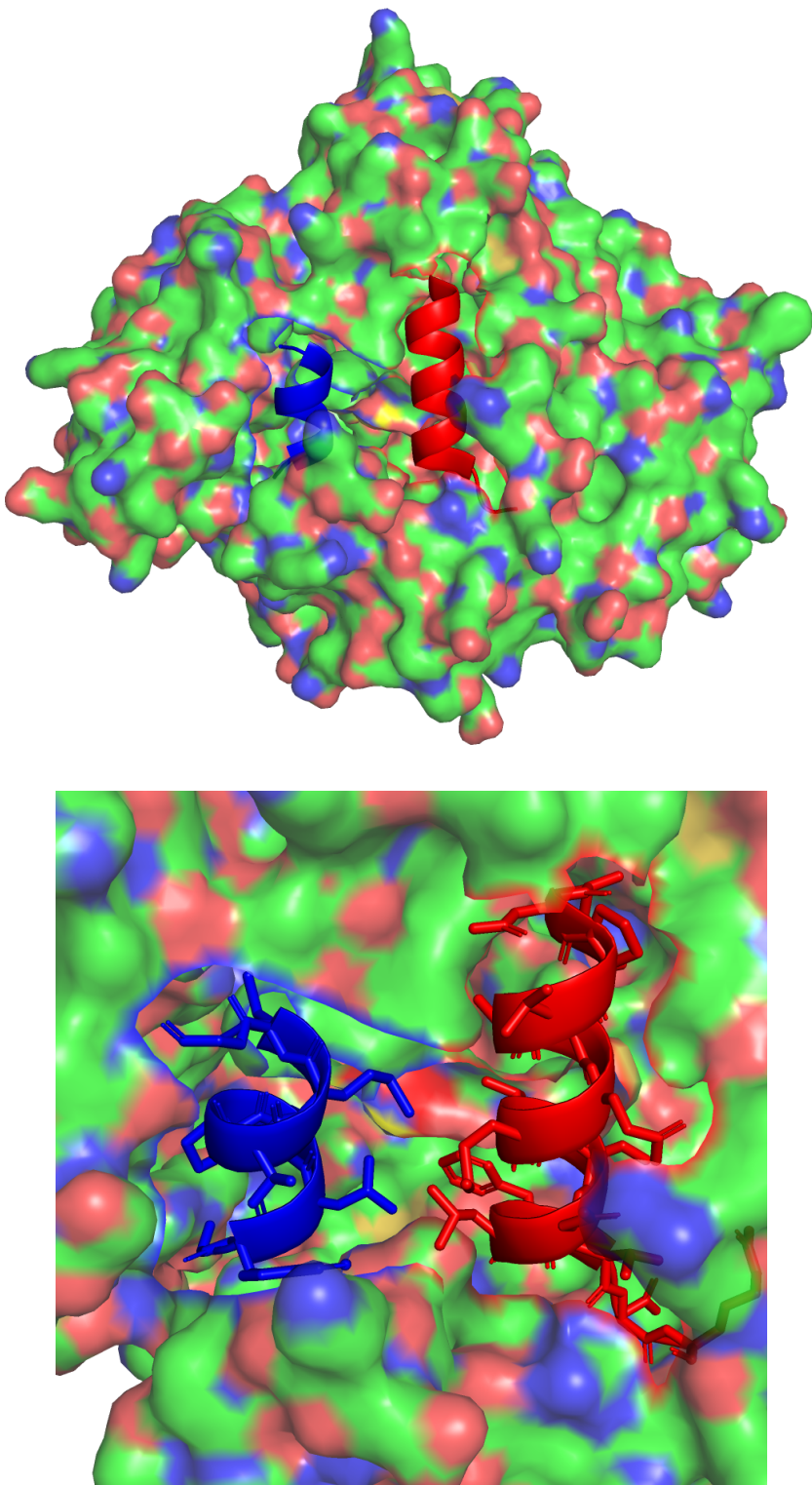


Figure 2.9.1: Illustration of the Entrance Channel, flanked by the two entrance helices, highlighted in blue and red. Image via PyMOL.⁷¹

CHAPTER 3: Fluorinated Alcohols: Powerful Promoters for Ring-Opening Reactions of Epoxides with Carbon Nucleophiles

3.1 Overview

The coupling of terminal alkynes and epoxides using mild catalytic methods remains a long-standing challenge in synthetic organic chemistry. Bolstered by its potential as a direct synthetic route to natural products containing skipped polyol moieties, this coupling is of great interest to the McDonald laboratory. The chemical literature documents numerous routes to 1,2- and 1,3-polyol moieties; however, these routes are often hindered by poor-to-moderate yields and selectivity, low functional group tolerance, and/or non-generalizable strategies for differing diastereomers.⁷⁵⁻⁷⁸ Additionally, few routes provide direct access to the 1,5-polyol moiety, a critical component found in the bastimolide family of anti-malarial natural products (Figure 3.1.1).⁷⁹⁻⁸¹ As such, the development of a general route to 1,3- and 1,5-polyol moieties represents an advance in not only synthetic chemistry, but also in medicinal chemistry.

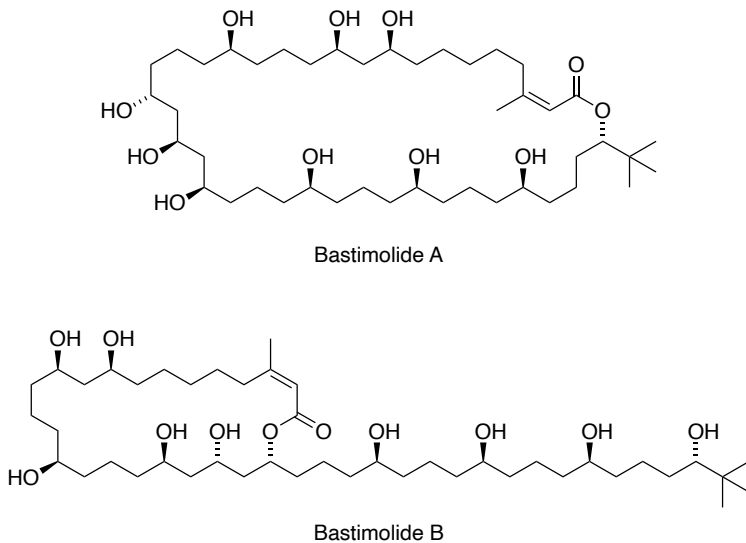


Figure 3.1.1: Proposed structures for bastimolide A and bastimolide B, two antimalarial natural products with moderate activity against drug-resistant *P. falciparum* strains.^{80, 81}

In our efforts to address these challenges, we sought to develop a widely applicable coupling strategy that employs dual activation of the epoxide electrophile and terminal alkyne nucleophile, drawing on the McDonald laboratory's previous experience with alkyne-epoxide cross-couplings (Figure 3.1.2). In addition to providing a direct route to polyol macrolide natural products such as those above, this accomplishment could allow for the creation of a library of all polyol stereoisomers—a feat that is far from trivial. An organometallic catalyst could plausibly activate the terminal alkyne, so we were particularly interested in the possibility of using fluorinated alcohol solvents to activate our epoxide. These solvents represented an interesting area to explore, owing to their demonstrated compatibility with organometallic transformations and their recent use in related transformations.⁸²⁻⁸⁴

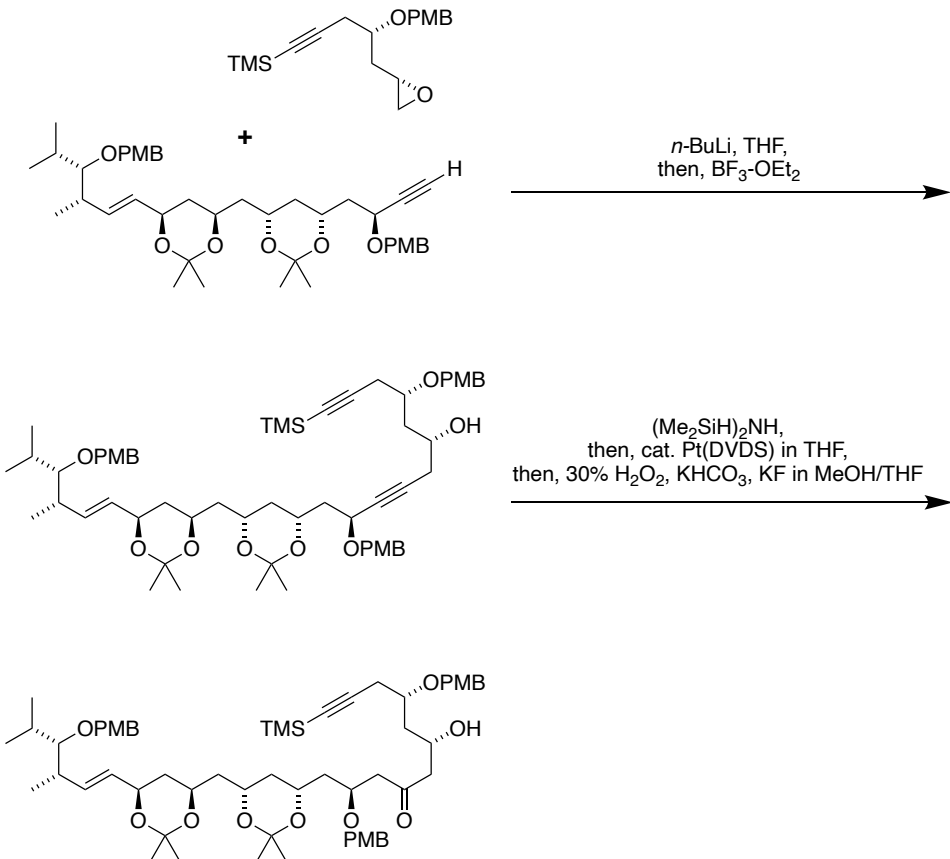


Figure 3.1.2: Excerpt from the synthesis of RK-397, an anti-cancer natural product. PMB = *para*-methoxybenzyl. Adapted from ref. 85.

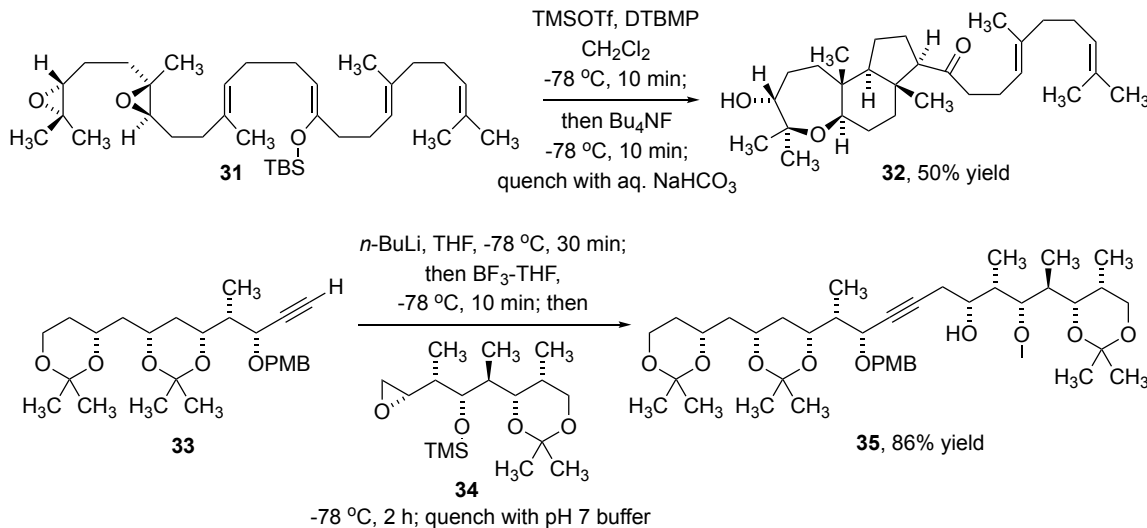
While preliminary studies with 1,1,1,3,3,3-hexafluoro-2-propanol (HFIP) and 2,2,2-trifluoroethanol (TFE) were not successful for our purposes, our early interest in these solvents provided an avenue to develop a review article on their broader uses. Aided by the closure of in-person laboratories as a result of the COVID-19 pandemic, this article came to fruition over the course of several months, and it was recently published in *Arkivoc*, an open-access journal.⁸⁶ The full text of this publication appears within the following sections of this chapter.

3.2.1 Introduction

Nucleophilic additions to epoxides are a common theme in chemical reactivity, ranging from preparations of poly(ethylene glycol) from ethylene oxide,⁸⁷ to DNA alkylations of carcinogenic epoxide metabolites of polycyclic aromatic hydrocarbons.⁸⁸ Despite the ring strain of the three-membered ring, epoxides are generally stable to long-term storage, due to the thermodynamic strength of the carbon-carbon and carbon-oxygen bonds. Therefore, many reactions of carbon nucleophiles with epoxides require either Lewis acidic reagents or catalysts to activate the latent electrophilicity of the epoxide, and/or highly nucleophilic main group organometallics, such as organolithium or organomagnesium compounds, which are also strongly basic.

Our interest in this topic arises from previous work from our laboratory involving epoxide electrophiles with carbon nucleophiles. These transformations have used strong Lewis acids, such as trimethylsilyl triflate (TMSOTf) for the intramolecular tricyclization of diepoxyenolsilane **31** to tricyclic ketone **32**,⁸⁹ and boron trifluoride-tetrahydrofuran (BF₃-THF) for the intermolecular addition of alkyne **33** with epoxide **34** to produce alkynyl alcohol **35** (Scheme 3.2.1.1).⁹⁰ Both examples required careful control of reaction time and temperature to attain the optimized yields.

In the past dozen years, other laboratories have reported several classes of ring-opening reactions of epoxides with carbon nucleophiles, *using fluorinated alcohol solvents* to promote these reactions under milder conditions or with greater efficiency than previously reported, including some transformations similar to those depicted in Scheme 3.2.1.1.



Scheme 3.2.1.1: Representative examples of epoxide electrophiles reacting with carbon nucleophiles, *without* fluorinated alcohol solvents. DTBMP = 2,6-di-*tert*-butyl-4-methylpyridine; PMB = *para*-methoxybenzyl; TMS = trimethylsilyl.

The substantive 2004 review of Bégué *et al.* described fluorinated alcohol solvents activating ring-opening reactions of epoxides with several classes of *heteroatom nucleophiles*, including amines, thiols, and carboxylic acids.⁹¹ Subsequent reviews have presented the broader scope and relevance of fluorinated alcohol solvents in modern synthetic applications.⁹²⁻⁹⁸ This review focuses on ring-opening reactions of epoxides with *carbon nucleophiles* promoted by the fluorinated alcohol solvents 1,1,1,3,3,3-hexafluoro-2-propanol (HFIP) and 2,2,2-trifluoroethanol (TFE, Figure 3.2.1.2). Our review will conclude with a few examples of ring-opening reactions of *aziridines* with carbon nucleophiles in fluorinated alcohol solvents.

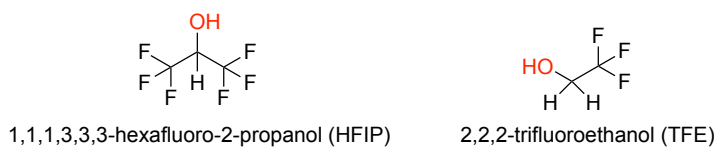


Figure 3.2.1.2: Structures of fluorinated alcohol solvents.

To maintain focus, we will not extend this review beyond the heterocyclic *epoxide* and *aziridine* electrophiles, even though the analogous ring-opening reaction of aryl-substituted *cyclopropanes* with electron-rich aromatic nucleophiles in HFIP may be mechanistically related.⁹⁹ Nonafluoro-*tert*-butyl alcohol (NFTB, also known as PFTB) promotes epoxide ring-opening with *oxygen nucleophiles*, including regioselective cascade cyclizations of polyepoxides terminated by alcohols,¹⁰⁰ but we have not yet uncovered examples of NFTB with *carbon nucleophiles* adding to epoxides.

3.2.2 Properties of Fluorinated Alcohol Solvents

The fluoroalkyl groups of these alcohols confer several synthetically useful benefits to these solvents. Among these are (1) increased acidity relative to their non-fluorinated analogs; (2) comparatively low boiling points; (3) strong hydrogen bond donating abilities; and (4) markedly low solvent nucleophilicities (Table 3.2.2.1).^{97, 102-107}

Table 3.2.2.1: Selected properties of HFIP and TFE, compared with ethanol and water.

Entry	Property	HFIP	TFE	CH ₃ CH ₂ OH	H ₂ O
1 [‡]	pK _a (25 °C, water) ^{97, 101}	9.3	12.4	15.9	14.0
2	b. p. (°C) ¹⁰²⁻¹⁰⁴	58	74.3	78.3	100
3	Hydrogen Bond Donor (α_1) ¹⁰⁵	1.86	1.36	0.75	1.54
4	Hydrogen Bond Acceptor (β_1) ¹⁰⁵	0.16	0.23	0.62	0.37
5 [‡]	Solvent Ionizing Power (Y, 2-adamantyl tosylate) ¹⁰⁶	3.61 ^a	1.83 ^b	-1.75	n.r. ^c
6 [‡]	Solvent Ionizing Power (Y, <i>tert</i> -butyl chloride) ¹⁰⁶	2.46 ^a	1.15 ^b	-2.03	3.49
7 [‡]	Nucleophilicity (N) ¹⁰⁷	-5.17 ^a	-3.25 ^b	0.55	-1.47

^a For 97% (w/w) HFIP-H₂O. ^b For 97% (w/w) TFE-H₂O. ^c not reported

[‡]Entries 1 and 5-7 are on logarithmic scales (log₁₀)

The electron-withdrawing fluoroalkyl groups are responsible for the low nucleophilicity and Brønsted acidity of fluorinated alcohol solvents. To illustrate, fluorinated alcohols exhibit enhanced acidity (pK_a, Table 3.2.2.1, entry 1) and strong hydrogen bond donating ability (entry 3),

especially with ethereal oxygens.^{108, 109} This results in an aggregation-induced decrease in the σ^*_{OH} orbital energy (Figure 3.2.2.2). For HFIP in the solid state, this complexation takes a helical form.¹⁰⁶ In addition, HFIP is a strongly ionizing solvent, and is more than five orders of magnitude less nucleophilic than ethanol (entries 5-7).^{106, 107, 110, 111} Fluorinated alcohol solvents are more expensive than the non-fluorinated congeners. However, bulk prices are currently as low as \$100 USD per kilogram, with TFE less expensive than HFIP. The low boiling points are desirable for recovering and recycling fluorinated alcohol solvents but present an upper limit on reaction temperature under refluxing conditions.^{112, 113}

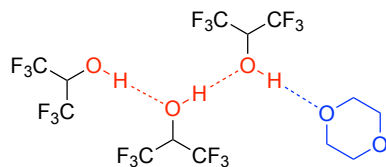


Figure 3.2.2.2: Aggregation of HFIP, depicting hydrogen bond donation with 1,4-dioxane.

3.2.3 Safety of Fluorinated Alcohol Solvents and Implications in Green Chemistry

Fluorinated alcohol solvents are about one order of magnitude more toxic than ethanol or 2-propanol via oral and/or intraperitoneal routes, with LD₅₀ values ranging from 300 - 600 mg/kg in mice (Table 3.2.3.1).^{114, 115} The toxicity of TFE arises from metabolic oxidation pathways.¹¹⁶ Most biological studies focus on the *in vivo* production of TFE and HFIP as metabolites from fluorinated anesthetics and other fluoroorganic drugs.¹¹⁷

Table 3.2.3.1: Toxicity of HFIP and TFE.

Entry	Route	LD₅₀ or LC₅₀ (mouse)	
		HFIP¹¹⁴	TFE¹¹⁵
1	oral	600 mg/kg	366 ± 106 mg/kg
2	intraperitoneal	300 mg/kg	350 ± 23 mg/kg

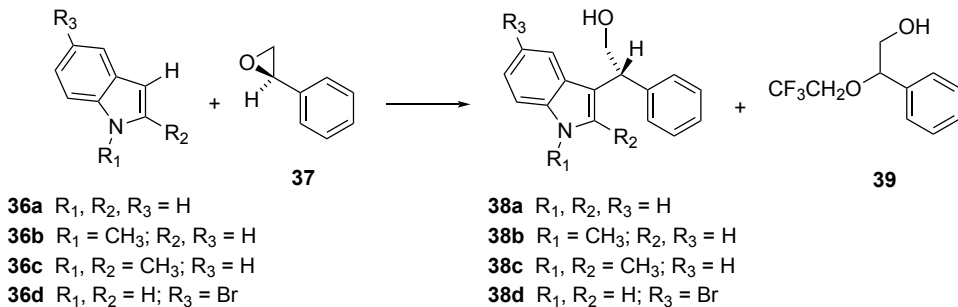
As mentioned in the last section, these solvents are amenable to recovery and reuse, lowering their impact on waste streams. While this feature is desirable from a green chemistry perspective, fluorinated alcohols raise significant environmental concerns. Notably, HFIP possesses a 100-year global warming potential (GWP) of 195, relative to CO₂.¹¹⁸ Although TFE falls at a less-concerning 18.3, these values are notable.¹¹⁹ Furthermore, HFIP meets the criteria necessary to be considered “Persistent, Mobile and Toxic (PMT)” and “very Persistent, very Mobile (vPvM)” under the EU REACH guidelines, although it is technically exempt from assessment.¹²⁰ This suggests that HFIP’s improper disposal may be hazardous to drinking water safety.

3.3.1 Intermolecular Carbon-Carbon Bond-Forming Reactions

The alkylation of indoles with epoxides has typically required Lewis acid catalysis to activate epoxide C-O bond cleavage. In 2008, Westermaier and Mayr reported that indoles **36a** - **36d** reacted with equimolar (*R*)-styrene oxide (**37**) in TFE solvent, *without additional Lewis acid*, to provide the alkylated products **38a** - **38d** (Table 3.3.1.1).¹²¹ The alkylations proceeded with regioselective addition at the benzylic carbon, and with complete stereospecificity, corresponding to inversion of configuration at the chiral carbon. For example, the parent indole (**36a**) reacted with styrene oxide (**37**) to give good yields of **38a** at room temperature in TFE, with only trace amounts of the trifluoroethoxy byproduct **39** (entry 1). This reaction proceeded more rapidly and cleanly at reflux (entry 2). The corresponding reaction of **36a** in aqueous acetone or aqueous ethanol solvent gave lower yield of product **38a**, and required significantly longer reaction times (entries 3, 4). Methyl-substituted indoles **36b** and **36c** also gave good yields of the corresponding alkylated products **38b** and **38c** in TFE (entries 5 - 7) vs. other solvents (entries 8, 9). However,

electron-withdrawing substituents on the indole diminished nucleophilicity, so that 5-bromoindole (**36d**) required 72 hours for partial conversion, with the yield of **38d** diminished by the competing reaction of TFE with the epoxide (entry 10).

Table 3.3.1.1: TFE-promoted alkylations of indoles **36** with (*R*)-styrene oxide (**37**).



Entry	Indole	Solvent	Temperature (°C)	Time (h)	Yield 38 (%)	Yield 39 (%)
1	36a	TFE	20	48	65	trace
2	36a	TFE	80	10	79	-
3	36a	acetone : H ₂ O (80 : 20)	60	72	9	
4	36a	ethanol : H ₂ O (40 : 60)	80	72	45	
5	36b	TFE	80	4	73	-
6	36c	TFE	20	24	77	-
7	36c	TFE	80	3	90	-
8	36c	acetone : H ₂ O (80 : 20)	60	14	17	
9	36c	ethanol : H ₂ O (40 : 60)	80	12	54	
10	36d	TFE	80	72	45	19

The regioselectivity and stereospecificity outcomes were consistent with the fluorinated alcohol solvent stabilizing partial positive charge on the benzylic position in the transition state for the alkylation reaction (Figure 3.3.1.2).

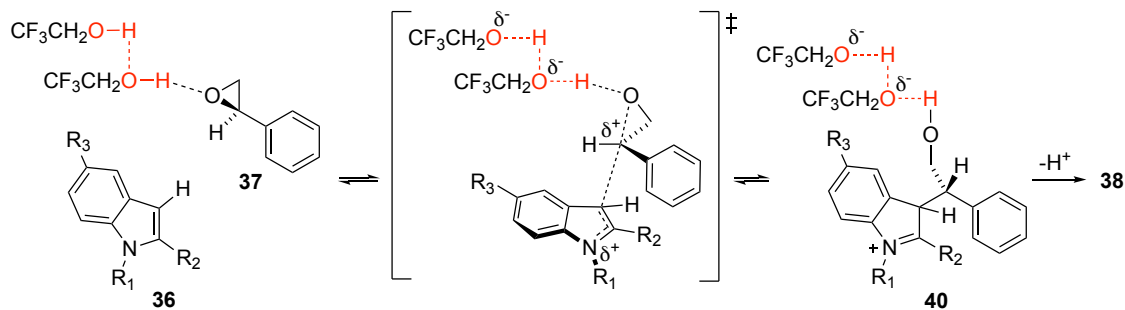
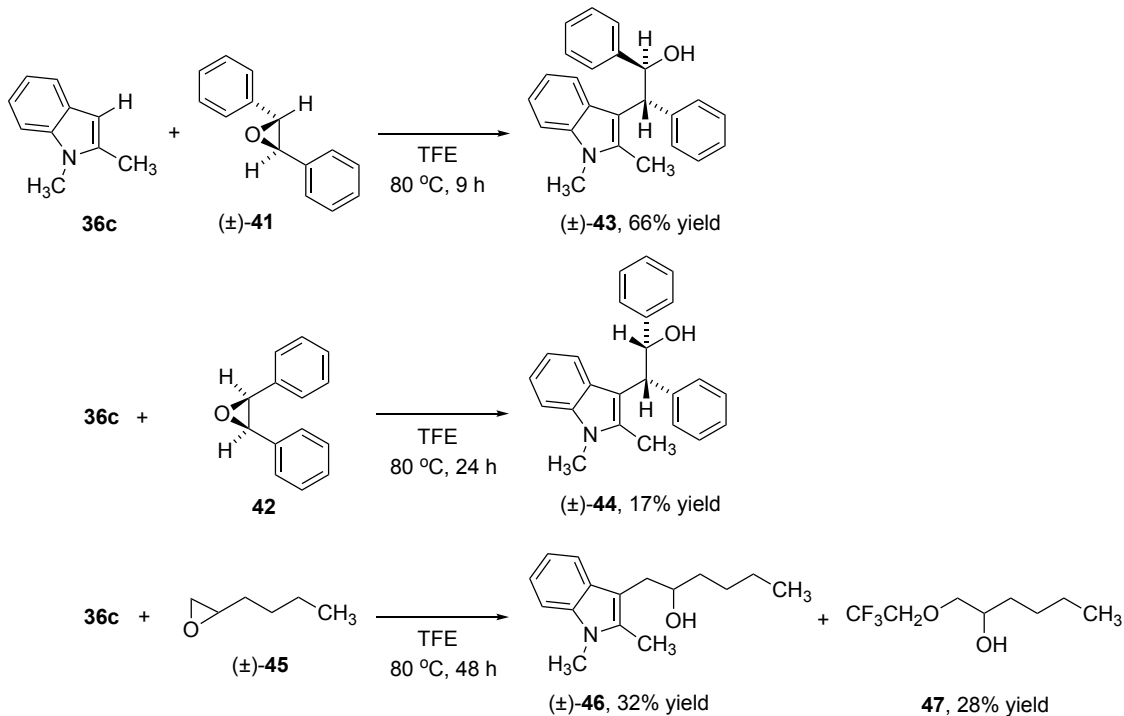


Figure 3.3.1.2 The electrophilic aromatic alkylation mechanism promoted by hydrogen bonding and the ionizing power of TFE.

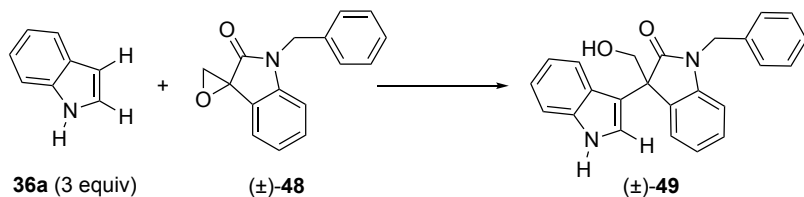
Westermaier and Mayr established that the scope of epoxide substrates with indoles was relatively limited: the reaction of **36c** with *trans*-stilbene oxide (**41**) provided **43** in good yield, but the corresponding reaction with *cis*-stilbene oxide (**42**) proceeded slowly—albeit with stereospecificity—to generate the expected diastereomer **44** (Scheme 3.3.1.3). The aliphatic epoxide 1,2-epoxyhexane (**45**) sluggishly underwent indole alkylation at the unsubstituted carbon to produce **46**, with the competing addition of TFE giving byproduct **47**.



Scheme 3.3.1.3: Representative scope of epoxide substrates in TFE-promoted alkylations of indoles.

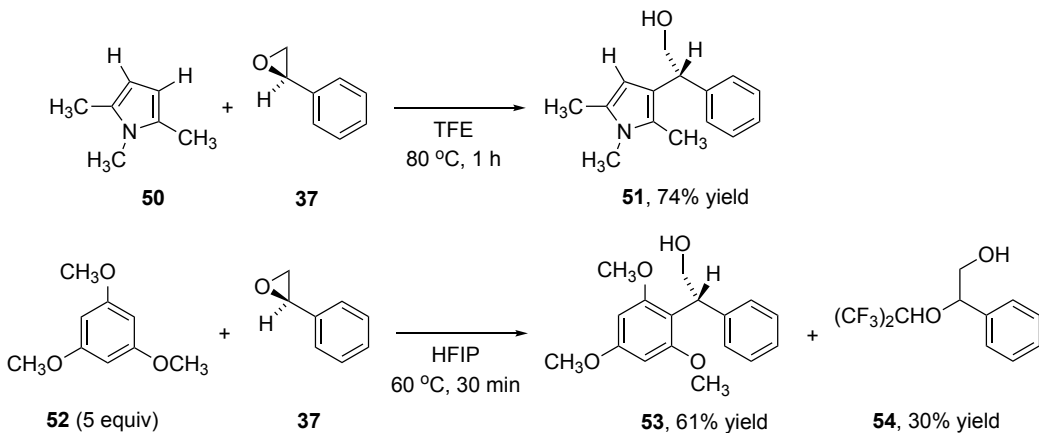
Sun, Hong, and Wang extended the alkylation of indole (**36a**) to spiroepoxyindole **48**, exploring several conditions with fluorinated alcohol solvents (Table 3.3.1.4).¹²² TFE promoted the reaction even at room temperature (entry 1), with a better yield and shorter reaction time upon warming (entry 2). The more acidic and highly ionizing solvent HFIP gave a considerably faster reaction, albeit with a slight loss of regioselectivity (entry 3). However, selectivity was regained in water containing some HFIP (9 : 1 ratio) to provide **49** in excellent yield, with carbon-carbon bond-formation at the more substituted position (entry 4). Other organic solvents such as dichloromethane, dimethyl sulfoxide, methanol, tetrahydrofuran, or toluene did not give product **49**.

Table 3.3.1.4: Comparing the effects of TFE vs. HFIP and water on alkylation with spiroepoxyxindole (**48**).



Entry	Solvent	Temperature (°C)	Time (h)	Yield 49 (%)
1	TFE	25	80	65
2	TFE	60	32	90
3	HFIP	25	12	66 ^a
4	H ₂ O / HFIP (9 : 1)	25	32	93

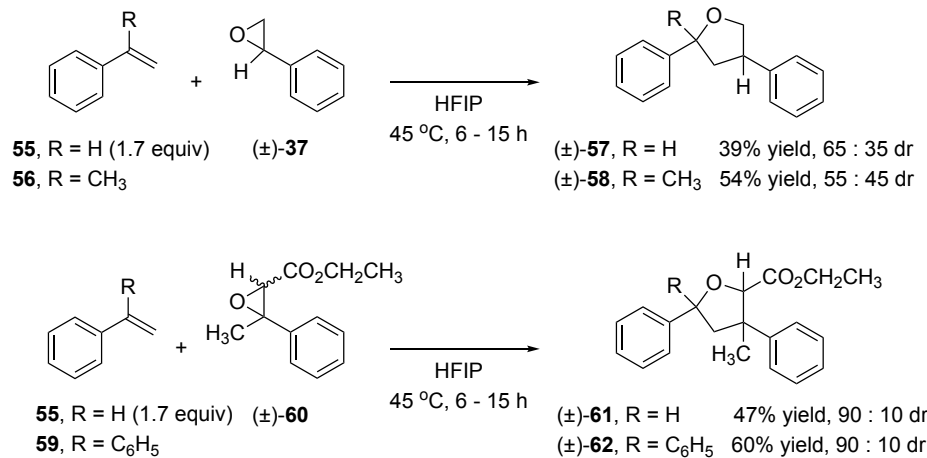
Westermaier and Mayr also described alkylations of pyrroles with styrene oxide (**37**) in TFE, affording regioisomer mixtures and double alkylation products with simpler pyrroles. Conversely, 1,2,5-trimethylpyrrole (**50**) selectively produced **51** as its major product (Scheme 3.3.1.5).¹²¹ Li and Qu subsequently reported alkylation of 1,3,5-trimethoxybenzene (**52**) in HFIP, with the electron-rich aromatic compound out-competing the HFIP solvent to favor the aromatic alkylation product **53** over the solvent addition product **54**.¹²³ Chiral non-racemic styrene oxide (*R*)-**37** stereospecifically led to both products **51** and **53**, with inversion of configuration. The yields were substantially lower with 1,4-dimethoxybenzene (35%) and with anisole (15%).



Scheme 3.3.1.5: Alkylations of other electron-rich aromatic compounds with (*R*)-styrene oxide.

The 3-atom + 2-atom annulations of epoxides with alkenes to form tetrahydrofurans have typically required transition metal catalysts, likely operating by radical or Lewis acid processes.^{124,125} However, Llopis and Baeza have reported catalyst-free conditions, simply by warming in HFIP solvent.¹²⁶ Although the scope is limited to aryl-substituted epoxides, the yields are modest, and the diastereoselectivity is generally low, metal-catalyzed versions of this transformation also share these limitations.^{124, 125} The reactions of styrene (**55**) and *alpha*-methylstyrene (**56**) with racemic styrene oxide (**37**) in HFIP solvent exemplify these results (Scheme 3.3.1.6). With chiral non-racemic styrene oxide (*R*)-**37**, the reaction with styrene (**55**) gives racemic product **57**, whereas only partial racemization occurs upon forming tetrahydrofuran **58** from *alpha*-methylstyrene (**56**) (not shown). Annulations with ethyl 3-methyl-3-phenylglycidate (**60**), sold as a mixture of diastereomers, give higher diastereoselectivities upon reaction with styrene (**55**) and 1,1-diphenylethene (**59**). The regioselectivity is consistent with the less substituted carbon of the alkene adding to the phenyl-substituted carbon of the epoxide, with carbon-oxygen bond formation at the phenyl-substituted carbon arising from the alkene reactant. The yields of tetrahydrofuran products are diminished by competing dimerizations and

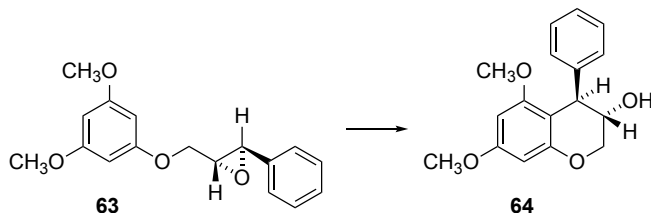
trimerizations of the aryl alkene,¹²⁷ and solvent addition to the epoxide, forming byproducts including ether **54** (see Scheme 3.3.1.5 for structure).



Scheme 3.3.1.6: 3 atom + 2 atom annulations of aryl-substituted epoxides with aryl alkenes.

3.3.2 Intramolecular carbon-carbon bond-forming reactions

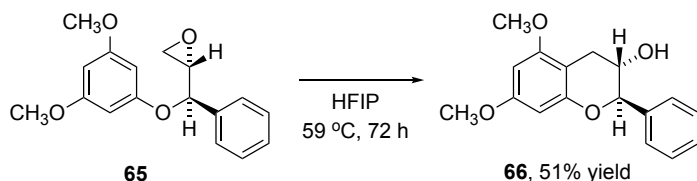
Li and Qu reported the intramolecular alkylation of epoxides tethered to electron-rich aromatic rings, using fluorinated alcohols to activate the epoxide.¹²³ Although the literature has described several Lewis acid-catalyzed methods for the cycloisomerization of **63** to **64**, these scientists explored the effects of highly ionizing solvents *in the absence of Lewis acids* (Table 3.3.2.1). In contrast to methanol or water (entries 1, 2), TFE promoted cyclization in excellent yield (entries 3, 4). HFIP was a more effective promoter, affording the cyclized product in only 5 min at reflux (entries 5, 6). Nucleophilic addition occurred with high regioselectivity for the 6-*endo*-mode of cyclization, and with inversion of configuration at the benzylic carbon to provide the *trans*-disubstituted benzopyran **64** from the *trans*-disubstituted epoxide **63**. The decrease in reaction time between TFE and HFIP is consistent with the increased acidity and ionizing power of HFIP, rather than hydrogen bond donation which diminishes with higher temperature.^{128, 129}

Table 3.3.2.1: Solvent screening for cycloisomerization of epoxide **63**.

Entry	Solvent	Temperature (°C)	Time	Yield 64 (%)
1	methanol	65	26 h	18
2	water	100	10 h	55 ^a
3	TFE	20	48 h	96
4	TFE	74	4.5 h	99
5	HFIP	20	4 h	99
6	HFIP	59	5 min	99

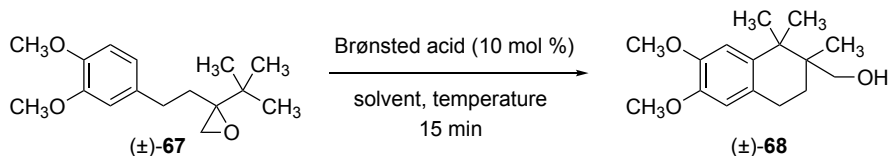
^a remainder was diol from epoxide hydrolysis

The epoxide substrate **65** with an acid-sensitive benzylic ether provided a valuable demonstration of the power of this HFIP-promoted transformation (Scheme 3.3.2.2). The previous synthesis of compound **66**, closely corresponding to the catechin natural products, required a specialized combination of Lewis acid and hydrogen bond donor catalysts ($\text{AuCl}_3 / \text{AgOTf} / \text{thiourea}$).¹³⁰ In contrast, HFIP solvent promoted the slow but clean conversion of epoxide **65** into benzopyranol **66**, arising from 6-*endo*-mode nucleophilic addition to the unsubstituted carbon of the epoxide.¹²³

**Scheme 3.3.2.2:** HFIP-promoted cyclization of the sensitive epoxyether **65**.

The Magauer laboratory reported the acid-catalyzed cycloisomerizations of neopentyl epoxides tethered to electron-rich aromatic rings.¹³¹ In the course of cyclization of substrate **67** into tetralin product **68**, a methyl group underwent 1,2-alkyl shift. Cyclizations were unsuccessful or proceeded in low yield in most solvents (Table 3.3.2.3, entry 1 for a representative example) but improved in fluorinated alcohol solvents, with HFIP outperforming TFE (entries 2 vs. 3). The optimized conditions used sulfuric acid in HFIP at 0 °C (entry 5). HFIP forms hydrogen bonds with the conjugate base of sulfuric acid, increasing its Brønsted acid activity.¹³²

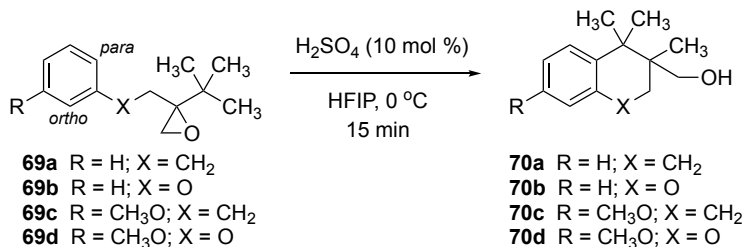
Table 3.3.2.3: Acid-catalyzed, HFIP-promoted cycloisomerization of neopentyl epoxide **67**.



Entry	Brønsted acid	Solvent	Temperature	Yield 68 (%) ^a
1	H ₂ SO ₄	toluene	23 °C	19%
2	H ₂ SO ₄	TFE	23 °C	43%
3	H ₂ SO ₄	HFIP	23 °C	77%
4	<i>p</i> -toluenesulfonic acid	HFIP	23 °C	77%
5	H ₂ SO ₄	HFIP	0 °C	83% ^b

^a ¹H NMR yields. ^b The isolated yield of compound **68** was 80%.

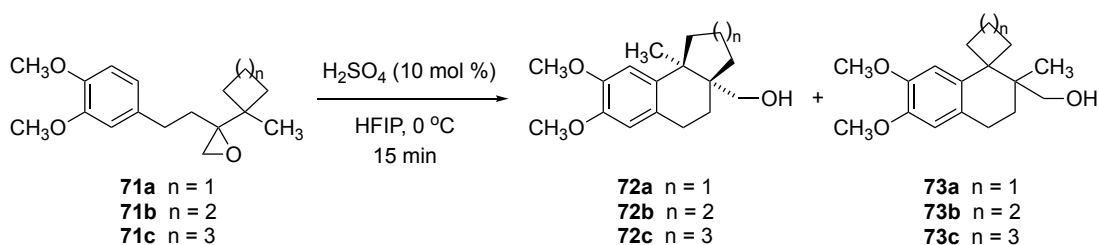
The phenyl substrate **69a** also produced the corresponding tetralin **70a** (Table 3.3.2.4, entry 1).¹³¹ The reaction conditions tolerated aryl ether tethers in **69b** to form chromane **70b** (entry 2). With electron-donating substituents, cycloisomerization favored the *para*-isomers **70c-d** with varying levels of regioselectivity (entries 3, 4). Aromatic rings with strongly electron-withdrawing substituents gave lower yields or did not cyclize.

Table 3.3.2.4: Alkyl vs. ether tethers, and regioselectivity of monomethoxy aromatic substrates.

Entry	Substrate	Yield 70 (%)	Regioselectivity
1	39a	70%	n. a.
2	39b	60%	n. a.
3	39c	69%	<i>para</i> only
4	39d	40%	<i>para</i> : <i>ortho</i> = 4.7 : 1 ^a

^a *ortho*-isomer not shown

Neopentyl epoxide substrates containing cycloalkyl rings gave divergent behavior, depending on the degree of ring strain (Table 3.3.2.5).¹³¹ The cyclobutyl and cyclopentyl substrates **71a**-**71b** favored the corresponding ring-expansion fused products **72a** and **72b** (entries 1, 2), whereas the cyclohexyl substrate **71c** produced exclusively the spiro isomer **73c** arising from a 1,2-methyl shift.

Table 3.3.2.5: Cycloisomerizations of methylcycloalkyl epoxide substrates **71**.

Entry	Substrate ^a	Yield 72 (%) ^a	Yield 73 (%) ^a
1	41a	76	0
2	41b	54	6
3	41c	0	71

^a substrates and products are racemic

The partitioning of mechanistic pathways leading to products **72** and **73** is consistent with carbenium ion intermediates.¹³¹ As depicted in Figure 3.3.2.6, ring expansion exclusively occurs (path a) with strained cyclobutyl epoxide **71a** and is favored with cyclopentyl epoxide **71b**. With the unstrained cyclohexane attached to epoxide **71c**, the 1,2-methyl shift (path b) exclusively occurs. From each tertiary carbenium ion intermediate **74** and **75**, intramolecular Friedel-Crafts alkylation provides the tetralin core structures of products **72** and **73**. Figure 4 also depicts the hydrogen bonding interaction between HFIP and sulfuric acid, and HFIP stabilization of the hydrogen sulfate conjugate base,¹³² which is also observed in other acid-catalyzed processes.^{133, 134}

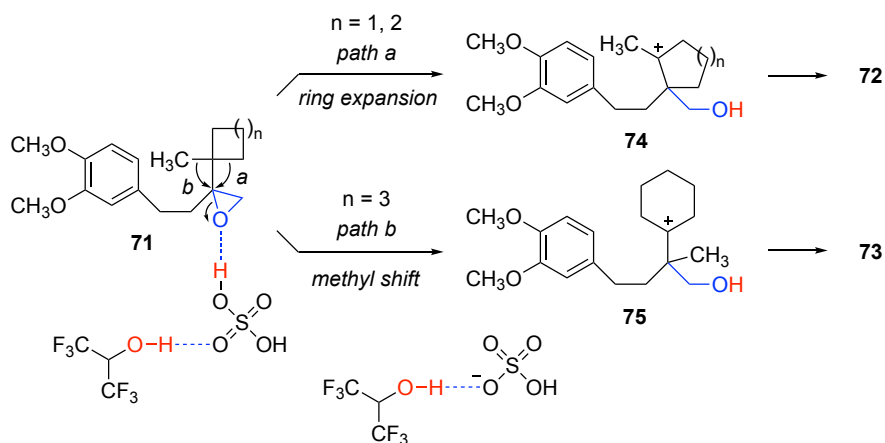
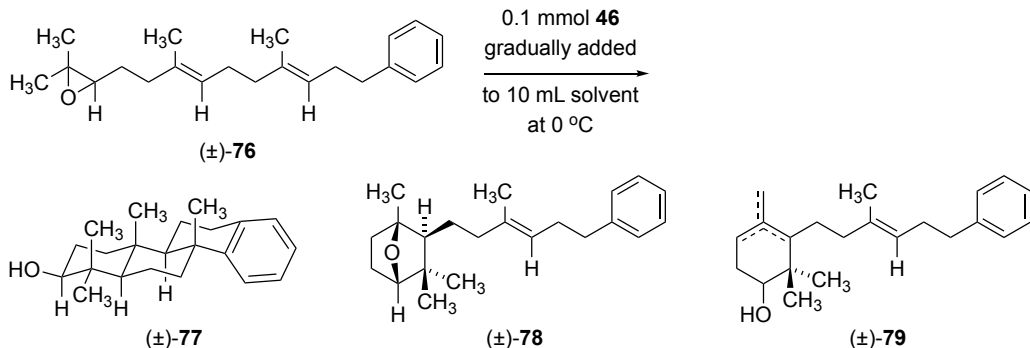


Figure 3.3.2.6: Possible mechanisms for cycloisomerization.

Biomimetic polyene-epoxide polycyclizations have typically required Lewis acid promoters or catalysts.^{135, 136} In contrast, the Qu laboratory observed slow conversion of epoxydiene **76** when diluted in HFIP, producing a mixture of tetracyclic product **77**, the oxabicyclo[2.2.1]heptane byproduct **78**, and an inseparable mixture of partially cyclized dienes **79** (Table 3.3.2.7, entry 1).¹³⁷ Remarkably, epoxydiene **76** was inert with other fluorinated alcohol solvents (entries 2, 3). *p*-Toluenesulfonic acid (*p*-TSA) rapidly catalyzed the reaction of **76**, but gave a mixture favoring the partially cyclized byproducts **79** (entry 4). The reaction rate

dramatically increased, with improved selectivity for tetracyclic product **77**, upon gradual addition of epoxydiene **76** to HFIP solutions of soluble organic salts with fluorine-containing non-nucleophilic anions (entries 5 - 7). Tetraphenylphosphonium tetrafluoroborate (Ph_4PBF_4) in HFIP gave the best yield of compound **77** (entry 7). Although excess water hydrolyzed the epoxide of **76** to form a diol, up to 20 equivalents of water were compatible with tricyclization (entry 8). Deliberately adding catalytic hydrogen fluoride to HFIP gave a similar enhancement in the reaction rate (entry 9), supporting a proposal that BF_4^- and PF_6^- provided trace amounts of HF. However, replacing HFIP with dichloromethane, while including Ph_4PBF_4 and HF as additives, gave no reaction (entry 10). The authors concluded that HFIP played an essential role in promoting the polycyclization, likely by stabilizing the fluoride conjugate base.

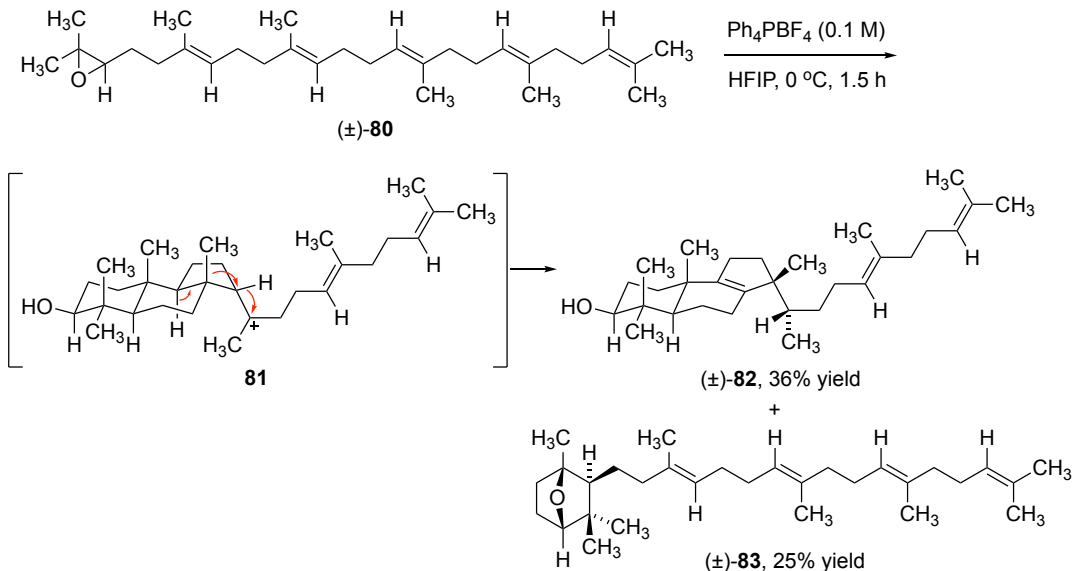
Table 3.3.2.7: HFIP / additive-promoted tricyclizations of epoxydiene **76**.

Entry	Solvent	Additive(s)	Time	Yield 77 (%)	Yield 78 (%)	Yield 79 (%)
1	HFIP	none	24 h	40	27	32
2	TFE	none	24 h		(no reaction)	
3	(CF ₃) ₃ COH	none	24 h		(no reaction)	
4	CH ₂ Cl ₂	p-TSA (0.1 equiv)	15 min	23	19	56
5	HFIP	Bu ₄ N ⁺ BF ₄ ⁻ (0.1 M)	5 min	51	n.r. ^a	n.r.
6	HFIP	Bu ₄ N ⁺ PF ₆ ⁻ (0.1 M)	5 min	51	n.r.	n.r.
7	HFIP	Ph ₄ P ⁺ BF ₄ ⁻ (0.1 M)	5 min	60	19	n.r.
8	HFIP	Ph ₄ P ⁺ BF ₄ ⁻ (0.1 M) + H ₂ O (0.2 M)	5 min	56	n.r.	n.r.
9	HFIP	HF (0.001 M)	5 min	37	n.r.	n.r.
10	CH ₂ Cl ₂	Ph ₄ P ⁺ BF ₄ ⁻ (0.1 M) + HF (0.001 M)	24 h	(no reaction)		

^a n.r. = not reported

These scientists then applied these conditions to the cyclization of squalene oxide (**80**), the biosynthetic precursor of lanosterol and other steroid natural products (Scheme 3.3.2.8).¹³⁷ The 36% yield of tricyclic product **82** was substantially higher than the outcomes from various Lewis acid-promoted transformations.¹³⁸⁻¹⁴² The formation of compound **82** is consistent with a mechanism involving concerted cyclization of the three alkenes closest to the epoxide, thereby generating a tertiary carbenium ion **81**. The authors proposed that the cations—including protonated epoxide and the tricyclic intermediate cation **81**—were stabilized by the non-nucleophilic solvent HFIP and/or the non-nucleophilic tetrafluoroborate anions. From **81**, an

intramolecular cascade of face-selective 1,2-hydride and 1,2-methyl migrations followed by deprotonation generated the principal product **82**.



Scheme 3.3.2.8: HFIP / Ph₄PBF₄-promoted cyclization of squalene oxide (**80**).

In summary, although most epoxide alkylations were limited to electron-rich aromatic compounds, fluorinated alcohol solvents effectively replaced the Lewis acidic reagents and catalysts customarily used for these transformations. The intramolecular alkylations of epoxides tethered to polyenes have demonstrated the powerful combination of additive Brønsted acid sources in combination with HFIP.

3.4.1 Ring-opening reactions with organopalladium intermediates arising from directed C-H functionalization

Directed C-H functionalization of aromatic rings has traditionally required strongly basic reagents, such as *tert*-butyllithium combined with *N,N,N,N*-tetramethylethylenediamine (TMEDA). Regioselectivity *ortho*- to a Lewis basic directing group (DG) arises from coordination

with the electropositive metal, bringing the electronegative alkyl ligand into proximity with the aromatic C-H bond.^{143, 144} The resulting functionalized aryllithium intermediates reacts with many electrophiles, and the literature documents several examples with epoxides.¹⁴⁵ However, transition-metal catalysts offer milder conditions for directed C-H functionalization. The literature provides several examples in which HFIP has favored palladium acetate-catalyzed directed metalations of benzene rings, coupled with *in situ* alkylation of epoxides, presumably also activated by HFIP for nucleophilic addition (Figure 3.4.1.1).^{84, 146-149} A variety of Lewis basic directing groups (DG) are effective, including 2-pyridyl (**84**), and a variety of carbonyl- or carboxyl-derived compounds **85 - 89**.

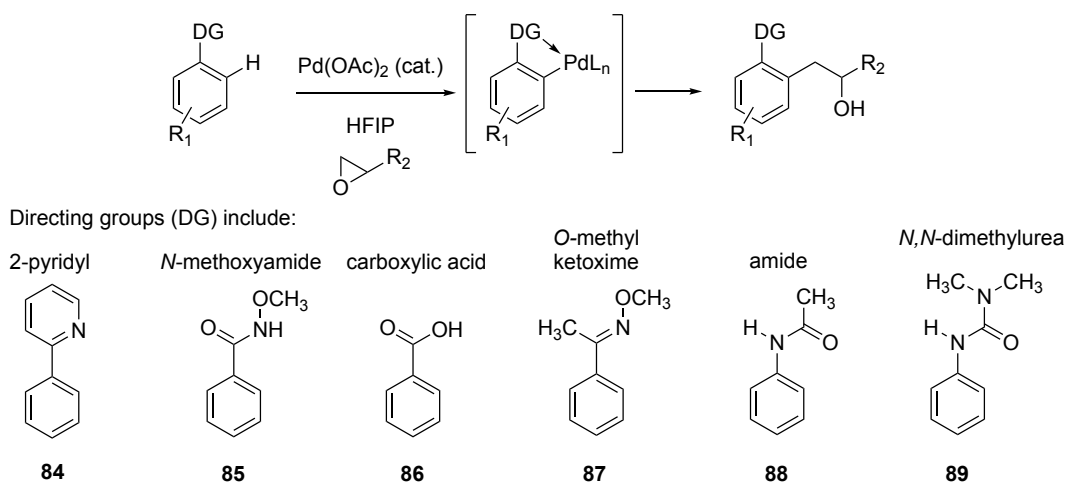


Figure 3.4.1.1: Directing groups for palladium acetate-catalyzed C-H functionalization / epoxide alkylation.

The methods published to date have several common features:

- All use palladium acetate as the catalyst,
- The methods show broad scope with many substituents R₁ on the benzene ring, and

- A variety of monosubstituted and 1,1-disubstituted epoxides give good yields (Figure 3.4.1.2).

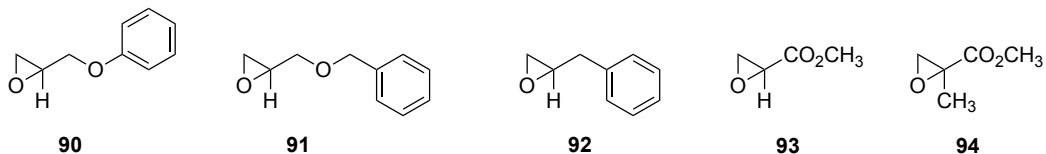


Figure 3.4.1.2: Representative epoxides for palladium-catalyzed C-H functionalization / epoxide alkylation.

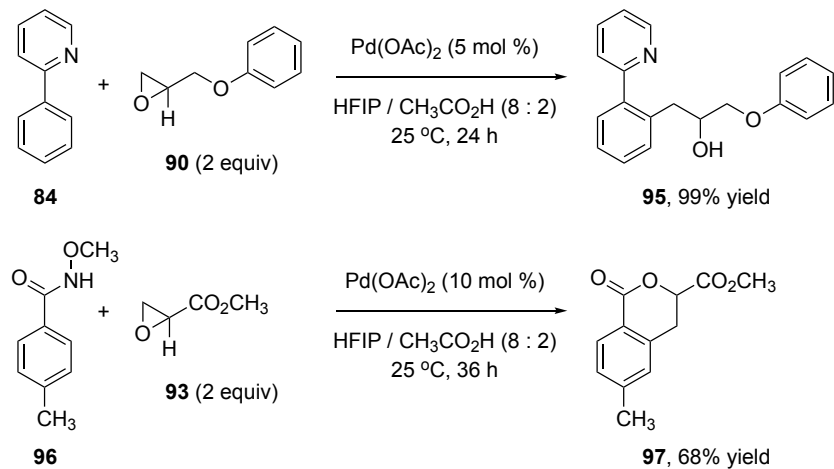
These methods also share common substrate limitations:

- To date, heterocyclic aromatic rings are not functionalized under these conditions, and
- 1,2-Disubstituted epoxides generally do not react, or give substantially lower yields.
- No examples are reported with styrene oxide (**37**) or other arylepoxides.

3.4.2 Scope of reactions and conditions

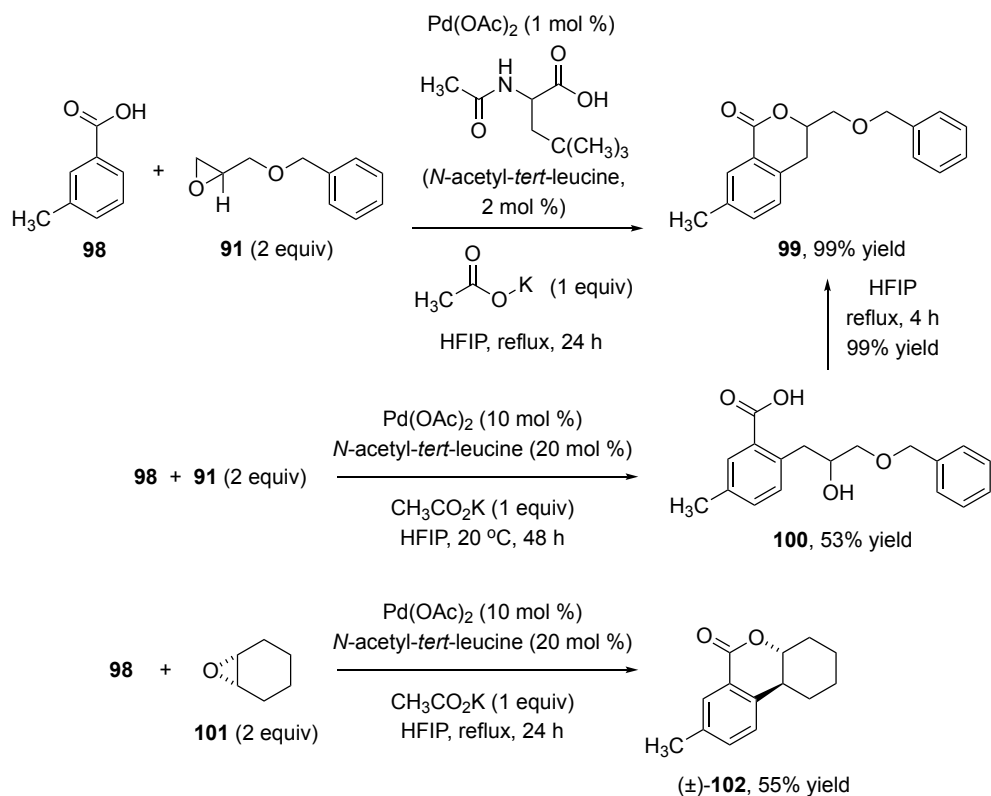
In 2015, the Kuninobu and Kanai laboratories collaboratively reported the regioselective alkylation of 2-phenylpyridine (**84**) and derivatives with epoxides including phenyl glycidyl ether (**90**), catalyzed by palladium acetate (Scheme 3.4.2.1).¹⁴⁶ The initial solvent choice, acetic acid, gave low yields due to acid-promoted decomposition of the epoxide. Diluting acetic acid with HFIP resulted in the substituted phenethyl alcohol **95** in excellent yield, provided that two equivalents of epoxide were used at room temperature, as epoxide decomposed under these conditions at higher temperatures. These scientists established that HFIP alone was not sufficient to promote this transformation. In addition to the example with **84** and **90**, they also reported the analogous transformation with the *N*-methoxyamide **96** and methyl glycidate (**93**). In this example,

the lactone ring of product **97** presumably formed via acid-catalyzed intramolecular transacylation after the carbon-carbon bond-forming step.



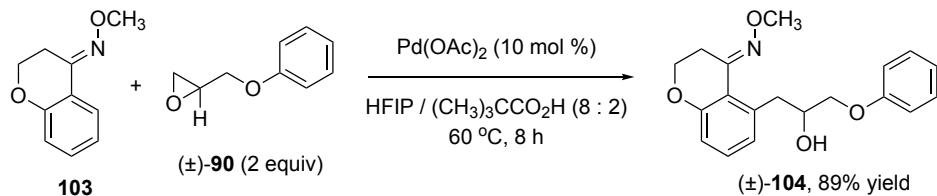
Scheme 3.4.2.1: Pd-catalyzed C-H functionalization with 2-pyridyl and *N*-methoxyamide directing groups, with regioselective epoxide alkylation.

Later in 2015, the Yu laboratory disclosed the directed alkylation of benzoic acids, including *meta*-toluic acid (**98**), with a broad scope of epoxide substrates (Scheme 3.4.2.2).⁸⁴ Essential components of this reaction system included palladium acetate, potassium acetate, and HFIP solvent. Cesium acetate led to lower yields, and little or no product was formed when using sodium acetate or lithium acetate. Yields increased from 75% to 99% with the mono-*N*-protected amino acid ligand *N*-acetyl-*tert*-leucine. In a highly optimized example with benzyl glycidyl ether (**91**), product **99** was isolated in 99% yield. At room temperature, the reaction proceeded more slowly and required higher catalyst loading but produced intermediate hydroxyacid **100**. This compound underwent HFIP-promoted lactonization at reflux to form **99**. By avoiding acetic acid as a cosolvent, a broad range of epoxide substrates were compatible with HFIP, even under reflux. This carboxyl directing group method was compatible with cyclohexene oxide (**101**), producing *trans*-fused **102** in satisfactory yield.



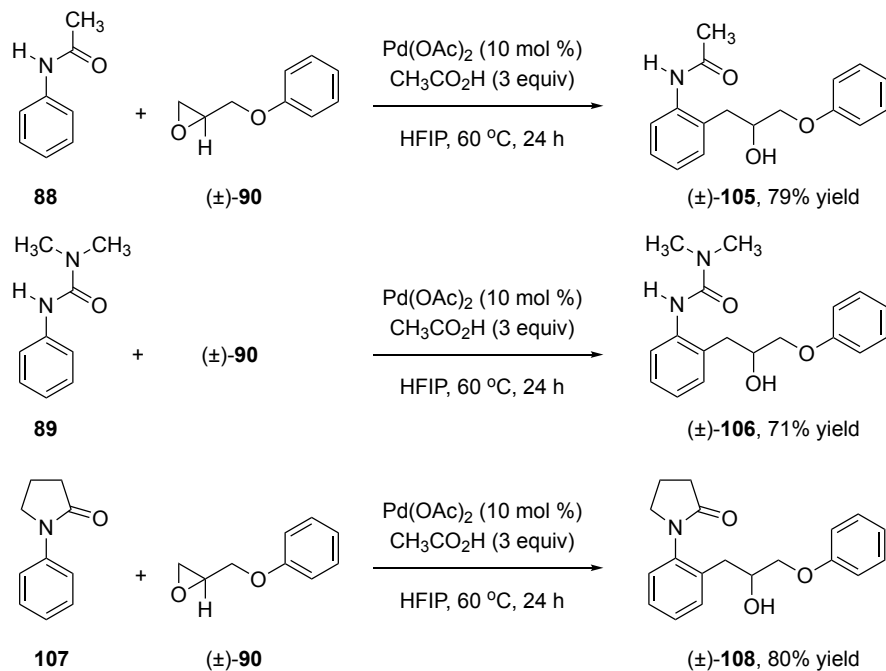
Scheme 3.4.2.2: Pd-catalyzed C-H functionalization with carboxylic acid directing group, with regioselective epoxide alkylation.

The Li laboratory optimized the directed alkylation of *O*-methyl ketoximes with epoxides, using HFIP and a carboxylic acid co-solvent. Pivalic acid gave much better yields than acetic acid. Neither HFIP nor pivalic acid alone were suitable solvents. The bicyclic substrate **103** with phenyl glycidyl ether (**90**, Scheme 3.4.2.3) afforded alcohol **104**.¹⁴⁷



Scheme 3.4.2.3: Pd-catalyzed C-H functionalization with an *O*-methyl ketoxime directing group, promoting regioselective epoxide alkylation.

In 2020, the Cheong and Lee laboratories collaboratively published the corresponding directed alkylations with equimolar amounts of epoxides, using *N*-acyl aniline derivatives as the directing groups, including acetanilide (**88**), the corresponding *N,N*-dimethylurea **89**, and 1-phenylpyrrolidin-2-one (**107**) (Scheme 3.4.2.4).¹⁴⁸ Notably, the Lewis basic oxygens of the directing groups were one atom further removed from the benzene carbon undergoing C-H functionalization, yet the optimized conditions were similar to those reported for most of the other directing groups.

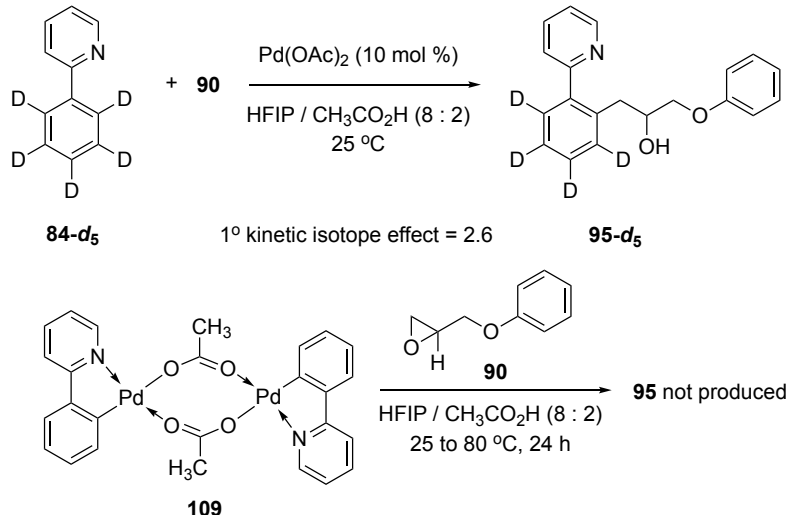


Scheme 3.4.2.4: Pd-catalyzed C-H functionalization with *N*-acyl directing groups, with regioselective epoxide alkylation.

3.4.3 Mechanistic Proposals

Wang, Kuninobu, and Kanai reported the relative rates of reaction of 2-phenylpyridine (**84**) vs. **84-d5** with phenyl glycidyl ether (**90**), measuring a primary kinetic isotope effect $k_{\text{H}} / k_{\text{D}} = 2.6$, indicating that the rate-determining step was C-H bond activation (Scheme 3.4.3.1).¹⁴⁶ These

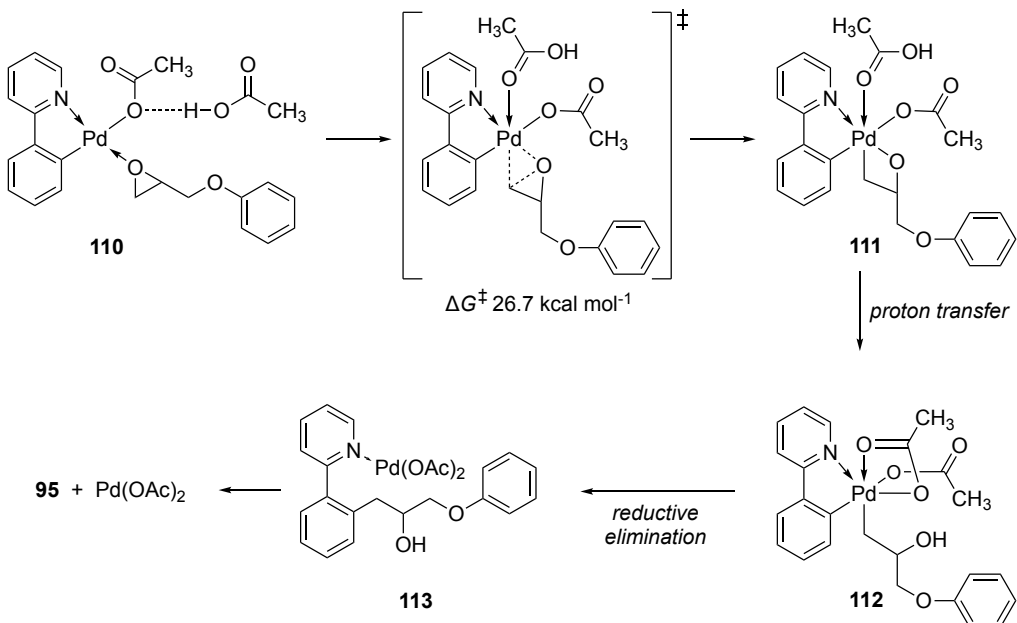
scientists prepared a plausible dimeric palladacycle intermediate **109**, but this palladacycle did not promote the ring-opening reaction with epoxide **90**. They speculated that oxidation to Pd(IV) might be required for alkylation of epoxides.



Scheme 3.4.3.1: Kinetic isotope rate study and a stoichiometric experiment with palladacycle **109** from 2-phenylpyridine (**84**).

The Fang laboratory explored these results via density functional theory (DFT) studies.¹⁴⁹ These scientists found that the lower energy pathway involved coordination of epoxide to a *mononuclear* palladacycle to form intermediate **110**, followed by oxidative addition of the coordinated epoxide to Pd(IV) metallocetane **111** (Figure 3.4.3.2, part a). The catalytic cycle concluded with proton transfer to form intermediate **112**, followed by reductive elimination to yield the palladium complex with the directing group **113**. In contrast, mechanisms involving only Pd(II) intermediates (Figure 3.4.3.2, part b) required much higher energy barriers for ring-opening coupled with carbon-carbon bond-formation. The theoretical study did not consider the effects of fluorinated solvent on the C-H functionalization stage (not shown) to form intermediate **110**, or on the epoxide reaction stage.

a) via Pd(IV) intermediate **111**:



b) redox-neutral pathway via Pd(II) intermediate **110**:

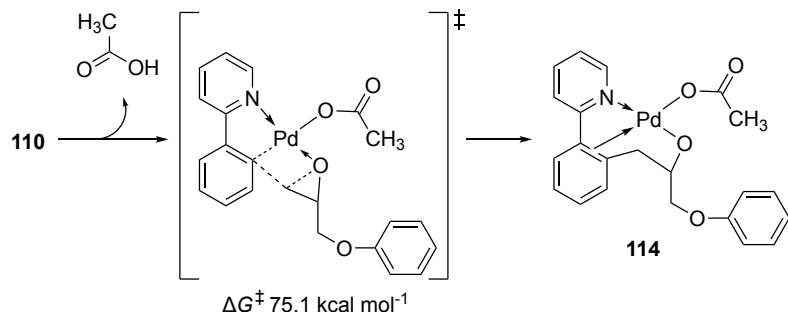
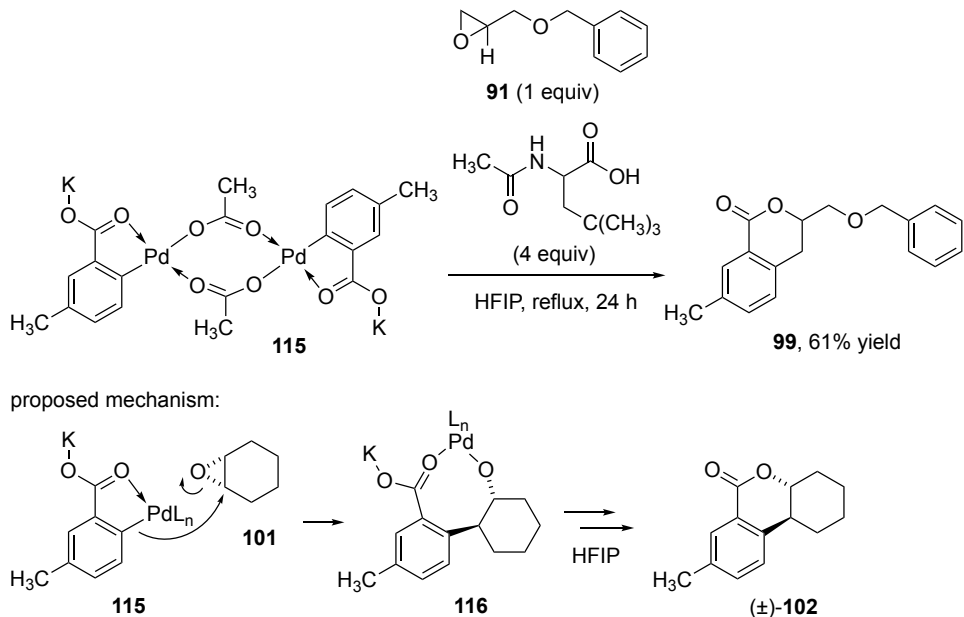


Figure 3.4.3.2. Partial catalytic cycles involving 2-phenylpyridine alkylation, with a Pd(IV) intermediate (path a) vs. redox-neutral pathway (path b). Determined at the B2PLYP/DGDZVP level of theory, in acetic acid ($\epsilon = 6.25$).

In contrast, the Yu laboratory conducted a stoichiometric experiment with *meta*-toluic acid-derived palladacycle **115**, which reacted with benzyl glycidyl ether (**91**) to produce the same compound **99** arising from catalytic conditions (Scheme 3.4.3.3). Moreover, the *trans*-

stereochemistry of **102** arising from the reaction with cyclohexene oxide (**101**) suggested that the arylpalladium intermediate **115** reacted with inversion of configuration at the reactive carbon from the epoxide, without requiring a change in oxidation state from Pd(II).⁸⁴



Scheme 3.4.3.3 A stoichiometric experiment with palladacycle **115** from *meta*-toluic acid, and a mechanistic proposal based on the stereochemistry of **102**.

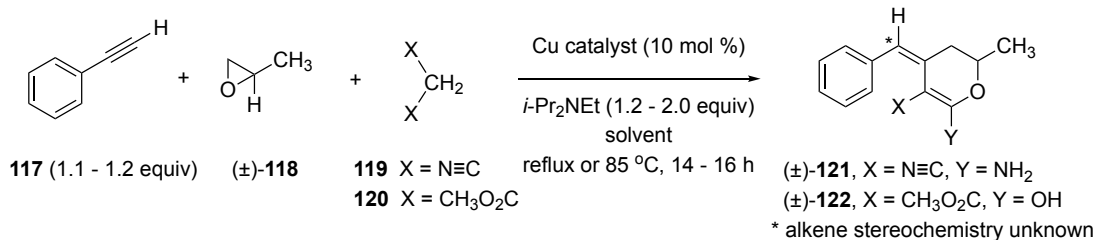
In summary, we note that the carboxylic acid readily forms the *anionic* carboxylate under the reaction conditions. This makes the attached aryl ligand in Pd(II) complex **115** more nucleophilic for alkylation with epoxides. *Neutral* directing groups may uniquely require a mechanism involving Pd(IV) for epoxide alkylations.

3.5 Ring-opening reactions with terminal alkyne nucleophiles

A pair of collaborative studies from the laboratories of Sedaghat and Khalaj have described three-component coupling / cyclization methods, combining terminal alkynes, epoxides, and the active methylene compounds malononitrile (**119**) or dimethyl malonate (**120**) (Table 3.5.1).^{82, 83}

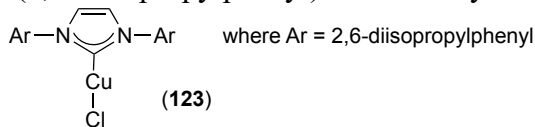
Several Cu(I) catalysts gave good to excellent yields of highly functionalized pyrans **121** or **122**, corresponding to the active methylene reactant. In all cases, the best yields arose with HFIP as solvent, although satisfactory results were also reported with polyethylene glycol 400 (PEG 400, entries 5, 13). Both solvents can activate the electrophilic epoxide by hydrogen bonding with the epoxide oxygen, however, these scientists did not propose a role for HFIP in alkyne activation. The non-nucleophilic nature of HFIP apparently prevented the competing addition of solvent to the epoxide, *even in the presence of tertiary amine*. The stereochemistry of the trisubstituted alkenes of **121** - **122** was not established in all cases, although the ¹H and ¹³C NMR data suggested that isolated products may correspond to only one alkene stereoisomer.

Table 3.5.1: Three-component reactions of phenylacetylene with propylene oxide and active methylene compounds.



Entry	Reactant	Cu Catalyst	Solvent	Product	Yield (%)
1	119	Cu_2O	HFIP	121	85
2	119	Cu_2O	acetonitrile	121	21
3	119	Cu_2O	dimethylformamide	121	26
4	119	Cu_2O	PEG-200	121	40
5	119	Cu_2O	PEG-400	121	70
6	119	CuI	HFIP	121	80
7	119	$\text{CuOSO}_2\text{CF}_3$	HFIP	121	80
8	119	$(\text{IPr})\text{CuCl}$ (122)^a	HFIP	121	68
9	120	Cu_2O	HFIP	122	52
10	120	CuI	HFIP	122	61
11	120	$\text{CuOSO}_2\text{CF}_3$	HFIP	122	65
12	120	$(\text{IPr})\text{CuCl}$ (122)^a	HFIP	122	80
13	120	$(\text{IPr})\text{CuCl}$	PEG-400	122	51

^a $(\text{IPr})\text{CuCl}$ is [1,3-bis(2,6-diisopropylphenyl)imidazol-2-ylidene]copper(I) chloride



This transformation shows relatively broad scope beyond phenylacetylene (**117**) and propylene oxide (**118**):

- trimethylsilylacetylene and 1-hexyne are reactive nucleophiles;
- the opposite regioselectivity is observed for styrene oxide (**37**), giving dihydropyrans **124** - **125**; and

- cyclohexene oxide (**101**) is a reactive electrophile, giving bicyclic dihydropyrans **126 - 127** (Figure 3.5.2).

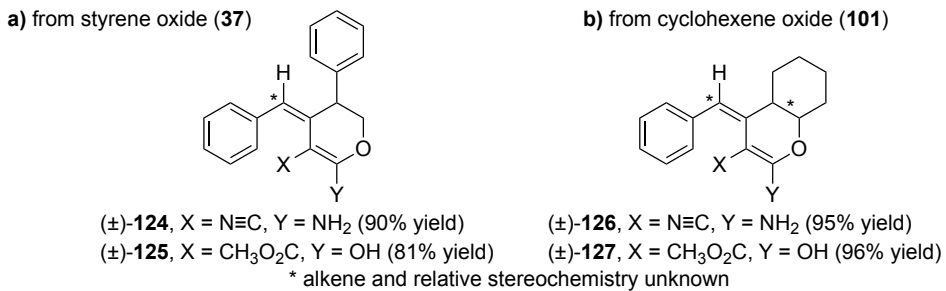


Figure 3.5.2: Scope of product dihydropyrans (**124-127**) arising from epoxide substrates **37** (a) and **101** (b).

Experiments that generated the alkynyl alcohol intermediate **128**, and related experiments that converted 4-phenylbut-3-yn-1-ol (**129**) into dihydropyran **131** provide some mechanistic hints (Figure 3.5.3):⁸⁴

- a) The combination of phenylacetylene (**117**), propylene oxide (**118**), and dimethyl malonate (**120**) in the presence of (IPr)CuCl and refluxing HFIP, *without added base*, afforded a good yield of the alkynyl alcohol product **128**.
- This suggests that HFIP promoted the copper-promoted formation of a copper acetylidyne intermediate, which has added to a hydrogen bonded-complex of epoxide with HFIP, giving **128**.
- b) The combination of 4-phenylbut-3-yn-1-ol (**129**) and dimethyl malonate (**120**) catalyzed by (IPr)CuCl *in the absence of base* and *in the polar aprotic solvent N,N-dimethylformamide (DMF)* gave the malonate addition product **130**, albeit in modest yield. The catalytic loading of (IPr)CuCl was not specified in this experiment.

- The (IPr)CuCl catalyst may have deprotonated malonate (the imidazolium cation has pK_a 21.1)¹⁵⁰ and promoted regioselective malonate addition to the alkyne, giving **130**, in a step that did not require HFIP.
- c) The combination of alkynyl alcohol **129** and dimethyl malonate (**120**) catalyzed by (IPr)CuCl *in the presence of tertiary amine* and HFIP produced the dihydropyran **131** in good yield.

- HFIP alone may have promoted the final intramolecular transacylation and tautomerization; the role of the tertiary amine in this scenario was unclear.

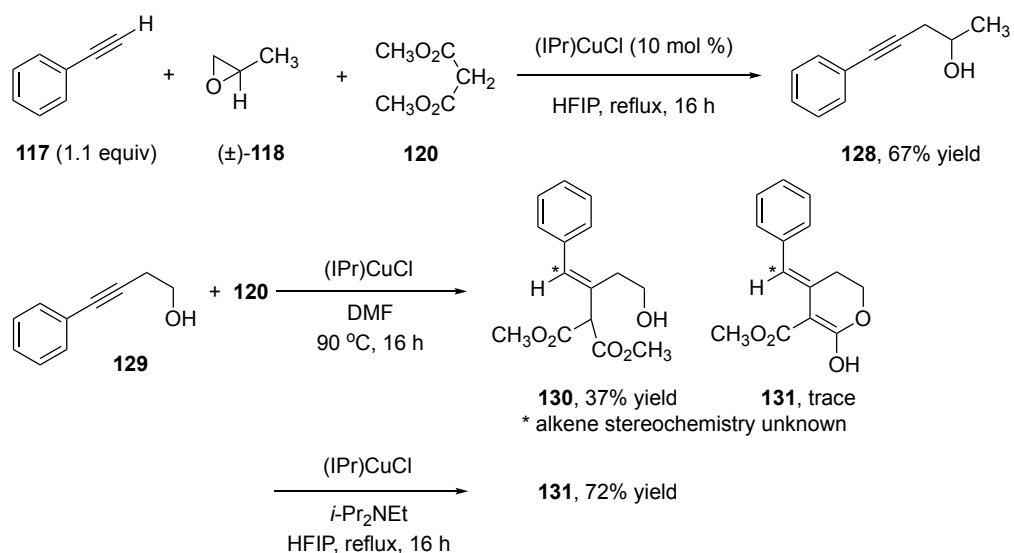
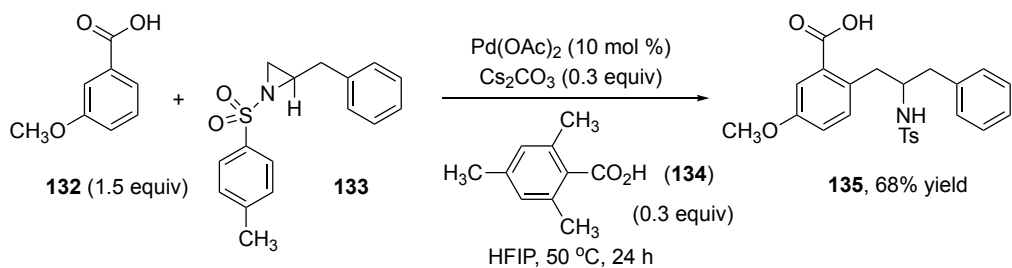


Figure 3.5.3: Individual steps via alkynyl alcohols **128** and **129**.

In summary, the combination of moderately acidic HFIP solvent with basic tertiary alkylamine *without solvent addition to the epoxide* is quite interesting, as similar conditions promote hexafluoroisopropoxide nucleophilic addition to phosgene and thionyl chloride electrophiles.^{151, 152} This work merits additional investigation and optimization, particularly the direct addition of alkyne to epoxide *in the absence of an active methylene compound*.

3.6 Ring-opening reactions of aziridines with carbon nucleophiles

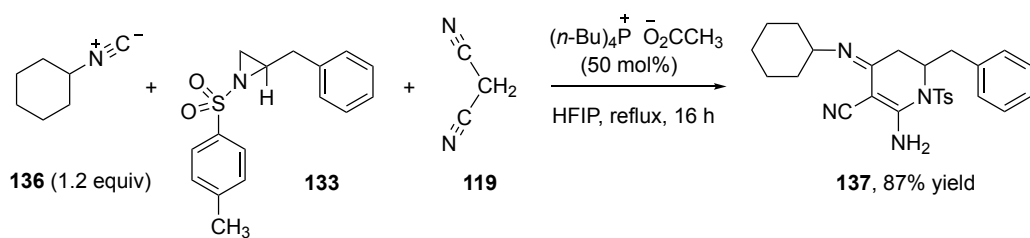
This review concludes with extensions of two approaches described earlier in this review, applied to aziridine electrophiles, promoted by HFIP. In 2019, the Zhao laboratory reported palladium-catalyzed C-H functionalization of 3-methoxybenzoic acid (**132**) and other arylcarboxylic acids, reacting with a relatively broad range of *N*-tosylaziridines including monosubstituted **133**, producing the protected *beta*-arylethylamine **135**, an important substructure in medicinal chemistry (Scheme 3.6.1).¹⁵³ The principal competing process was ring-opening of aziridine with the carboxylic acid, which was suppressed by diminishing the cesium carbonate loading to substoichiometric amounts. The conversion increased with 2,4,6-trimethylbenzoic acid (**134**) as a substoichiometric additive. A solvent screen revealed that a protic alcohol solvent was required, with HFIP giving the best yields.



Scheme 3.6.1: Palladium-catalyzed C-H functionalization of an arylcarboxylic acid with addition to an *N*-tosylaziridine, promoted by HFIP.

In 2019, Samzadeh-Kermani described an organocatalytic synthesis of tetrahydropyridone imines, including compound **137** (Scheme 3.6.2).¹⁵⁴ The carbon nucleophile was an aryl- or alkylisonitrile, with cyclohexyl isonitrile (**136**) as a representative case. Several Lewis acids gave competing isomerization of monosubstituted aziridine **133** to a *N*-tosylimine, but tetrabutylphosphonium acetate in refluxing HFIP promoted aziridine ring-opening with

nucleophilic addition of the isonitrile. The base for deprotonating malononitrile (**119**) may have been the anionic *N*-tosylamide from ring opening, or the acetate counteranion. Nucleophilic addition of dinitrile-stabilized carbanion to the alkynitrilium cation from the initial isonitrile addition step explains the remaining carbon–carbon bond-forming step. The author proposed that the tetrabutylphosphonium cation may coordinate with one of the nitriles to promote intramolecular nucleophilic addition of the tosylamide to close the tetrahydropyridine ring.



Scheme 3.6.2: Three-component coupling of an isonitrile, an *N*-tosylaziridine, and malononitrile (**119**) to form tetrahydropyridone imines, promoted by tetrabutylphosphonium acetate in HFIP.

3.7 Conclusions

This review describes the benefits of fluorinated alcohol solvents in promoting the ring-opening reactions of epoxides and aziridines with carbon nucleophiles. The advances presented herein fall into two categories:

- **significant electrophilic activation, due to the formation of complex structures and aggregations**, such as the formation of an activating HFIP complex with epoxides, thereby allowing reactions with weak and neutral nucleophiles; and
- **safety and environmental benefits**, especially where fluorinated alcohol solvents replace Lewis acid reagents, and even more so when the solvent is recycled.

We anticipate that other researchers will find that fluorinated alcohol solvents enable other synthetically valuable transformations that have not been previously developed. The role of these

solvents in activating C-H bonds is not well-established, warranting further investigation to increase our understanding of fluorinated alcohol solvents. Additionally, there is clearly room for significant future work in aziridine ring-opening reactions in fluorinated alcohols, an area with potential for synthesizing pharmaceutical substances.

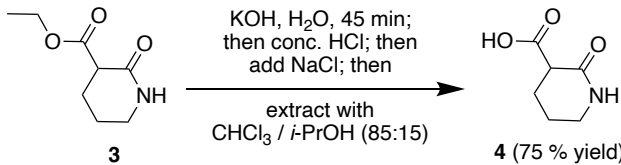
CHAPTER 4: Experimental Details

4.1 Notes

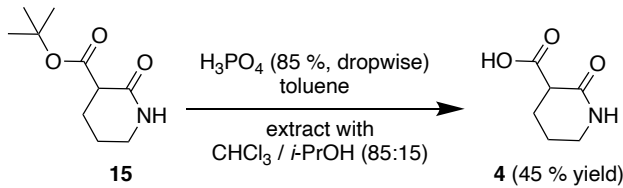
- 1.) It is not completely clear if pure **4** was prepared from **15**. The process provided an oil, which, upon trituration, provided some solid material. The material was not further purified or analyzed.
 - 2.) Upon the start of the computation, we received a warning that our search area was >27,000 cubic Å, which might lead to dubious results with low exhaustiveness parameters. We have used 1024 as this parameter in all cases to account for this. The default exhaustiveness is 8.
 - 3.) Enzymatic hydrolysis of ethyl 2-oxopiperidine-3-carboxylate (**3**) was completed using the ratios determined from Hu *et al.*, 2007.⁴⁴ The conversion was determined using:

$$Conversion = \frac{\int 1.00 \text{ ppm}}{\int (1.00 \text{ ppm} + 1.12 \text{ ppm})} \quad (Eq. 4.1.1)$$

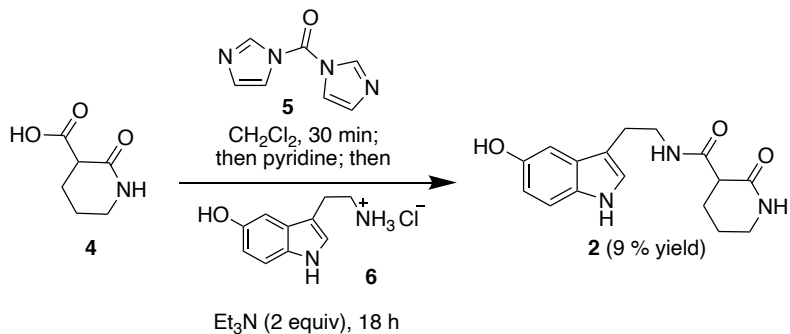
4.2 Protocols



2-oxopiperidine-3-carboxylic acid (4): To a round-bottom flask equipped with a stir bar was added ethyl 2-oxopiperidine-3-carboxylate (**2**, 1.025 g, 5.99 mmol), solid KOH (1.436 g, 25.59 mmol, 4.3 equiv.) and 10mL H₂O. The solution was stirred at room temperature for 45 min, followed by the dropwise addition of concentrated HCl until a pH of 3-4 was reached. Solid NaCl (15.2 g) was added to the solution and stirred, followed by extraction with an 85:15 solution of CHCl₃/i-PrOH (5 x 200mL, twice). The organic phase was dried over MgSO₄, filtered, and concentrated *in vacuo* to yield 2-oxopiperidine-3-carboxylic acid (**4**, 0.639 g, 4.46 mmol, 75% yield) as a white powder. In some instances, the isopropyl ester **14** was observed in the NMR of the product. mp: 113-119 °C (decomp. with vigorous bubbling); IR(±30cm⁻¹): 3270, 2960, 2865, 1935, 1670, 1340, 1220 cm⁻¹; ¹H-NMR (600 MHz, DMSO-d₆): δ 12.57 (s, 1H), 7.74 (s, 1H), 3.15-3.08 (m, 3H), 1.97-1.92 (m, 1H), 1.83-1.78 (m, 1H), 1.74-1.69 (m, 1H), 1.61-1.54 (m, 1H); ¹³C-NMR (150 MHz, DMSO-d₆): δ 172.5, 167.8, 48.4, 41.6, 24.8, 20.6; HRMS calculated for C₆H₁₀O₃N [M+H]⁺ 144.06552, found 144.06544, 172.09679.

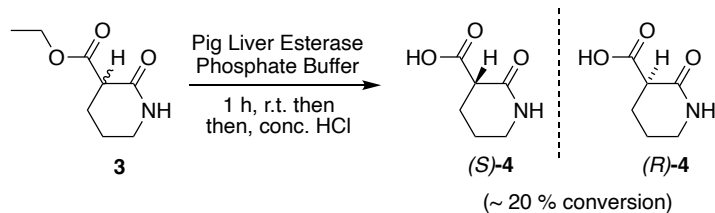


2-oxopiperidine-3-carboxylic acid (4) (*via* *tert*-butyl ester hydrolysis): To a round-bottom flask equipped with a stir bar was added *tert*-butyl 2-oxopiperidine-3-carboxylate (**15**, 0.2117 g, 1.06 mmol) and 1.5 mL toluene. The solution was briefly stirred, and phosphoric acid (85 %) was added dropwise via syringe (~0.36 mL, 5.3 mmol, 5 equiv.). The reaction was then allowed to stir overnight, after which 10 mL of H₂O was added. The combined solution was the extracted with ethyl acetate (4 x 30 mL), dried over MgSO₄, filtered, and concentrated *in vacuo* to provide 0.068 g of an oil. This oil was placed on a vacuum pump, leading to a waxy material, which was triturated in ethyl acetate to provide a small quantity of solid material. This material was not analyzed further.

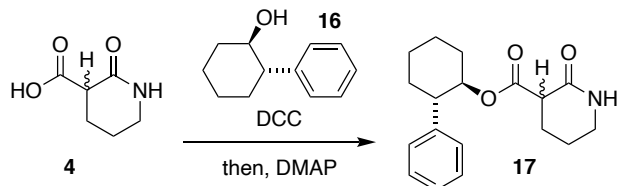


N-[2-(5-hydroxy-1*H*-indol-3-yl)ethyl]-2-oxopiperidine-3-carboxamide (HIOC, **2):** To an oven-dried three-neck flask equipped with a stir bar was added 2-oxopiperidine-3-carboxylic acid (**4**, 0.250 g, 1.74 mmol), carbonyldiimidazole (CDI, **5**, 0.287 g, 1.77 mmol) and anhydrous CH₂Cl₂ (5.8 mL). The mixture was purged with argon, and stirred at room temperature for 30 min, followed by addition of serotonin-HCl (**6**, 0.378 g, 1.78 mmol) and anhydrous pyridine (5.8 mL). The reaction was stirred until the serotonin-HCl was completely dissolved, followed by the addition of triethylamine (0.48 mL, 2 equiv.). The reaction was left to stir for an additional 18 hours, after which no starting material was visible via TLC (eluent: 9:1 EtOAc / MeOH; stained purple with *p*-anisaldehyde). The solution was concentrated *in vacuo*, followed by dissolution in a minimal amount of a 9:1 mixture of EtOAc / MeOH, and dry silica gel was added. The mixture was then concentrated *in vacuo*, and the free-flowing silica-adsorbed product was dry-loaded onto a packed chromatography column. The product was initially eluted with 98:2 EtOAc / MeOH, then 95:5 EtOAc / MeOH after TLC initially revealed the presence of the desired product (eluent: 9:1 EtOAc / MeOH; stained purple with *p*-anisaldehyde; UV-active). The relevant fractions were combined into a round-bottom flask, and concentrated *in vacuo*, yielding a brown viscous oil, which was washed with warm diethyl ether to remove traces of imidazole. The resultant white solid was then loaded onto a fritted funnel and washed with acetone, followed by drying with argon, to furnish *N*-[2-(5-hydroxy-1*H*-indol-3-yl)ethyl]-2-oxopiperidine-3-carboxamide (HIOC, **1**) as a white powder (0.0456 g, 0.15 mmol, 9 % yield); mp 181–183.5°C (found), 205–208°C (literature),

decomp.; IR(\pm 30cm $^{-1}$): 3255, 2930, 1650, 1590, 1555, 1495, 1470, 1375 cm $^{-1}$; 1 H-NMR (600 MHz, DMSO-d $_6$): δ 10.45 (s, 1H), 8.55 (s, 1H), 8.03 (dd, J = 5.9 Hz, 5.3 Hz, 1H), 7.62 (s, 1H), 7.07 (d, J = 8.8 Hz, 1H), 7.01 (d, J = 2.3 Hz, 1H), 6.79 (d, J = 2.3 Hz, 1H), 6.54 (dd, J = 6.44 Hz, 2.35 Hz, 2.34 Hz, 1H), 3.29-3.21 (m, 2H), 3.10-3.07 (m, 2H), 3.02 (dd, J = 7.6 Hz, 6.4 Hz, 1H), 2.67 (t, J = 7.6 Hz, 2H), 1.88-1.86 (m, 1H), 1.80-1.73 (m, 2H), 1.58-1.51 (m, 1H); 13 C-NMR (150 MHz, DMSO-d $_6$): δ 170.1, 168.7, 150.6, 131.2, 128.3, 123.6, 112.1, 111.6, 111.0, 102.6, 48.4, 41.7, 39.5, 25.6, 24.9, 20.9; HRMS calculated for C₁₆H₂₀O₃N₃ [M+H] $^+$ 302.15101, found 302.14970. We have also observed the monohydrate ([M+H] $^+$ =320.15988) and protonated dimer ([M+H] $^+$ =603.29201) in another run of this experiment. Additionally, up to 40 % yield has been obtained in a distinct experiment; however, more characterization data is available for the 9 % yield run (only 1 H-NMR available for 40 % yield run).

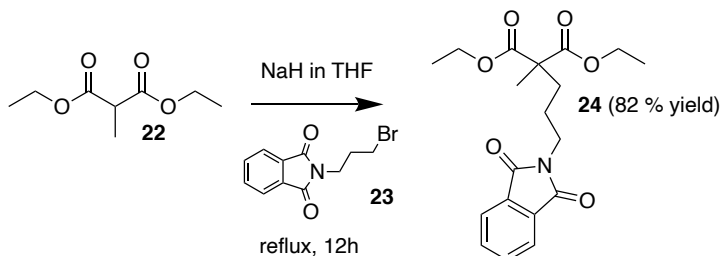


2-oxopiperidine-3-carboxylic acid (4) (Chemoenzymatic Preparation): To a round bottom flask equipped with stir bar was added ethyl 2-oxopiperidine-3-carboxylate (**3**, 0.750 g, 4.38 mmol) in phosphate buffer (pH=7, 50 mM, Fisher Sci.) (6 mL). The reaction was stirred until a suspension was formed, followed by the addition of Pig Liver Esterase (0.012 g, 71.43 nanomoles). A 2 N solution of NaOH was added as needed to keep the pH between 6.8 and 7.2, and the reaction was stirred at room temperature for one hour, then immediately placed in an ice bath to prevent further conversion. On average, approximately 20% conversion was observed via ¹H-NMR analysis of the sample. A suitable work-up and purification procedure has not yet been determined. ¹H-NMR (600 MHz, DMSO-d₆): δ 7.65 (s, 1H), 4.02 (q, *J* = 7.1 Hz, 2H), 3.39 (q, *J* = 6.9 Hz, 1H), 3.19 (dd, *J* = 8.9, 6.4 Hz, 1 H), 3.09 (td, *J* = 5.7, 2.7 Hz, 2H), 1.92 (dtd, *J* = 13.4, 6.8, 3.4 Hz, 1H), 1.78 (dtd, *J* = 13.0 6.4, 3.3 Hz, 1H), 1.69 (ddq, *J* = 12.2, 8.5, 4.7 Hz, 1H), 1.57 (dddd, *J* = 17.0, 13.8, 6.4, 3.3 Hz, 1H), 1.12 (t, *J* = 7.1 Hz, 3H [exact: 2.91]), 1.00 (t, *J* = 7.0 Hz, 1H [exact: 0.68]). Procedure modeled after Hu *et al.*, 2007.⁴⁴

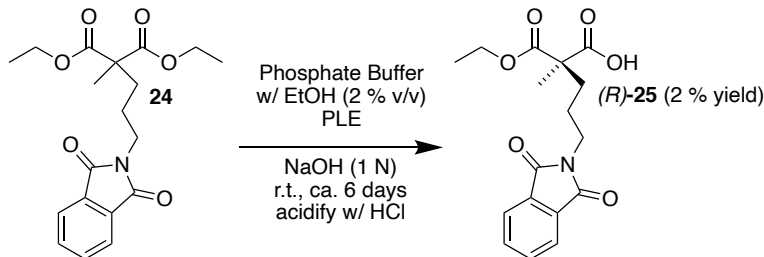


(1*R*,2*S*)-2-phenylcyclohexyl 2-oxopiperidine-3-carboxylate: To a round bottom flask equipped with a stir bar was added 2-oxopiperidine-3-carboxylic acid (**4**, 4.1 mg, 0.029 mmol), (1*R*,2*S*)-*trans*-2-phenyl-1-cyclohexanol (5.4 mg, 0.031 mmol, ~1 equiv.), dicyclohexylcarbodiimide (DCC, 6.7 mg, 0.032 mmol, ~1.1 equiv.), and acetonitrile (3 mL). The reaction was briefly stirred until a solution formed, and then DMAP was added (19.4 mg, 0.159 mmol, 5.48 equiv., [only 10

mol % was needed per the literature; this presented a challenge due to the small scale of the reaction]). The reaction was stirred, covered, for 24 hours, followed by filtration. The filter was then washed with four 5-mL portions of hexanes. The hexanes were previously used to wash the reaction flask to ensure the desired material was transferred wholly. The filtrates were combined and then washed with a cold 1 N solution of hydrochloric acid in water (2 x 3 mL), saturated sodium bicarbonate solution (2 x 3 mL), and saturated sodium chloride solution (2 x 3 mL). The organic phase was then dried with anhydrous MgSO₄, filtered, and concentrated *in vacuo* to yield a white crystalline material, which was then placed inside a desiccator. While a spectrum was obtained, it was too convoluted for effective analysis. See in-text discussion. Procedure adapted from Trost et al., 1986.⁵³

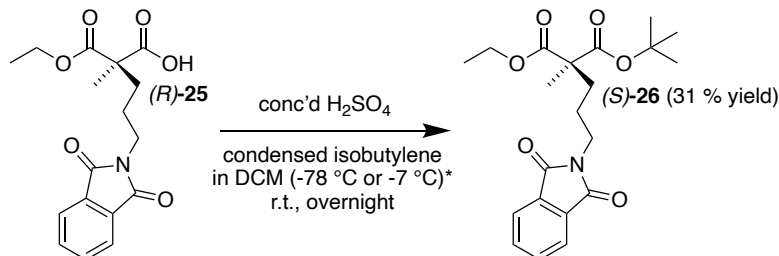


diethyl 2-(3-(1,3-dioxoisindolin-2-yl)propyl)-2-methylmalonate (24): A three-neck round-bottom flask under argon was fitted with a reflux condenser and an addition funnel. The flask was charged with anhydrous THF (10 mL), NaH (60% dispersion in mineral oil, 0.277 g, 6.92 mmol), and a stir bar, yielding a grey solution. The flask was then placed in an ice bath while stirring. After reaching 0 °C, a solution of diethyl-2-methylmalonate in anhydrous THF (0.9785 mL of 22 in 4 mL THF; 5.74 mmol, 0.83 equiv.) was added slowly via the addition funnel, and the solution was stirred at room temperature for 1 hour. Then, a solution of *N*-(bromopropyl)-phthalimide in anhydrous THF (1.542 g of 23 in 10 mL THF; 5.75 mmol, 0.83 equiv.) was added slowly via the addition funnel, yielding a light orange solution. After refluxing for 24 hours, the solution was white and was diluted with diethyl ether (30 mL). It was then washed with 2 N HCl and brine, twice each, and the organic phase was dried over anhydrous MgSO₄. The dried solution was then filtered and concentrated *in vacuo* to yield a yellow oil. This oil was purified via column chromatography (solvent gradient, up to 30:70 EtOAc/hexanes). The pure fractions were combined and concentrated *in vacuo* to yield a viscous clear oil (24, 1.699 g, 81.9 % yield). In one instance, this oil provided a crystalline material upon standing. ¹H NMR (600 MHz, CDCl₃) δ 7.86 – 7.80 (m, 2H), 7.74 – 7.68 (m, 2H), 4.20 – 4.07 (m, 7H [exp. 4H; if presumed solvent omitted: qd, 4H]), 3.68 (dd, *J* = 8.1, 6.4 Hz, 2H), 2.03 (s, 4H [likely solvent impurity]), 2.06 – 2.01 (m, 1H [likely solvent impurity]), 1.93 – 1.86 (m, 2H), 1.69 – 1.60 (m, 2H), 1.38 (s, 3H), 1.28 – 1.18 (m, 11H [exp. 6H; if presumed solvent omitted: t, 6H]). Procedure adapted from Banerjee et al., 2013⁵⁴



(R)-5-(1,3-dioxoisindolin-2-yl)-2-(ethoxycarbonyl)-2-methylpentanoic acid ((R)-25): To a round-bottom flask containing rapidly stirring phosphate buffer (pH 7.0, 0.05 M) with absolute ethanol cosolvent (169.9 mL buffer + 3.4 mL EtOH [exp. 2 % (v/v)]) was added diethyl 2-(3-(1,3-dioxoisindolin-2-yl)propyl)-2-methylmalonate (**24**, 1.699 g, 4.70 mmol). After stirring briefly, porcine liver esterase (PLE, 24 units per mg of PLE; Actual: 17 mg, 87 units/mmol substrate; Literature: 17.63 mg, 90 units/mmol substrate) was added to the solution. The pH of the solution was measured periodically with a Hanna Checker pH meter, and dilute aqueous NaOH (0.5 N) was added as necessary to maintain a pH of 7.4-7.5, until a total of one equivalent of NaOH had been added, after which the reaction was stopped. The solution was then extracted with diethyl ether (4 x 100 mL). The aqueous phase was then acidified to pH 1 with concentrated HCl, yielding a cloudy yellow solution (yellow is likely due to dye present in buffer), which was then extracted again with diethyl ether (8 x 100 mL). The organic phase was dried over MgSO₄, filtered, and concentrated *in vacuo*, yielding a brown oil. The oil was then purified using column chromatography with a gradient of ethyl acetate/hexanes from 30 % to 40 %. The desired fractions were identified with ¹H NMR and combined, followed by concentration *in vacuo* to yield **(R)-25** (0.014 g, 2 %). ¹H NMR (600 MHz, CDCl₃) δ 7.83 – 7.77 (m, 2H), 7.71 – 7.64 (m, 2H), 4.15 (qd, *J* = 7.2, 0.9 Hz, 2H), 3.66 (t, *J* = 7.1 Hz, 2H), 1.96 – 1.82 (m, 2H), 1.72 – 1.59 (m, 2H), 1.39 (s, 3H), 1.20 (t, *J* = 7.1 Hz, 3H). Protocol adapted from Banerjee *et al.*, 2013⁵⁴

Protocol to prepare 0.1 N, pH 7.4 Phosphate Buffer: In later desymmetrization experiments, we prepared our own buffer to match with the literature. To a 1000 mL volumetric flask was added 3.1 g of sodium phosphate monobasic monohydrate and 10.9 g of sodium phosphate dibasic (anhydrous). The flask was then filled with deionized water to the fill line and mixed thoroughly, before transferring the solution to a bottle. The resultant buffer may be stored in the refrigerator for up to one month before disposal. Procedure adapted from ref. 155.



1-(tert-butyl) 3-ethyl (S)-2-(3-(1,3-dioxoisooindolin-2-yl)propyl)-2-methylmalonate ((S)-26): To a sealable tube was added (*R*)-5-(1,3-dioxoisooindolin-2-yl)-2-(ethoxycarbonyl)-2-methylpentanoic acid ((*R*)-25, 0.625 g, 1.88 mmol) in anhydrous dichloromethane (10 mL). A catalytic amount of concentrated H₂SO₄ (ca. 200 µL, 4 drops) was added to the tube, and the tube was allowed to stir while cooling to -78 °C in an acetone/dry ice bath, yielding a dark grey solution. When the temperature desired was reached, isobutylene (2 mL) was condensed in a small test tube at -78 °C, then added immediately to the sealed tube, which was then sealed tightly and placed behind a blast shield. The reaction was allowed to stir overnight with the bath removed, after which the tube was slowly opened, and allowed to stir for an additional two hours. This produced a dark green solution which was then diluted with dichloromethane (10 mL) and washed with 1 N NaOH and brine (3 x 20mL). The organic phase was dried over MgSO₄, filtered, and concentrated *in vacuo*. The resultant material was dissolved in EtOAc and purified via column chromatography on a Biotage with a gradient of EtOAc/hexanes of 10 % to 80 %. The desired fractions were combined and concentrated *in vacuo* to provide the desired product. In reviewing my notes, it seems that the provided yield of 31 % may be for an incorrect sample, and thus a revised yield will need to be reported. ¹H NMR (600 MHz, CDCl₃) δ 7.80 (ddt, *J* = 5.8, 2.9, 1.5 Hz, 2H), 7.71 – 7.65 (m, 2H), 4.17 – 4.05 (m, 4H [Exp. 2H, solvent impurities likely]), 3.65 (tq, *J* = 7.1, 1.4 Hz, 3H [Exp. 2H, solvent impurities likely]), 2.03 – 1.99 (m, 2H) [Impurity?], 1.86 – 1.80 (m, 3H [Exp. 2H]), 1.66 – 1.58 (m, 2H), 1.55 (d, *J* = 1.4 Hz, 1H) [Impurity?], 1.38 (t, *J* = 1.5 Hz, 12H [Exp. 9H & 1.48 ppm]), 1.36 – 1.29 (m, 4H [Exp. 3H & 1.39 ppm]), 1.21 (dtt, *J* = 13.0, 7.1, 1.5 Hz, 7H [Exp. 3H]). Clearly, more work is needed to definitively claim success in this protocol. See the in-text discussion for some comments on this protocol. Adapted from Banerjee *et al.*, 2015.⁵⁵

4.3 Computational Details

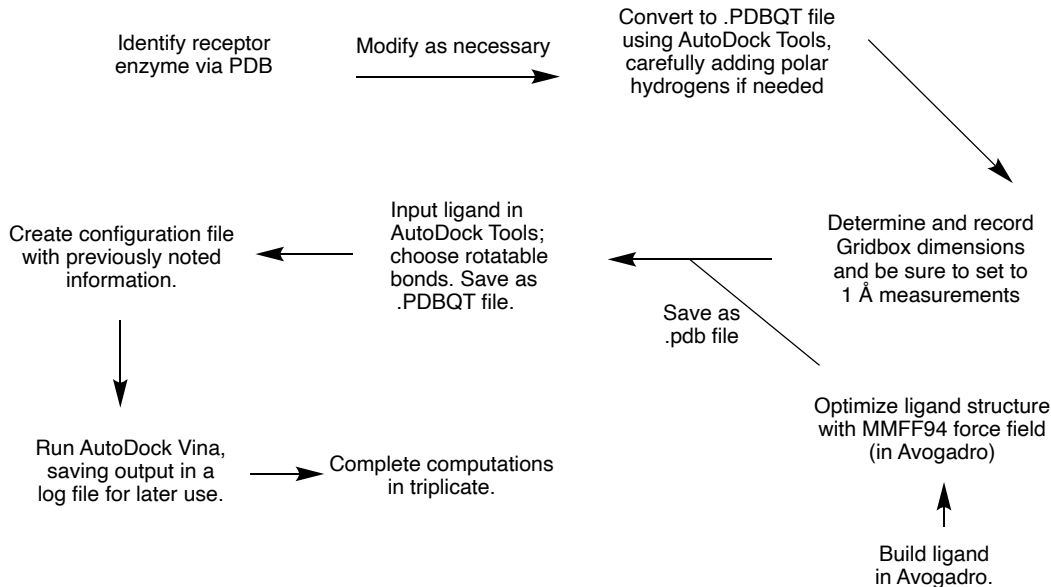


Figure 4.3.1: Sample Workflow for AutoDock Vina Docking Calculations. Avogadro^{156, 157} and the MMFF94 force field¹⁵⁸⁻¹⁶² are distinct from AutoDock Vina.

References

1. Yuen, E. C.; Howe, C. L.; Li, Y.; Holtzman, D. M.; Mobley, W. C. Nerve growth factor and the neurotrophic factor hypothesis. *Brain Dev.* **1996**, *18* (5), 362-368.
2. Kaplan, D. R.; Miller, F. D. Neurotrophin signal transduction in the nervous system. *Curr. Opin. Neurobiol.* **2000**, *10* (3), 381-391.
3. Hamburger, V.; Levi-Montalcini, R. Proliferation, differentiation and degeneration in the spinal ganglia of the chick embryo under normal and experimental conditions. *J. Exp. Zool.* **1949**, *111* (3), 457-501.
4. Schecterson, L. C.; Bothwell, M. Novel roles for neurotrophins are suggested by BDNF and NT-3 mRNA expression in developing neurons. *Neuron* **1992**, *9* (3), 449-463.
5. Acheson, A.; Conover, J. C.; Fandl, J. P.; DeChiara, T. M.; Russell, M.; Thadani, A.; Squinto, S. P.; Yancopoulos, G. D.; Lindsay, R. M. A BDNF autocrine loop in adult sensory neurons prevents cell death. *Nature* **1995**, *374* (6521), 450-453.
6. Merlio, J. P.; Ernfors, P.; Jaber, M.; Persson, H. Molecular cloning of rat trkB and distribution of cells expressing messenger RNAs for members of the trkB family in the rat central nervous system. *Neuroscience* **1992**, *51* (3), 513-532.
7. Yuen, E. C.; Mobley, W. C. Therapeutic applications of neurotrophic factors in disorders of motor neurons and peripheral nerves. *Mol. Med. Today* **1995**, *1* (6), 278-286.
8. Lu, B.; Pang, P. T.; Woo, N. H. The yin and yang of neurotrophin action. *Nature Reviews Neuroscience* **2005**, *6* (8), 603-614.
9. Lee, R.; Kermani, P.; Teng, K. K.; Hempstead, B. L. Regulation of Cell Survival by Secreted Proneurotrophins. *Science* **2001**, *294* (5548), 1945.
10. Hamanoue, M.; Middleton, G.; Wyatt, S.; Jaffray, E.; Hay, R. T.; Davies, A. M. p75-Mediated NF-κB Activation Enhances the Survival Response of Developing Sensory Neurons to Nerve Growth Factor. *Mol. Cell. Neurosci.* **1999**, *14* (1), 28-40.
11. Huang, E. J.; Reichardt, L. F. Neurotrophins: Roles in Neuronal Development and Function. *Annu. Rev. Neurosci.* **2001**, *24* (1), 677-736.
12. Skaper, S. D. The Neurotrophin Family of Neurotrophic Factors: An Overview. In *Neurotrophic Factors: Methods and Protocols*, Skaper, S. D., Ed. Humana Press: Totowa, NJ, 2012; pp 1-12.
13. Encinas, M.; Iglesias, M.; Llecha, N.; Comella, J. X. Extracellular-Regulated Kinases and Phosphatidylinositol 3-Kinase Are Involved in Brain-Derived Neurotrophic Factor-Mediated Survival and neuritogenesis of the Neuroblastoma Cell Line SH-SY5Y. *J. Neurochem.* **1999**, *73* (4), 1409-1421.
14. Boulle, F.; Kenis, G.; Cazorla, M.; Hamon, M.; Steinbusch, H. W. M.; Lanfumey, L.; van den Hove, D. L. A. TrkB inhibition as a therapeutic target for CNS-related disorders. *Prog. Neurobiol. (Oxford, U. K.)* **2012**, *98* (2), 197-206.
15. Middlemas, D. S.; Meisenhelder, J.; Hunter, T. Identification of TrkB autophosphorylation sites and evidence that phospholipase C-gamma 1 is a substrate of the TrkB receptor. *J. Biol. Chem.* **1994**, *269* (7), 5458-5466.
16. Jang, S.-W.; Liu, X.; Pradoldej, S.; Tosini, G.; Chang, Q.; Iuvone, P. M.; Ye, K. N-acetylserotonin activates TrkB receptor in a circadian rhythm. *Proc. Natl. Acad. Sci. U. S. A.* **2010**, *107* (8), 3876.
17. Minichiello, L. TrkB signalling pathways in LTP and learning. *Nat. Rev. Neurosci.* **2009**, *10* (12), 850-860.

18. Rui, T.; Wang, Z.; Li, Q.; Wang, H.; Wang, T.; Zhang, M.; Tao, L.; Luo, C. A TrkB receptor agonist N-acetyl serotonin provides cerebral protection after traumatic brain injury by mitigating apoptotic activation and autophagic dysfunction. *Neurochem. Int.* **2020**, *132*, 104606.
19. Iuvone, P. M.; Boatright, J. H.; Tosini, G.; Ye, K. In *N-Acetylserotonin: Circadian Activation of the BDNF Receptor and Neuroprotection in the Retina and Brain*, Retinal Degenerative Diseases, New York, NY, 2014; Ash, J. D.; Grimm, C.; Hollyfield, J. G.; Anderson, R. E.; LaVail, M. M.; Bowes Rickman, C., Eds. Springer New York: New York, NY, 2014; pp 765-771.
20. Chen, S.-D.; Wu, C.-L.; Hwang, W.-C.; Yang, D.-I. More Insight into BDNF against Neurodegeneration: Anti-Apoptosis, Anti-Oxidation, and Suppression of Autophagy. *Int. J. Mol. Sci.* **2017**, *18* (3).
21. Hicks, R. R.; Martin, V. B.; Zhang, L.; Seroogy, K. B. Mild Experimental Brain Injury Differentially Alters the Expression of Neurotrophin and Neurotrophin Receptor mRNAs in the Hippocampus. *Exp. Neurol.* **1999**, *160* (2), 469-478.
22. Hicks, R. R.; Numan, S.; Dhillon, H. S.; Prasad, M. R.; Seroogy, K. B. Alterations in BDNF and NT-3 mRNAs in rat hippocampus after experimental brain trauma. *Mol. Brain Res.* **1997**, *48* (2), 401-406.
23. Hicks, R. R.; Zhang, L.; Dhillon, H. S.; Prasad, M. R.; Seroogy, K. B. Expression of trkB mRNA is altered in rat hippocampus after experimental brain trauma. *Mol. Brain Res.* **1998**, *59* (2), 264-268.
24. Yang, K.; Perez-Polo, J. R.; Mu, X. S.; Yan, H. Q.; Xue, J. J.; Iwamoto, Y.; Liu, S. J.; Dixon, C. E.; Hayes, R. L. Increased expression of brain-derived neurotrophic factor but not neurotrophin-3 mRNA in rat brain after cortical impact injury. *J. Neurosci. Res.* **1996**, *44* (2), 157-164.
25. Webster, N. J. G.; Pirrung, M. C. Small molecule activators of the Trk receptors for neuroprotection. *BMC Neurosci.* **2008**, *9* (2), S1.
26. Thorne, R. G.; Frey, W. H. Delivery of Neurotrophic Factors to the Central Nervous System. *Clin. Pharmacokinet.* **2001**, *40* (12), 907-946.
27. Longo, F. M.; Massa, S. M. Small-molecule modulation of neurotrophin receptors: a strategy for the treatment of neurological disease. *Nat. Rev. Drug Discovery* **2013**, *12* (7), 507-525.
28. Saragovi, H. U.; Gehring, K. Development of pharmacological agents for targeting neurotrophins and their receptors. *Trends in Pharmacol. Sci.* **2000**, *21* (3), 93-98.
29. Obianyo, O.; Ye, K. Novel small molecule activators of the Trk family of receptor tyrosine kinases. *Biochim. Biophys. Acta Proteins Proteomics* **2013**, *1834* (10), 2213-2218.
30. Shen, J.; Ghai, K.; Sompal, P.; Liu, X.; Cao, X.; Iuvone, P. M.; Ye, K. N-acetyl serotonin derivatives as potent neuroprotectants for retinas. *Proc. Natl. Acad. Sci. U. S. A.* **2012**, *109* (9), 3540.
31. Setterholm, N. A.; McDonald, F. E.; Boatright, J. H.; Iuvone, P. M. Gram-scale, chemoselective synthesis of N-[2-(5-hydroxy-1H-indol-3-yl)ethyl]-2-oxopiperidine-3-carboxamide (HIOC). *Tetrahedron Lett.* **2015**, *56* (23), 3413-3415.
32. Paul, R.; Anderson, G. W. N,N'-Carbonyldiimidazole, a New Peptide Forming Reagent1. *J. Am. Chem. Soc.* **1960**, *82* (17), 4596-4600.
33. Montalbetti, C. A. G. N.; Falque, V. Amide bond formation and peptide coupling. *Tetrahedron* **2005**, *61* (46), 10827-10852.

34. Rannard, S. P.; Davis, N. J. The Selective Reaction of Primary Amines with Carbonyl Imidazole Containing Compounds: Selective Amide and Carbamate Synthesis. *Org. Lett.* **2000**, *2* (14), 2117-2120.
35. Staab, H. A. New Methods of Preparative Organic Chemistry IV. Syntheses Using Heterocyclic Amides (Azolides). *Angew. Chem., Int. Ed. Engl.* **1962**, *1* (7), 351-367.
36. Zhang, J.; Wu, H.; Kim, E.; El-Shourbagy, T. A. Salting-out assisted liquid/liquid extraction with acetonitrile: a new high throughput sample preparation technique for good laboratory practice bioanalysis using liquid chromatography-mass spectrometry. *Biomed. Chromatogr.* **2009**, *23* (4), 419-425.
37. Wang, Z.; Richter, S. M.; Rozema, M. J.; Schellinger, A.; Smith, K.; Napolitano, J. G. Potential Safety Hazards Associated with Using Acetonitrile and a Strong Aqueous Base. *Org. Process Res. Dev.* **2017**, *21* (10), 1501-1508.
38. Gunawardena, N. R.; Brill, T. B. Spectroscopy of Hydrothermal Reactions 15. The pH and Counterion Effects on the Decarboxylation Kinetics of the Malonate System. *J. Phys. Chem. A* **2001**, *105* (10), 1876-1881.
39. McConathy, J.; Owens, M. J. Stereochemistry in Drug Action. *Prim. Care Companion J. Clin. Psychiatry* **2003**, *5* (2), 70-73.
40. Tokunaga, E.; Yamamoto, T.; Ito, E.; Shibata, N. Understanding the Thalidomide Chirality in Biological Processes by the Self-disproportionation of Enantiomers. *Sci. Rep.* **2018**, *8* (1), 17131.
41. Kim, J. H.; Scialli, A. R. Thalidomide: The Tragedy of Birth Defects and the Effective Treatment of Disease. *Toxicol. Sci.* **2011**, *122* (1), 1-6.
42. Nguyen, L. A.; He, H.; Pham-Huy, C. Chiral drugs: an overview. *Int. J. Biomed. Sci.* **2006**, *2* (2), 85-100.
43. Giannini, G.; Vesci, L.; Battistuzzi, G.; Vignola, D.; Milazzo, F. M.; Guglielmi, M. B.; Barbarino, M.; Santaniello, M.; Fantò, N.; Mor, M.; Rivara, S.; Pala, D.; Taddei, M.; Pisano, C.; Cabri, W. ST7612AA1, a Thioacetate- ω (γ -lactam carboxamide) Derivative Selected from a Novel Generation of Oral HDAC Inhibitors. *J. Med. Chem.* **2014**, *57* (20), 8358-8377.
44. Hu, B.; Prashad, M.; Har, D.; Prasad, K.; Repič, O.; Blacklock, T. J. An Efficient Synthesis of (R)-2-Butyl-3-hydroxypropionic Acid. *Org. Process Res. Dev.* **2007**, *11* (1), 90-93.
45. Yaşa, H.; Yusufoglu, A. S. Synthesis of New Medium- and Large- Sized Racemic and Chiral Lactones. *J. Turk. Chem. Soc., Sect. A* **2018**, *5* (2), 539 - 550.
46. Kołodziejska, R.; Studzińska, R. Reverse Stereoselectivity in the Lipase-Catalyzed Hydrolysis of Diacetylated Pyrimidine Acyclonucleosides. *ChemCatChem* **2016**, *8* (23), 3644-3649.
47. Amano Lipase powder, beige-brown, \geq 20,000U/g | 9001-62-1 | Sigma-Aldrich. <https://www.sigmaaldrich.com/catalog/product/aldrich/534730?lang=en®ion=US> (accessed Mar 22, 2021).
48. Kojima, Y.; Yokoe, M.; Mase, T. Purification and Characterization of an Alkaline Lipase from *Pseudomonas fluorescens* AK102. *Biosci., Biotechnol., and Biochem.* **1994**, *58* (9), 1564-1568.
49. Fernández-Lorente, G.; Palomo, J. M.; Fuentes, M.; Mateo, C.; Guisán, J. M.; Fernández-Lafuente, R. Self-assembly of *Pseudomonas fluorescens* lipase into bimolecular aggregates dramatically affects functional properties. *Biotechnol. Bioeng.* **2003**, *82* (2), 232-237.

50. Lipase powder fine, ~ 200U/g | 9001-62-1 | Sigma-Aldrich. <https://www.sigmaaldrich.com/catalog/product/sigma/62301?lang=en®ion=US> (accessed Mar 23, 2021).
51. Ferreiro, M. J.; Latypov, S. K.; Quiñoá, E.; Riguera, R. Assignment of the Absolute Configuration of α -Chiral Carboxylic Acids by ^1H NMR Spectroscopy. *J. Org. Chem.* **2000**, *65* (9), 2658-2666.
52. Seco, J. M.; Quiñoá, E.; Riguera, R. The Assignment of Absolute Configuration by NMR. *Chem. Rev.* **2004**, *104* (1), 17-118.
53. Trost, B. M.; Belletire, J. L.; Godleski, S.; McDougal, P. G.; Balkovec, J. M.; Baldwin, J. J.; Christy, M. E.; Ponticello, G. S.; Varga, S. L.; Springer, J. P. On the use of the O-methylmandelate ester for establishment of absolute configuration of secondary alcohols. *J. Org. Chem.* **1986**, *51* (12), 2370-2374.
54. Banerjee, S.; Wiggins, W. J.; Geoghegan, J. L.; Anthony, C. T.; Woltering, E. A.; Masterson, D. S. Novel synthesis of various orthogonally protected Ca -methyllysine analogues and biological evaluation of a Vapretide analogue containing (S)- α -methyllysine. *Org. Biomol. Chem.* **2013**, *11* (37), 6307-6319.
55. Banerjee, S.; Vogel, E. R.; Hinton, D.; Sterling, M.; Masterson, D. S. An enantiodivergent synthesis of Ca -methyl nipecotic acid analogues from δ -lactam derivatives obtained through a highly stereoselective cyclization strategy. *Tetrahedron: Asymmetry* **2015**, *26* (21), 1292-1299.
56. Provencher, L.; Jones, J. B. A Concluding Specification of the Dimensions of the Active Site Model of Pig Liver Esterase. *J. Org. Chem.* **1994**, *59* (10), 2729-2732.
57. Smith, M. E.; Banerjee, S.; Shi, Y.; Schmidt, M.; Bornscheuer, U. T.; Masterson, D. S. Investigation of the Cosolvent Effect on Six Isoenzymes of PLE in the Enantioselective Hydrolysis of Selected α,α -Disubstituted Malonate Esters. *ChemCatChem* **2012**, *4* (4), 472-475.
58. McCloskey, A. L.; Fonken, G. S.; Kluiber, R. W.; Johnson, W. S. DI-tert-BUTYL MALONATE [I. ISOBUTYLENE METHOD]. *Org. Synth.* **1954**, *34*, 26.
59. Harrane, A.; Meghabar, R.; Belbachir, M. A Protons Exchanged Montmorillonite Clay as an Efficient Catalyst for the Reaction of Isobutylene Polymerization. *Int. J. Mol. Sci.* **2002**, *3* (7), 790-800.
60. Hasenpusch, D.; Bornscheuer, U. T.; Langel, W. Simulation on the structure of pig liver esterase. *J. Mol. Model.* **2011**, *17* (6), 1493-1506.
61. Toone, E. J.; Werth, M. J.; Jones, J. B. Enzymes in organic synthesis. 47. Active-site model for interpreting and predicting the specificity of pig liver esterase. *J. Am. Chem. Soc.* **1990**, *112* (12), 4946-4952.
62. Jencks, W. P. Binding Energy, Specificity, and Enzymic Catalysis: The Circe Effect. In *Advances in Enzymology and Related Areas of Molecular Biology*, 1975; pp 219-410.
63. Kazemi, M.; Himo, F.; Åqvist, J. Enzyme catalysis by entropy without Circe effect. *Proc. Natl. Acad. Sci. U.S.A.* **2016**, *113* (9), 2406.
64. PDB ID: 5fv4; Werten, S., Palm, G. J., Berndt, L., Hinrichs, W. (2016) Pig liver esterase 5 (PLE5) doi: 10.2210/pdb5FV4/pdb
65. Lam, L. K. P.; Brown, C. M.; De Jeso, B.; Lym, L.; Toone, E. J.; Jones, J. B. Enzymes in organic synthesis. 42. Investigation of the effects of the isozymal composition of pig liver esterase on its stereoselectivity in preparative-scale ester hydrolysis of asymmetric synthetic value. *J. Am. Chem. Soc.* **1988**, *110* (13), 4409-4411.

66. Hummel, A.; Brüsehaber, E.; Böttcher, D.; Trauthwein, H.; Doderer, K.; Bornscheuer, U. T. Isoenzymes of Pig-Liver Esterase Reveal Striking Differences in Enantioselectivities. *Angew. Chem. Int. Ed.* **2007**, *46* (44), 8492-8494.
67. Moseley, J. D.; Staunton, J. Influence of ester chain length on lipase catalysed hydrolyses of meso-oxiranedimethanol esters. *Tetrahedron: Asymmetry* **1998**, *9* (20), 3619-3623.
68. Moseley, J. D.; Staunton, J. Influence of ester chain length, enzyme, and physical parameters on lipase-catalysed hydrolyses of meso-oxiranedimethanol esters. Part 2. *Tetrahedron: Asymmetry* **2000**, *11* (15), 3197-3209.
69. Ji, L.; Xiaoling, T.; Hongwei, Y. Prediction of the enantioselectivity of lipases and esterases by molecular docking method with modified force field parameters. *Biotechnol. Bioeng.* **2010**, *105* (4), 687-696.
70. Trott, O.; Olson, A. J. AutoDock Vina: Improving the speed and accuracy of docking with a new scoring function, efficient optimization, and multithreading. *J. Comp. Chem.* **2010**, *31* (2), 455-461.
71. PyMOL; The PyMOL Molecular Graphics System, Version 2.4.1 Schrödinger, LLC.
72. Barton, P.; Laws, A. P.; Page, M. I. Structure–activity relationships in the esterase-catalysed hydrolysis and transesterification of esters and lactones. *J. Chem. Soc., Perkin Trans. 2* **1994**, (9), 2021-2029.
73. Bianco, G.; Forli, S.; Goodsell, D. S.; Olson, A. J. Covalent docking using autodock: Two-point attractor and flexible side chain methods. *Protein Science* **2016**, *25* (1), 295-301.
74. Hasenpusch, D.; Möller, D.; Bornscheuer, U. T.; Langel, W. Substrate-Enzyme Interaction in Pig Liver Esterase. [arXiv:1204.6186](https://arxiv.org/abs/1204.6186)
75. Bode, S. E.; Wolberg, M.; Müller, M. Stereoselective Synthesis of 1,3-Diols. *Synthesis* **2006**, *2006* (04), 557-588.
76. Kumar, P.; Tripathi, D.; Sharma, B. M.; Dwivedi, N. Transition metal catalysis—a unique road map in the stereoselective synthesis of 1,3-polyols. *Org. Biomol. Chem.* **2017**, *15* (4), 733-761.
77. Gamba-Sánchez, D.; Prunet, J. Synthesis of 1,3-Diols by O-Nucleophile Additions to Activated Alkenes. *Synthesis* **2018**, *50* (20), 3997-4007.
78. Sperandio, C.; Rodriguez, J.; Quintard, A. Catalytic strategies towards 1,3-polyol synthesis by enantioselective cascades creating multiple alcohol functions. *Org. Biomol. Chem.* **2020**, *18* (6), 1025-1035.
79. Friedrich, R. M.; Friestad, G. K. Inspirations from tetrafibracin and related polyketides: new methods and strategies for 1,5-polyol synthesis. *Nat. Prod. Rep.* **2020**, *37* (9), 1229-1261.
80. Shao, C.-L.; Linington, R. G.; Balunas, M. J.; Centeno, A.; Boudreau, P.; Zhang, C.; Engene, N.; Spadafora, C.; Mutka, T. S.; Kyle, D. E.; Gerwick, L.; Wang, C.-Y.; Gerwick, W. H. Bastimolide A, a Potent Antimalarial Polyhydroxy Macrolide from the Marine Cyanobacterium Okeania hirsuta. *J. Org. Chem.* **2015**, *80* (16), 7849-7855.
81. Shao, C.-L.; Mou, X.-F.; Cao, F.; Spadafora, C.; Glukhov, E.; Gerwick, L.; Wang, C.-Y.; Gerwick, W. H. Bastimolide B, an Antimalarial 24-Membered Marine Macrolide Possessing a tert-Butyl Group. *J. Nat. Prod.* **2018**, *81* (1), 211-215.
82. Varmazyar, A.; Sedaghat, S.; Goli-Kand, A. N.; Khalaj, M.; Arab-Salmanabadi, S. Copper Salt Catalyzed Synthesis of Functionalized 2H-Pyranes. *J. Heterocycl. Chem.* **2019**, *56* (6), 1850-1856.

83. Varmazyar, A.; Sedaghat, S.; Goli-Kand, A. N.; Khalaj, M.; Arab-Salmanabadi, S. Domino ring opening/cyclization of oxiranes for synthesis of functionalized 2H-pyran-5-carboxylate. *Mol. Diversity* **2020**, *24* (3), 707-716.
84. Cheng, G.; Li, T.-J.; Yu, J.-Q. Practical Pd(II)-Catalyzed C–H Alkylation with Epoxides: One-Step Syntheses of 3,4-Dihydroisocoumarins. *J. Am. Chem. Soc.* **2015**, *137* (34), 10950-10953.
85. Burova, S. A.; McDonald, F. E. Total Synthesis of the Polyene-Polyol Macrolide RK-397, Featuring Cross-Couplings of Alkynylepoxyde Modules. *J. Am. Chem. Soc.* **2004**, *126* (8), 2495-2500.
86. Dover, T. L.; McDonald, F. E. Fluorinated alcohols: powerful promoters for ring-opening reactions of epoxides with carbon nucleophiles. *Arkivoc* **2021**, (iii), 85-114.
87. Reed, N. N.; Janda, K. D. A One-Step Synthesis of Monoprotected Polyethylene Glycol Ethers. *J. Org. Chem.* **2000**, *65* (18), 5843-5845.
88. Harvey, R. G. Activated metabolites of carcinogenic hydrocarbons. *Acc. Chem. Res.* **1981**, *14* (7), 218-226.
89. Boone, M. A.; Tong, R.; McDonald, F. E.; Lense, S.; Cao, R.; Hardcastle, K. I. Biomimetic Syntheses from Squalene-Like Precursors: Synthesis of ent-Abudinol B and Reassessment of the Structure of Muzitone. *J. Am. Chem. Soc.* **2010**, *132* (14), 5300-5308.
90. Robles, O.; McDonald, F. E. Modular Synthesis of the C9–C27 Degradation Product of Aflastatin A via Alkyne–Epoxide Cross-Couplings. *Org. Lett.* **2008**, *10* (9), 1811-1814.
91. Bégué, J.-P.; Bonnet-Delpon, D.; Crousse, B. Fluorinated Alcohols: A New Medium for Selective and Clean Reaction. *Synlett* **2004**, (1), 18-29.
92. Shuklov, I. A.; Dubrovina, N. V.; Börner, A. Fluorinated Alcohols as Solvents, Cosolvents and Additives in Homogeneous Catalysis. *Synthesis* **2007**, (19), 2925-2943.
93. Wencel-Delord, J.; Colobert, F. A remarkable solvent effect of fluorinated alcohols on transition metal catalysed C–H functionalizations. *Org. Chem. Front.* **2016**, *3* (3), 394-400.
94. Colomer, I.; Chamberlain, A. E. R.; Haughey, M. B.; Donohoe, T. J. Hexafluoroisopropanol as a highly versatile solvent. *Nat. Rev. Chem.* **2017**, *1*, 0088.
95. Sinha, S. K.; Bhattacharya, T.; Maiti, D. Role of hexafluoroisopropanol in C–H activation. *React. Chem. Eng.* **2019**, *4* (2), 244-253.
96. Yu, C.; Sanjosé-Orduna, J.; Patureau, F. W.; Pérez-Temprano, M. H. Emerging unconventional organic solvents for C–H bond and related functionalization reactions. *Chem. Soc. Rev.* **2020**, *49* (6), 1643-1652.
97. An, X.-D.; Xiao, J. Fluorinated Alcohols: Magic Reaction Medium and Promoters for Organic Synthesis. *Chem. Rec.* **2020**, *20* (2), 142-161.
98. Pozhydaiev, V.; Power, M.; Gandon, V.; Moran, J.; Lebœuf, D. Exploiting hexafluoroisopropanol (HFIP) in Lewis and Brønsted acid-catalyzed reactions. *Chem. Commun.* **2020**, *56* (78), 11548-11564.
99. Richmond, E.; Yi, J.; Vuković, V. D.; Sajadi, F.; Rowley, C. N.; Moran, J. Ring-opening hydroarylation of monosubstituted cyclopropanes enabled by hexafluoroisopropanol. *Chem. Sci.* **2018**, *9* (30), 6411-6416.

100. Li, F.-X.; Ren, S.-J.; Li, P.-F.; Yang, P.; Qu, J. An *Endo*-Selective Epoxide-Opening Cascade for the Fast Assembly of the Polycyclic Core Structure of Marine Ladder Polyethers. *Angew. Chem. Int. Ed.* **2020**, *59* (42), 18473-18478.
101. Silverstein, T. P.; Heller, S. T. pKa Values in the Undergraduate Curriculum: What Is the Real pKa of Water? *J. Chem. Ed.* **2017**, *94* (6), 690-695.
102. Bentley, T. W.; Roberts, I. Structural and solvent effects on rates of solvolysis of secondary alkyl substrates—an update. *J. Phys. Org. Chem.* **2005**, *18* (2), 96-100.
103. Atik, Z. Experimental Isobaric Vapor-Liquid Equilibria of Binary Mixtures of 2,2,2-Trifluoroethanol with Benzene or Toluene. *J. Chem. Eng. Data* **2007**, *52* (3), 1086-1088.
104. Mejía, A.; Segura, H.; Cartes, M. Vapor-Liquid Equilibria and Interfacial Tensions of the System Ethanol + 2-Methoxy-2-methylpropane. *J. Chem. Eng. Data* **2010**, *55* (1), 428-434.
105. Laurence, C.; Legros, J.; Chantzis, A.; Planchat, A.; Jacquemin, D. A Database of Dispersion-Induction DI, Electrostatic ES, and Hydrogen Bonding α_1 and β_1 Solvent Parameters and Some Applications to the Multiparameter Correlation Analysis of Solvent Effects. *J. Phys. Chem. B* **2015**, *119* (7), 3174-3184.
106. Schadt, F. L.; Bentley, T. W.; Schleyer, P. v. R. The SN₂-SN₁ spectrum. 2. Quantitative treatments of nucleophilic solvent assistance. A scale of solvent nucleophilicities. *J. Am. Chem. Soc.* **1976**, *98* (24), 7667-7674.
107. Kevill, D. N.; Anderson, S. W. An improved scale of solvent nucleophilicity based on the solvolysis of the S-methyldibenzothiophenium ion. *J. Org. Chem.* **1991**, *56* (5), 1845-1850.
108. Middleton, W. J.; Lindsey, R. V. Hydrogen Bonding in Fluoro Alcohols *J. Am. Chem. Soc.* **1964**, *86* (22), 4948-4952.
109. Berkessel, A.; Adrio, J. A.; Hüttenhain, D.; Neudörfl, J. M. Unveiling the “Booster Effect” of Fluorinated Alcohol Solvents: Aggregation-Induced Conformational Changes and Cooperatively Enhanced H-Bonding. *J. Am. Chem. Soc.* **2006**, *128* (26), 8421-8426.
110. Minegishi, S.; Kobayashi, S.; Mayr, H. Solvent Nucleophilicity. *J. Am. Chem. Soc.* **2004**, *126* (16), 5174-5181.
111. Ammer, J.; Mayr, H. Solvent nucleophilicities of hexafluoroisopropanol/water mixtures. *J. Phys. Org. Chem.* **2013**, *26* (1), 59-63.
112. Tavener, S. J.; Clark, J. H. Can fluorine chemistry be green chemistry? *J. Fluorine Chem.* **2003**, *123* (1), 31-36.
113. Brenek, S. J.; Caron, S.; Chisowa, E.; Delude, M. P.; Drexler, M. T.; Ewing, M. D.; Handfield, R. E.; Ide, N. D.; Nadkarni, D. V.; Nelson, J. D.; Olivier, M.; Perfect, H. H.; Phillips, J. E.; Teixeira, J. J.; Weekly, R. M.; Zelina, J. P. Development of a Practical and Convergent Process for the Preparation of Sulopenem. *Org. Process Res. Dev.* **2012**, *16* (8), 1348-1359.
114. Crank, G.; Harding, D. R. K.; Szinai, S. S. Perfluoroalkyl carbonyl compounds. 2. Derivatives of hexafluoroacetone. *J. Med. Chem.* **1970**, *13* (6), 1215-1217.
115. Blake, D. A.; Cascorbi, H. F.; Rozman, R. S.; Meyer, F. J. Animal toxicity of 2,2,2-trifluoroethanol. *Toxicol. Appl. Pharmacol.* **1969**, *15* (1), 83-91.

116. Kaminsky, L. S.; Fraser, J. M.; Seaman, M.; Dunbar, D. Rat liver metabolism and toxicity of 2,2,2-trifluoroethanol. *Biochem. Pharmacol.* **1992**, *44* (9), 1829-1837.
117. Johnson, B. M.; Shu, Y.-Z.; Zhuo, X.; Meanwell, N. A. Metabolic and Pharmaceutical Aspects of Fluorinated Compounds. *J. Med. Chem.* **2020**, *63* (12), 6315-6386.
118. Mandatory Reporting of Greenhouse Gases.
<https://www.federalregister.gov/documents/2009/10/30/E9-23315/mandatory-reporting-of-greenhouse-gases> (accessed Apr 5, 2021).
119. Sellevåg, S. R.; Nielsen, C. J.; Søvde, O. A.; Myhre, G.; Sundet, J. K.; Stordal, F.; Isaksen, I. S. A. Atmospheric gas-phase degradation and global warming potentials of 2-fluoroethanol, 2,2-difluoroethanol, and 2,2,2-trifluoroethanol. *Atmos. Environ.* **2004**, *38* (39), 6725-6735.
120. Örtl, E. REACH: Improvement of guidance and methods for the identification and assessment of PMT/vPvM substances. <https://www.umweltbundesamt.de/en/publikationen/reach-improvement-of-guidance-methods-for-the> (accessed Apr 5, 2021).
121. Westermaier, M.; Mayr, H. Regio- and Stereoselective Ring-Opening Reactions of Epoxides with Indoles and Pyrroles in 2,2,2-Trifluoroethanol. *Chem. – Eur. J.* **2008**, *14* (5), 1638-1647.
122. Li, G.; Bao, G.; Zhu, G.; Li, Y.; Huang, L.; Sun, W.; Hong, L.; Wang, R. Regio- and stereospecific Friedel–Crafts alkylation of indoles with spiro-epoxyxindoles. *Org. Biomol. Chem.* **2018**, *16* (19), 3655-3661.
123. Li, G.-X.; Qu, J. Friedel–Crafts alkylation of arenes with epoxides promoted by fluorinated alcohols or water. *Chem. Commun.* **2010**, *46* (15), 2653-2655.
124. Hilt, G.; Bolze, P.; Harms, K. An Improved Catalyst System for the Iron-Catalyzed Intermolecular Ring-Expansion Reactions of Epoxides. *Chem. Eur. J.* **2007**, *13* (15), 4312-4325.
125. Shuler, W. G.; Combee, L. A.; Falk, I. D.; Hilinski, M. K. Intermolecular Electrophilic Addition of Epoxides to Alkenes: [3+2] Cycloadditions Catalyzed by Lewis Acids. *Eur. J. Org. Chem.* **2016**, *(20)*, 3335-3338.
126. Llopis, N.; Baeza, A. HFIP-Promoted Synthesis of Substituted Tetrahydrofurans by Reaction of Epoxides with Electron-Rich Alkenes. *Molecules* **2020**, *25* (15), 3464.
127. Mayo, F. R. The dimerization of styrene. *J. Am. Chem. Soc.* **1968**, *90* (5), 1289-1295.
128. Ioganson, A. V. Direct proportionality of the hydrogen bonding energy and the intensification of the stretching $\nu(XH)$ vibration in infrared spectra. *Spectrochim. Acta, Part A* **1999**, *55* (7-8), 1585-1612.
129. Lu, J.; Brown, J. S.; Liotta, C. L.; Eckert, C. A. Polarity and hydrogen-bonding of ambient to near-critical water: Kamlet–Taft solvent parameters. *Chem. Commun.* **2001**, *(7)*, 665-666.
130. Liu, Y.; Li, X.; Lin, G.; Xiang, Z.; Xiang, J.; Zhao, M.; Chen, J.; Yang, Z. Synthesis of Catechins via Thiourea/AuCl₃-Catalyzed Cycloalkylation of Aryl Epoxides, *J. Org. Chem.* **2008**, *73* (12), 4625-4629.
131. Schmid, M.; Sokol, K. R.; Wein, L. A.; Torres Venegas, S.; Meisenbichler, C.; Wurst, K.; Podewitz, M.; Magauer, T. Synthesis of Vicinal Quaternary All-Carbon Centers via Acid-catalyzed Cycloisomerization of Neopentylic Epoxides. *Org. Lett.* **2020**, *22* (16), 6526-6531.

132. Fărcașiu, D.; Ghenciu, A.; Marino, G.; Kastrup, R. V. Strength of liquid acids in solution and on solid supports. The anion stabilization by solvent and its consequences for catalysis. *J. Mol. Cat. A: Chem.* **1997**, *126* (2-3), 141-150.
133. Iskra, J.; Bonnet-Delpo, D.; Bégué, J.-P. Comparative study of the ring opening of 1-CF₃-epoxy ethers mediated by Brönsted acids and hexafluoro-2-propanol. *J. Fluorine Chem.* **2005**, *126* (4), 551-556.
134. Palladino, P.; Stetsenko, D. A. New TFA-Free Cleavage and Final Deprotection in Fmoc Solid-Phase Peptide Synthesis: Dilute HCl in Fluoro Alcohol. *Org. Lett.* **2012**, *14* (24), 6346-6349.
135. Zhao, J.-F.; Zhao, Y.-J.; Loh, T.-P. Indium tribromide-promoted arene-terminated epoxy olefin cyclization. *Chem. Commun.* **2008**, (11), 1353-1355.
136. Surendra, K.; Corey, E. J. Rapid and Enantioselective Synthetic Approaches to Germanicol and Other Pentacyclic Triterpenes. *J. Am. Chem. Soc.* **2008**, *130* (27), 8865-8869.
137. Tian, Y.; Xu, X.; Zhang, L.; Qu, J. Tetraphenylphosphonium Tetrafluoroborate/1,1,1,3,3,3-Hexafluoroisopropanol (Ph₄PBF₄/HFIP) Effecting Epoxide-Initiated Cation–Olefin Polycyclizations. *Org. Lett.* **2016**, *18* (2), 268-271.
138. van Tamelen, E. E.; Willet, J.; Schwartz, M.; Nadeau, R. Nonenzymic Laboratory Cyclization of Squalene 2,3-Oxide. *J. Am. Chem. Soc.* **1966**, *88* (24), 5937-5938.
139. Kitahara, Y.; Kato, T.; Kishi, M. Cyclization of Polyenes. III Cyclization of Squalene-oxides. *Chem. Pharm. Bull.* **1968**, *16* (11), 2216-2222.
140. Kolesnikova, M. D.; Obermeyer, A. C.; Wilson, W. K.; Lynch, D. A.; Xiong, Q.; Matsuda, S. P. T. Stereochemistry of Water Addition in Triterpene Synthesis: The Structure of Arabidiol. *Org. Lett.* **2007**, *9* (11), 2183-2186.
141. Tsangarakis, C.; Raptis, C.; Arkoudis, E.; Stratakis, M. Zeolite NaY-Promoted Monocyclization of Epoxy Polyene Terpenes: A Unique Route for the Direct Synthesis of Incompletely Cyclized Naturally Occurring Terpenols. *Adv. Synth. Catal.* **2008**, *350* (10), 1587-1600.
142. Quilez del Moral, J. F.; Domingo, V.; Pérez, A.; Martínez Andrade, K. A.; Enríquez, L.; Jaraiz, M.; López-Pérez, J. L.; Barrero, A. F. Mimicking Halimane Synthases: Monitoring a Cascade of Cyclizations and Rearrangements from Epoxypolyprenes. *J. Org. Chem.* **2019**, *84* (21), 13764-13779.
143. Gschwend, H. W.; Rodriguez, H. R. Heteroatom-Facilitated Lithiations. *Org. React.* **1979**, *26*, 1-360.
144. Snieckus, V. Directed ortho metalation. Tertiary amide and O-carbamate directors in synthetic strategies for polysubstituted aromatics. *Chem. Rev.* **1990**, *90* (6), 879-933.
145. Nicolaou, K. C.; Gray, D.; Tae, J. Total Synthesis of Hamigerans: Part 1. Development of Synthetic Technology for the Construction of Benzannulated Polycyclic Systems by the Intramolecular Trapping of Photogenerated Hydroxy-*o*-quinodimethanes and Synthesis of Key Building Blocks. *Angew. Chem. Int. Ed.* **2001**, *40* (19), 3675-3678.
146. Wang, Z.; Kuninobu, Y.; Kanai, M. Palladium-Catalyzed Oxirane-Opening Reaction with Arenes via C–H Bond Activation. *J. Am. Chem. Soc.* **2015**, *137* (19), 6140-6143.

147. Li, D.-D.; Niu, L.-F.; Ju, Z.-Y.; Xu, Z.; Wu, C. Palladium-Catalyzed C(sp₂)–H Bond Alkylation of Ketoximes by Using the Ring-Opening of Epoxides. *Eur. J. Org. Chem.* **2016**, (18), 3090-3096.
148. Thombal, R. S.; Feoktistova, T.; González-Montiel, G. A.; Cheong, P. H.-Y.; Lee, Y. R. Palladium-catalyzed synthesis of β-hydroxy compounds via a strained 6,4-palladacycle from directed C–H activation of anilines and C–O insertion of epoxides. *Chem. Sci.* **2020**, *11* (27), 7260-7265.
149. Lian, B.; Zhang, L.; Li, S.-J.; Zhang, L.-L.; Fang, D.-C. Pd^{IV} Species Mediation in Pd^{II}-Catalyzed Direct Alkylation of Arenes with Oxiranes: A DFT Study. *J. Org. Chem.* **2018**, *83* (6), 3142-3148.
150. Higgins, E. M.; Sherwood, J. A.; Lindsay, A. G.; Armstrong, J.; Massey, R. S.; Alder, R. W.; O'Donoghue, A. C. pK_as of the conjugate acids of N-heterocyclic carbenes in water. *Chem. Commun.* **2011**, *47* (5), 1559-1561.
151. Cisar, J. S.; Weber, O. D.; Clapper, J. R.; Blankman, J. L.; Henry, C. L.; Simon, G. M.; Alexander, J. P.; Jones, T. K.; Ezekowitz, R. A. B.; O'Neill, G. P.; Grice, C. A. Identification of ABX-1431, a Selective Inhibitor of Monoacylglycerol Lipase and Clinical Candidate for Treatment of Neurological Disorders. *J. Med. Chem.* **2018**, *61* (20), 9062-9084.
152. De Marco, R. A.; Kovacina, T. A.; Fox, W. B. Polyfluoroalkyl sulfites: Preparation and properties. *J. Fluorine Chem.* **1975**, *5* (3), 221-230.
153. Zhou, K.; Zhu, Y.; Fan, W.; Chen, Y.; Xu, X.; Zhang, J.; Zhao, Y. Late-Stage Functionalization of Aromatic Acids with Aliphatic Aziridines: Direct Approach to Form β-Branched Arylethylamine Backbones. *ACS Catal.* **2019**, *9* (8), 6738-6743.
154. Samzadeh-Kermani, A. Organo-catalytic synthesis of tetrahydropyridines via a domino ring opening/cyclization reaction of aziridines. *Monatsh. Chem.* **2019**, *150*, 1495-1501.
155. Sodium phosphate. <http://cshprotocols.cshlp.org/content/2006/1/pdb.rec8303> (accessed Mar 23, 2021).
156. Avogadro: an open-source molecular builder and visualization tool. Version 1.2.0. <http://avogadro.cc/>
157. Hanwell, M. D.; Curtis, D. E.; Lonie, D. C.; Vandermeersch, T.; Zurek, E.; Hutchison, G. R. Avogadro: an advanced semantic chemical editor, visualization, and analysis platform. *J. Cheminform.* **2012**, *4*:17.
158. Halgren, T. A. Merck molecular force field. I. Basis, form, scope, parameterization, and performance of MMFF94. *J. Comput. Chem.* **1996**, *17* (5-6), 490-519.
159. Halgren, T. A. Merck molecular force field. II. MMFF94 van der Waals and electrostatic parameters for intermolecular interactions. *J. Comput. Chem.* **1996**, *17* (5-6), 520-552.
160. Halgren, T. A. Merck molecular force field. III. Molecular geometries and vibrational frequencies for MMFF94. *J. Comput. Chem.* **1996**, *17* (5-6), 553-586.
161. Halgren, T. A.; Nachbar, R. B. Merck molecular force field. IV. conformational energies and geometries for MMFF94. *J. Comput. Chem.* **1996**, *17* (5-6), 587-615.

162. Halgren, T. A. Merck molecular force field. V. Extension of MMFF94 using experimental data, additional computational data, and empirical rules. *J. Comput. Chem.* **1996**, *17* (5-6), 616-641.